University of New Orleans

ScholarWorks@UNO

Synthesis and Applications of Mutimodal Hybrid Albumin Nanoparticles for Chemotherapeutic Drug Delivery and Phototherml Therapy Platforms

Donna V. Peralta
University of New Orleans, dvweaver@uno.edu

Follow this and additional works at: https://scholarworks.uno.edu/td

Part of the Analytical Chemistry Commons, Biotechnology Commons, Materials Chemistry Commons, Medicinal-Pharmaceutical Chemistry Commons, and the Polymer Chemistry Commons

Recommended Citation

Synthesis and Applications of Multimodal Hybrid Albumin Nanoparticles for Chemotherapeutic
Drug Delivery and Photothermal Therapy Platforms

A Dissertation

Submitted to the Graduate Faculty of the
University of New Orleans
in partial fulfillment of the
requirements for the degree of

Doctor of Philosophy
in
Chemistry

By

Donna V. Peralta

B.S. Loyola University, New Orleans, 2002
M.B.A University of Phoenix, 2008
August 2014

Dedication

I would like to dedicate this dissertation to my favorite husband, George. His love, care, encouragement and enthusiasm are unending. I'm so grateful for him, every day.

To my biggest supporter, my mother Beverly. You are, without question, the sweetest person I will ever know. Thank you for always believing the best of me.

Truly, this work is dedicated to God. Without Him, I could not have accomplished it.

Acknowledgments

I would like to thank my research advisor Professor Matthew A. Tarr for his support and encouragement during my time at UNO. I thank Dr. Leroy Morgan for his financial support, guidance and sense of humor. I express my sincere gratitude to my advisory committee members: Professor Mark Trudell, Professor John Wiley and Professor Yang Cai for their help and kind words throughout my graduate research career. Thank you to Dr. Jibao He from Tulane University for all the TEM instruction and analysis.

I express my gratitude to AMRI for providing instrumentation and monetary support. Thank you to Dr. Benjamin Lee, Cameron Callaghan and Tulane University for your collaboration. Thank you to Dr. Jin Zhang and Damon Wheeler at the University of Santa Cruz for your collaboration. I give special thanks to Professor Richard Cole for always giving a kind word of encouragement and for urging me to do my best during my second chance. I am appreciative of the chemistry faculty at Loyola University, especially Dr. Kurt Birdwhistell, for supplying me with the chemistry building blocks. I am sincerely grateful to my past and present research group members for their instruction, help, and laughs; especially my lab mates Kristen and Parisa. Thanks for listening, ladies.

I give a very special thanks to my Aunt Libby for always, always being there. You are the best! I also thank my sister Tina for always for always being so proud of me and sharing so many laughs. Thank you to Caydee and Cody for that one day that you came to the lab and I got the best results ever. For my parents, family and friends; I cannot thank you enough for your prayers and for believing I could accomplish this.

Table of Contents

List of Tables

List of Figures

Abstract

Progress has been made in using human serum albumin nanoparticles (HSAPs) as carrier systems for targeted treatment of cancer. Human serum albumin (HSA), the most abundant human blood protein, can form HSAPs via a desolvation and crosslinking method, with the size of the HSAPs having crucial importance for drug loading and *in vivo* performance. Gold nanoparticles have also gained medicinal attention due to their ability to absorb near-infrared (NIR) light. These relatively non-toxic particles offer combinational therapy via imaging and photothermal therapy (PPTT) capabilities.

A desolvation and crosslinking approach was employed to encapsulate gold nanoparticles (AuNPs), hollow gold nanoshells (AuNSs), and gold nanorods (AuNRs), into efficiently sized HSAPs for future tumor heat ablation via PPTT. The AuNR-HSAPs, AuNP-HSAPs and AuNS-HSAPs had average particle diameters of 222 ± 5, 195 ± 9 and 156 ± 15, respectively.

We simultaneously encapsulated AuNRs and the anticancer drug paclitaxel (PAC), forming PAC-AuNR-HSAPs with overall average particle size of 299 ± 6 nm. Loading of paclitaxel into PAC-AuNR-HSAPs reached 3μg PAC/mg HSA. PAC-AuNR-HSAPs experienced photothermal heating of 46 ˚C after 15 minutes of NIR laser exposure; the temperature necessary to cause severe cellular hyperthermia. There was a burst release of paclitaxel up to 188 ng caused by the irradiation session, followed by a temporal drug release.

AuNR-HSAPs were tested for ablation of renal cell carcinoma using NIR irradiation *in vitro*. Particles created with the same amount of AuNRs, but varying HSA (1, 5 or 20 mg) showed overall particle size diameters 409 ± 224, 294 ± 83 and 167 ± 4 nm, respectively. Increasing HSAPs causes more toxicity under non-irradiated treatment conditions: AuNR-

HSAPs with 20 mg versus 5 mg HSA caused cell viability of 64.5% versus 87%, respectively. All AuNR-HSAPs batches experienced photothermal heating above 42 ˚C. Coumarin-6, was used to visualize the cellular uptake of AuNR-HSAPs via fluorescence microscopy.

Finally, camptothecin (CPT) an antineoplastic agent and BACPT (7-butyl-10-aminocamptothecin) were loaded into HSAPs to combat their aqueous insolubility. BACPT-HSAPs loaded up to 5.25 micrograms BACPT/ mg of HSA. CPT encapsulation could not be determined. BACPT-HSAPs and CPT-HSAPs showed cytotoxicity to human sarcoma cells *in vitro*.

Chapter 1

Introduction

1.1 Objectives and Aims

The objective of this research project was to develop hybrid gold nanomaterial and drug-loaded human serum albumin nanoparticles (HSAP) for custom chemotherapeutic/photothermally active cancer therapy platforms. HSAPs offer a combination of diagnostic and treatment functionalities which are unique to them, when considering their natural biological protein makeup. They have the inherent ability to seek out areas of increased blood flow, such a tumor sites, and accumulate there. This accumulation can prove diagnostically helpful when HSAPs are conjugated to a contrast agent. Due to the accumulation of the particles at tumor sites, they have the potential for controlled release of drugs as well as the capacity for inclusion of other therapy outlets, such as hyperthermia.

The advantages characteristic of a hybrid treatment system allow for simultaneous targeting, detection and multimodal therapy avenues, which do not currently exist in any one clinical therapy option. This research work was specifically designed to 1) develop and understand a preparation method for encapsulating gold nanomaterials into HSAPs, 2) prove the near-infrared triggered heating capabilities of the gold nanomaterials even while they were encapsulated in the protein shell, 3) simultaneously include proven chemotherapeutic drugs into the gold-HSAPs and determine the loading efficiencies and 4) test the heating and drug delivery effects of the drug-gold-HSAPs as compared to particle controls *in vitro*.

1.2 Significance

Cancer is an enormous global health problem, accounting for 1 in 8 deaths worldwide.[1] The financial cost of a disease of this magnitude is also staggering, so there is a definite crucial

1

need for more efficient, less invasive, and cheaper treatments that eliminate the severe symptoms of the therapies currently available. Human serum albumin (HSA), the most abundant human blood protein, offers natural biocompatibility and biodegradability and is capable of conjugating drugs, metallic nanoparticles, and other organic and inorganic substances via covalent and non-covalent attachment of its many functional groups [2, 3, 4, 5]. This research work focused on encapsulating solid gold nanoparticles, hollow gold nanoshells and gold nanorods into human serum albumin nanoparticles (HSAPs), as well as four other chemotherapeutics: paclitaxel, camptothecin, and 7-butyl-10-aminocamptothecin (BACPT) to show that the combination and size optimization of these hybrid particles can serve as platforms for preparing new drug therapies. Despite the clinical success of drug loaded HSAPs, there is a current lack of multi-functional HSAP hybrids that offer combinational therapies. This particle template allows for potential simultaneous inclusion of anti-cancer drugs, biomarkers, or other imaging/photodynamic molecules, along with photothermally active gold nanomaterials. The strategy also allows for subsequent external surface functionalizing to improve control of HSAP behavior in the body.

The combined approach will permit killing of cancer cells by both hyperthermal treatment and localized chemotherapy treatment. The combination of treatments is more likely to eliminate all cancer cells. The simplicity in the HSAP synthesis and entrapment of the gold materials, and the effectiveness of maintaining the HSA's stability and ability to bind internal and external molecules, provide a better approach in the field of photothermal therapies using nanoparticles. This novel approach will provide significant contributions in the fields of nano-scale drug delivery and photothermal/photodynamic therapy. Since our findings could be

2

utilized to further site-specific, targeted anti-cancer therapy approaches, it can potentially boost effectiveness and reduce damage to healthy tissue.

1.3 Human Serum Albumin Nanoparticles

Human serum albumin (HSA) is a heart-shaped, globular protein made up of 585 amino acid residues with only one central, fluorescent tryptophan.[3] HSA offers natural biocompatibility and biodegradability, as well as the capability to be surface functionalized due to its high content of charged amino acids.[2, 5, 6] Molecular HSA has a blood concentration of 7×10^{-4} M and a total mass of approximately 120 g, making up 50% of the protein present in plasma.[3, 4, 7] Each HSA molecule makes about 15,000 passes through the circulatory system during its 28-36 day lifespan; picking up and unloading numerous endogenous and exogenous compounds. This vital protein is able to make its way into the central nervous system and even across the blood-brain barrier.[3, 4, 7]

HSAPs have been utilized in promising controlled release studies due to enhanced permeability and retention effects (EPR), where molecules or particles of certain sizes accumulate at tumor sites upon stimulation of the production of blood vessels during rapid, irregular growth.[8, 9] This effect is especially true for molecules greater than 40 kDa, which are more readily trapped. Malignant tumors induce and increase angiogenesis and consequently, hypervascularization. Rapid blood vessel growth in tumors causes an irregular structure with pore sizes of 200-600 nm, thus allowing particles of ~200 nm to easily be taken into the tumor site.[9, 10] Once particles enter the tumor, there is not sufficient lymphatic drainage to remove them; thus longer retention of carrier systems such as liposomes and albumin particles is accomplished. [10, 11, 12, 13] Because of the natural tendency for blood accumulation at tumor sites,

a prominent blood protein like HSA is a strong candidate for this type of EPR substantiated cancer treatment vehicle.

The primary protein structure of molecular HSA allows for conjugating drugs, metallic nanoparticles and other organic and inorganic substances via covalent attachment of its functional groups, such as amine and carboxylic acid groups.[2] The creation of HSAPs as a colloidal drug carrier system multiplies this ability and allows for transport of toxic or low solubility drugs with high loading efficiency (better than liposomes), good storage competence, and minor leakage.[11,14]

Chemotherapeutic drugs have severe symptoms associated with them including drug resistance and myelosuppression, where bone marrow activity is decreased, resulting in fewer red blood cells, white blood cells, and platelets; so a contained transport method that delivers drug only to the site of disease is desired.[15, 16] HSA's natural biocompatibility makes it capable of conjugating drugs and hiding them, thus changing their pharmacokinetic profiles for stealth drug delivery.[3, 17] HSAPs have already been proven as safe medical transporters by the clinical formulations of Albunex[TM], an echocardiographic contrast agent made of sonicated, air-filled HSA microspheres and Abraxane[TM], paclitaxel filled HSAPs for the treatment of lung, ovarian, breast, head, and neck cancer. [11, 15]

1.3.1 Synthesis of HSAPs

Desolvation is a simple, thermodynamically driven self-assembly process for polymeric materials by the addition of a desolvating, or denaturing, agent which coacervates the polypeptide molecules in the aqueous phase, thus facilitating electrostatic and hydrophobic interactions.[14, 18] Because of this dependence on the attractive and repulsive forces, the pH of the

HSA aqueous solution prior to the addition of ethanol plays a pivotal role in the ultimate size of the formed particles, and the later influences cancer extracellular matrix interactions.[14,19]

Glutaraldehyde is used as a cross-linking reagent to covalently bond two amine groups. The glutaraldehyde is needed to strengthen the HSA acervates into place after denaturation and aggregation. The HSA amines of the 59 lysine residues and 23 arginine moieties in guanidino side chains are crosslinked by a condensation reaction with the aldehyde groups of glutaraldehyde.[20] It has been calculated that the lowest required amount of glutaraldehyde needed to quantitatively crosslink all 59 ε-amino groups present in 100 mg of HSA is approximately 4.7×10^{-5} moles of glutaraldehyde (58.8 μL of 8% by volume glutaraldehyde in H_2O).[20]

1.5 Photothermal Therapy and Cell Hyperthermia

Plasmonic photothermal therapy (PPTT) is the phenomena whereby a metal's surface electrons interact with a frequency of light that matches the resonant frequency of the electrons. Oscillations of the surface electrons, called plasmons, move in harmony with the wave resulting in absorption.[21] Through a photothermal conversion, the absorbed light is transferred to heat energy. The therapeutic capability occurs if the wavelength of the radiation is in the biologically safe water window (700-900 nm); with near infrared light being able to penetrate tissue *in vivo* at a tumor site up to 10 cm below the skin, without affecting surrounding healthy cells. [21, 22, 23] This particular phenomenon of heating gold nanomaterials has previously been successfully proven safe for *in vivo* applications. [21, 24, 25]

Moderate cell hyperthermia occurs at 43˚C and can cause increases in endocytosis and blood flow, resulting in not only an increase in uptake of drugs, but a break down intracellular structure [26]. Increasing the induced temperature to over 46˚C will cause severe hyperthermia and

eventual cell death through heat ablation. [27] This type of induced heat therapy shows immediate

anticancer effects, however the full benefits are hindered due to the distribution of energy within

the beam and the gradual reduction of heat in the tissues farther from the AuNR. [28] Therefore,

developing a hybrid mechanism which would also carry a proven chemotherapeutic drug along

with the AuNRs, with relatively long-lasting effects, was in order.

1.6 Gold Nanoparticles, Nanoshells and Nanorods

There has also been an emergence of new synthesis routes to manipulate gold into

nanomaterials of various shapes and sizes for therapeutics and other applications. [29, 30, 31, 32] Gold

nanorods (AuNRs), nanoparticles (AuNPs), and nanoshells (AuNSs) have the ability to absorb

and/or elastically scatter light, depending on the gold's shape and size. The scattering ability

makes them remarkable contrast imaging agents *in vivo* and the absorption of photons with

matching frequencies causes the subsequent release of energy via heat, which can be harnessed

for use in plasmonic photothermal therapy. [33, 34, 35, 36] Nano-sized gold's unique absorption

properties are due to surface plasmon resonance, with the resonant frequency varying with the

shape, size, and environment of the gold particle. [21]

AuNPs are inert with bio-conjugation ability, especially with thiolated molecules,

fluorophores and blood proteins like HSA. Since these particles are usually small (2-80 nm), they

are perfect for endocytosis (25-80 nm caveolae mediated uptake and up to 100 nm clatherin

mediated uptake). When the particles are encapsulated within a larger matrix, like an HSAP,

phagocytosis is a more common uptake mechanism. [31, 37, 38, 39, 40]

In particular, AuNRs absorption maxima can span a wide range of wavelengths due to the

fact that the particles have two distinct plasmon bands created by the transverse (short) axis and

the longitudinal (long) axis. Longer rods usually yield larger plasmon frequencies. [32] Also,

unlike spherical gold nanoparticles which are more likely to quench fluorescence via fluorescence resonance energy transfer (FRET), AuNRs can enhance quantum yields of fluorescent molecules at certain distances.[30] This could be very useful for imaging if a fluorophore is maximally loaded into the HSAP shell surrounding the gold nanorod.

PEGylated gold nanorods have shown to be the least toxic type of gold nanoparticle both *in vitro* and *in vivo* and have ideal photothermally active traits. However, one study found that they have a down side: they are rapidly excreted from the body and usually have a half-life of approximately 1 hour. [41] Therefore, for *in vivo* efficiency, the composite particle size range of 100-500 nm is still ideal.[42] During the rapid development of new, irregular blood vessels, normal vascular structures are impeded, thus resulting in openings in the capillaries from 200 to 2000 nm, which allow larger particles in. [43] From there, lymphatic drainage of interstitial fluids in the tumor site is abnormal; causing smaller particles to freely move back into circulation, while larger particles are maintained in the tumor. [44] Therefore, it would be beneficial to encapsulate rod-shaped gold particles into spherical HSAPs to increase overall size and loading capabilities. The majority of this work focuses on the encapsulation of gold nanorods into HSAPs.

1.7 CPT and BACPT

Natural products are successful sources of antineoplastic agents, accounting for greater than 60% of the anticancer pharmaceuticals in use. [45] Camptothecin (CPT), an alkaloid isolated from Camptotheca acuminata (the "happy tree" in China) was first isolated and reported in 1966.[46, 47] Camptothecin is greatly used on primary and metastatic colon carcinoma, platinum-refractory ovarian cancer, and small cell lung carcinoma. It acts by poisoning the DNA target enzyme topoisomerase I (top I) during its catalytic cycle of DNA relaxation, leading to the

generation of DNA double-strand breaks and cell death by apoptosis.[46,48,49,50] The problem associated with camptothecin is that it possesses extremely low aqueous solubility; consequently it failed in initial clinical trials conducted in the 1970s.

To reduce side effects and enhance potency, water soluble analogues of camptothecins, namely topotecan (TPT) and irinotecan (CPT-11), were created and are increasingly in clinical use for colorectal, ovarian and lung cancers. Despite their success, major side effects are caused by the water-solubilizing functionalities, such as severe to life-threatening diarrhea and myelosuppression (where bone marrow activity is decreased, resulting in fewer red blood cells, white blood cells, and platelets).[,15,16, 51] Because of this, these camptothecin derivatives are dose-limiting. [52]

Other methods have been explored to keep the camptothecins in their most effective state such as: encapsulating them within dendrimers (large, branched molecules), delivering them in conjunction with surfactants and linking them to large water-soluble polymers (e.g., PEGylation).[52,53] In most cases, there are still side effects and reduced anticancer efficacy. Hiding the highly effective CPT (or BACPT) in a biocompatible protein shield will accomplish the task of maximizing efficiency while minimizing harmful effects.

BACPT, 7-butyl-10-aminocamptothecin, was developed in an effort to improve potency and cross-resistance profiles in connection with the stability of the cleavage complex created when bound to the over expressed top I and DNA.[54] BACPT is promising because it has been found that substitutions at the C-10 position on the molecule can increase lipophilicity, while substitutions at the C-7 position enhances potency *in vitro*. BACPT is of particular interest because it exhibits increased activity at the acidic extracellular pH environment, which is common to many solid tumors.[54,55] Large metastatic solid tumors usually have hypoxic

8

environments, which promote expression of stress response genes, tumor angiogenesis and drug resistance. [55,56,57] The cancer cell's increased pHi (internal pH) causes cancer to spread by avoiding apoptosis, metabolic adaptation and directed cell migration. The decreased pHe (extracellular pH) limits buffering, changes the extracellular matrix and enables tumor cell invasion. [19] Drug pK_a has the ability to affect many biological processes: solubility, dissolution rate, reaction kinetics, formulation, cell permeability, tissue distribution, renal elimination, metabolism, protein binding and receptor interactions.[58]

1.8 Paclitaxel

Paclitaxel (PAC) is also a natural chemotherapeutic, isolated from the bark of the western yew tree. PAC has been established as having major effectiveness in the treatment of metastatic breast cancer, however it is also dose limited because it has low water solubility and can cause neurotoxicity and myelosuppression, amongst other complications. [59, 60, 61] The mechanism of PAC toxicity involves disruption of the microtubule system and blocking of cells in the late G2 and M phases of the cell cycle. [62]

PAC has poorly water solubility and a broad tissue distribution profile, so it is normally delivered in Cremophor EL (a derivative of castor oil), ethanol and saline; a formulation which also carries toxicity. [62] With the FDA approval of Abraxane®, an HSAP with paclitaxel inside, the paclitaxel can be used at the most antitumor efficient doses without introducing further toxicity to the patient. [60, 63] Our hybrid particles seek to draw on the success of Abraxane with the addition of other treatment functionalities.

1.8 Renal Cell Carcinoma

Renal cell carcinoma was as one of the most common malignancies in Europe and the U.S. as of 2008 and continues to make the list of most common cancers throughout the world. [1, 64] There is a worldwide annual increase in incidence of about 2%, with an estimated 63,000 new cases predicted for the United States alone. [1, 64] The incidence of renal cell carcinoma (RCC) is usually asymptomatic and is mostly diagnosed during imaging examinations which are usually being performed for unrelated reasons. [65]

Surgery, where the diseased portion of the kidney is removed, has traditionally been the only curative therapeutic approach for renal cell carcinoma, with a focus on nephron-sparing techniques, if possible. [64] Deterioration in health, tumor size, age and tumor location do not always allow for the best surgical outcome. Therefore, other treatment approaches have been developed to allow for minimum invasiveness. Treatment alternatives for RCC include percutaneous radiofrequency ablation (RFA), cryoablation, microwave ablation, laser ablation, and high intensity focused ultrasound ablation. [64] Potential advantages of these techniques include increased quality of life, the ability to treat high-risk surgical candidates and reduced complications caused by surgery. [64] Repeat ablation is necessary more frequently following RFA and local progression rates for cryotherapy and RFA are poorer than rates for surgical procedures. [64] However, if a treatment option possessed both the ability to ablate the RCC with more heating control and also contained a mechanism for temporal, controlled release of a proven RCC anticancer drug, such as sorafenib, the hybrid treatment could potentially eliminate the need for repeated ablation and allow for the non-surgical treatment of tumors larger than ~3 cm.

Overall, the dual chemotherapeutic and heating therapies supplied by the hybrid nanoparticles described within this research are customizable and allow for: future drug combinations, controllable heating for direct ablation and increased induced drug uptake and contrasting and targeting amalgamations not previously seen in current clinical applications.

Chapter 2

Encapsulating Gold Nanomaterials into Size-Controlled Human Serum Albumin Nanoparticles for Cancer Therapy Platforms

2.1 Abstract

Progress has been made in using human serum albumin nanoparticles (HSAPs) as promising colloidal carrier systems for the early detection and targeted treatment of cancer and other diseases. Despite this success, there is a current lack of multi-functional HSAP hybrids that offer combinational therapies. The size of the HSAPs has crucial importance on drug loading and *in vivo* performance and has previously been controlled via manipulation of pH and crosslinking parameters. Gold nanomaterials have also gained attention for medicinal use due to their ability to absorb near-infrared light, thus offering photothermal capabilities. In this study, the desolvation and crosslinking approach was employed to encapsulate gold nanorods, nanoparticles, and nanoshells into HSAPs. Incorporation of gold nanomaterials caused some changes in HSAP sizes, but the general size trends remained. This encasement strategy facilitated size-controlled HSAPs, in the range of 100-300 nm, loaded with gold nanostructures; providing composite particles which incorporate photothermally active components.

2.2 Introduction

Some previous studies have focused on binding very small gold nanoparticles with HSA molecules, surface functionalizing a protein corona monolayer (dynamic surface layer) of HSA onto gold nanomaterials, and self-assembly of gold into AuNPs using HSA as the driving medium. [29, 37, 66, 67, 68]   In the body a corona layer of proteins form on a nanoparticle surface when they are in contact with human biological proteins. These layers determine interactions with living systems and are responsible for cellular responses to the nanoparticles. Coronas are composed of an inner layer (hard corona) and outer layer (soft corona).[69]   The inner layer is selected proteins with a lifetime of several hours.[70] These manifest a slow exchange with the environment around them. The outer layer consists of weakly bound proteins and has a faster exchange with the environment.[66,71] More biological impact comes from hard corona and their specificity and orientation for a receptor than from the soft corona, which are replaced quickly.[66, 72] Some studies on particles designed for intravenous use show there can be a suppressed immune responses because of these interactions.[73]   There has also been a variety of work on surface modifying drug-loaded HSAPs with other molecules such as biomarkers, fluorophores, and antibodies; however, the creation of an optimally-sized gold-HSAP functional hybrid is lacking. [8, 74, 75]

This research focuses on encapsulating the nano-sized gold described above into a shell of HSAP big enough to bind and hold an extremely high, maximum payload of drug, while succumbing to the enhanced permeability and retention effects that will cause it to be trapped in a cancerous matrix. Also, the HSAPs should not induce such a detrimental corona response by biological proteins because it is seen by the body as commonplace as opposed to other capping agents that are put onto gold nanoparticles. Capping agents, such as CTAB

(cetyltrimethylammonium bromide), are becoming increasingly prevalent in nanoparticle synthesis and are primarily used to stabilize the highly reactive nanoparticle surfaces to aggregation and dissolution.[76] Encapsulating otherwise unmodified gold nanomaterials in albumin will alleviate problems associated with the toxicity of capping ligands.

The novelty of this research is in successfully combining two proven treatment approaches: photothermally active gold nanomaterials with HSAP transporters of controllable size. This research supplies promising template hybrids that could prove useful for future simultaneous, custom drug-loading and photothermal therapy. We have created Au-HSAP hybrid composites with overall diameters of 125-300 nm as a proof of concept model that has a conceivable future as flexible, multimodal platforms for the detection and selective treatment of cancer and other diseases. [32, 77, 78, 79]

2.3 Experimental Methods

2.3.1 Materials and Reagents

Human serum albumin, lyophilized powder $\geq$ 97%, potassium bromide, and 8% aqueous glutaraldehyde were obtained from Sigma Aldrich (St. Louis, MO). Ethanol, 200-proof, ACS/USP grade was obtained from Pharmco-AAPER (CT, USA). Two types of spherical gold nanoparticles were prepared at the University of California, Santa Cruz: Approximately 28 nm diameter solid (still slightly porous) gold nanoparticles (2.4×10^{12} AuNPs/mL in water) and ~53 nm outer diameter hollow gold nanoshells with ~4 nm thick shells (7.9×10^{10} AuNSs/mL in water). Both the AuNPs and AuNSs were created with a polyvinylpyrrolidone (PVP) coating that was used to drive the formation during the galvanic replacement of cobalt nanoparticles by Au^{3+} ions [80]. Phosphate buffer (pH 7.2) was obtained from VWR International (Radnor, PA). Water was distilled, deionized, and then further purified with a Barnstead Nanopure system.

Bare gold nanorods (10 nm average axial diameter, 43 nm average length, surface plasmon resonance ~ 808-829 nm, OD = 1, 5.9×10^{11} AuNR/mL in water) were obtained from Nanopartz, Inc. (Loveland, CO). The AuNRs used were advertised by the vendor as "bare", but they did contain trace amounts of cetyltrimethylammonium bromide. To prepare a solution of 1.2×10^{13} AuNR/mL, 2 mL of the original stock solution (5.9×10^{11} AuNR/mL) was centrifuged at 13,000 RPM (16,060 g) for 1 hour until a pellet resulted. The pellet was dispersed in ~ 0.1 mL of water. The process was the same for creating a AuNR solution of 1.77×10^{13} AuNRs/mL from 3 mL of the original 5.9×10^{11} AuNR/mL gold solution.

2.3.2   Synthesis of HSAPs and Au-HSAPs

The HSAPs were prepared using a conventional desolvation technique. [6, 81, 82, 83] The standard method for preparation included the addition of 20 mg of solid HSA to 1 mL of water. After dissolving, the pH was around 7. Any manipulation of pH was completed at this point by addition of 0.1 M NaOH (aq.). A small stir bar was added to the solution, and 3 mL of 100% ethanol was added at a rate of 1 mL/min using a peristaltic pump. Upon addition of the ethanol, the solution became turbid. Finally, 4.7 µL of 8% glutaraldehyde (aq.) was added to crosslink the HSA within the particles. After 24 h of stirring, the particles were centrifuged at 13,000 rpm (16,060 g) for 30 minutes to 1 hour. The supernatant was removed and the remaining pellet was resuspended and washed twice with water. The particles were stored at 4 °C. In order to encapsulate gold nano-materials into the HSAPs, various amounts of gold nanomaterials were added to the aqueous albumin solution prior to addition of ethanol.

The synthesis was also done in a scaled-down manner whereby the mass of HSA, volume of water, volume of ethanol, and amount of glutaraldehyde used were all reduced by

one-fourth to create smaller batches of HSAPs. Parameters used for preparing HSAPs with and

without gold are provided in Table 2.1.

Table 2.1. **Preparation Parameters used to create HSAPs with and without gold nanomaterials.**

Sample	HSA (mg)	Water (mL)	pH	EtOH (mL)	Aq. gold nanomaterial solution (mL)	Theoretical Gold:HSA particle number ratio[a]	Glutaraldehyde (μL of 8% aqueous solution)
HSAP-1	20	1	7	3	None	0	4.7
HSAP-2	20	1	8	3	None	0	4.7
HSAP-3	20	1	9	3	None	0	4.7
HSAP-4	20	1	7	3	None	0	9.4
HSAP-5	20	1	9	3	None	0	9.4
HSAP-6	5	0.25	7	0.75	None	0	9.4 (2% glutaraldehyde)
AuNR-HSAP-1	5	0	7	3	1.0 AuNR[b]	1:1.5	2.4
AuNR-HSAP-2	6	0	7	1.5	0.5 AuNR[b]	1:3.7	2.4
AuNR-HSAP-3	2	0	7	5	2 AuNR[b]	3.2:1	2.4
AuNR-HSAP-4	2	0	7	1.5	0.1 AuNR[c]	3.2:1	2.4
AuNR-HSAP-5	5	0	7	3	0.1 AuNR[d]	1.9:1	2.4
AuNP-HSAP-1	5	0.25	7	1.5	0.25 AuNP[e]	1:1.5	2.4
AuNP-HSAP-2	5	0.25	7	2.25	0.5 AuNP[e]	1.3:1	4.8
AuNP-HSAP-3	2.5	0.125	7	3	0.75 AuNP[e]	3.9:1	2.4
AuNP-HSAP-4	2	0.1	7	3	0.9 AuNP[e]	5.9:1	2.4 (2% glutaraldehyde)
AuNP-HSAP-5	0.5	0.025	7	3	0.95 AuNP[e]	25:1	2.4
AuNP-HSAP-6	5	0	7	3	1.0 AuNP[e]	2.6:1	2.4
AuNS-HSAP-1	5	0.25	7	1.5	0.25 AuNS[f]	1:46	2.4
AuNS-HSAP-2	5	0.25	7	3.75	1.0 AuNS[f]	1:12	4.8
AuNS-HSAP-3	2.5	0.125	7	3	0.75 AuNS[f]	1:7.7	2.4
AuNS-HSAP-4	2	0.1	7	3	0.9 AuNS[f]	1:5.1	2.4 (2% glutaraldehyde)
AuNS-HSAP-5	0.5	0.025	7	3	0.95 AuNS[f]	1:1.2	2.4

[a]Based on all HSA forming 200 nm diameter spherical particles with d = 1.3 g/cm^3; [b]5.9 × 10^{11} AuNR/mL; [c]1.18 × 10^{13} AuNR/mL; [d]1.77 × 10^{13} AuNR/mL; [e]2.4 × 10^{12} AuNP/mL; [f]7.9 × 10^{10} AuNS/mL

2.3.3   Density Separation

A potassium bromide solution was prepared by mixing ~75 g KBr with water (total solution volume was 100 mL) and stirring at 100°C for 4 hours. The density was calculated to be ~1.45 g/cm^3. AuNR-HSAPs were prepared via their respective parameters (Table 2.1) and centrifuged at 13,000 rpm for 1 hour to create a pellet. After removing the aqueous supernatant, 1 mL of the KBr solution was added to the pellet and the sample was homogenized by sonication for 10 seconds. The particles resuspended in the aqueous KBr were then centrifuged at 13,000 rpm for 30 minutes to one hour. The supernatant (containing any particles with a density of ~1.45 g/cm^{3}or less) was removed from the red precipitate. Particles in the supernatant were washed several times by centrifugation with pure water. The remaining red pellet from the KBr centrifugation was also washed several times with water.

2.3.4   Absorbance

Absorbance measurements of the HSAPs and AuNS/NP/NR-HSAPs were performed with a Cary 60 absorbance spectrometer (Agilent Technologies).

2.3.5   Dynamic Light Scattering

The completed HSAPs were characterized by measuring the diameter and zeta potential using a Mobius dynamic light scattering (DLS) instrument (Wyatt Technology Corporation, Santa Barbara, CA). Samples were diluted with water prior to analysis.

2.3.6 SEM and TEM

Particles were imaged using a field emission-scanning electron microscope FESEM, LEO 1530VP (LEO Elektronenmikroskopie GmbH, Oberkochen, Germany). HSAPs were sputtered with a thin film of gold or silver to facilitate imaging. Transmission electron microscope (TEM) images were acquired with a JEOL Model 2010 TEM or with cryo-TEM using an FEI G2 F30

Tecnai TEM (FEI, Hillsboro, OR) with a Gatan-626 cryo-specimen holder and cryotransfer system (Gatan, Warrendale, PA).

2.4   Results and Discussion

2.4.1 HSAP Formation

Desolvation is a simple, thermodynamically driven self-assembly process for polymeric materials by the addition of a denaturing agent, which coacervates the polypeptide molecules in the aqueous phase, thus facilitating electrostatic and hydrophobic interactions. [14,18] Because of this dependence on the attractive and repulsive forces, the pH of the HSA aqueous solution, as well as the amount of cross-linker added, play pivotal roles in the ultimate size of the formed particles. Particle size also influences interactions of the particles with the cancer extracellular matrix. [14,19] Experiments were done to confirm preparation parameters, which have been previously well documented, that would yield 150-300 nm diameter unloaded HSAPs and to compare the preparation-based sizing trends to size outcomes of the gold-loaded HSAPs. Figure 2.1 shows an FESEM image of HSAPs with no gold or drug loaded inside.
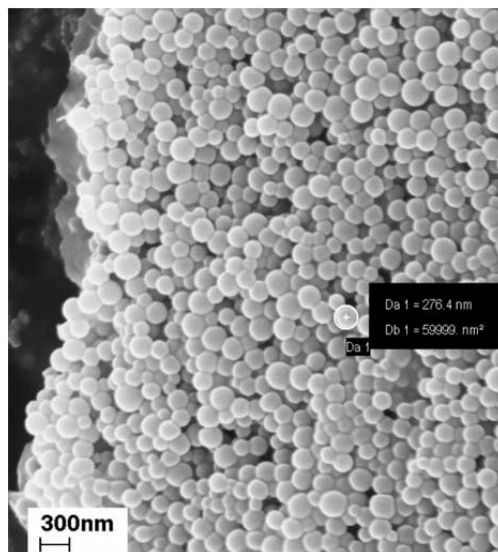
Figure 2.1. FESEM image of 200-300 nm diameter HSA particles.

19

Experiments were done to find a starting pH that would yield 150-300 nm diameter HSAPs by adjusting the pH from ~6.8 – 10. Because the isoelectric point (pI) of HSA is ~4.7 to 5.4, it is not fruitful to try to form particles under pH 6. HSA has a zero net charge at these pH values, which causes unwanted, excessive aggregation of the particles and erratic size outcomes.

Table 2.2. Averaged DLS data for HSAPs

Sample	Initial pH	Theoretical % Crosslinked	Diameter (nm)	Polydispersity (%)	ζ (mV)
HSAP-1	7	40	248 ± 66	14	-14
HSAP-2	8	40	151 ± 23	8	-27
HSAP-3	9	40	140 ± 29	21	-28

Error represents one standard deviation with N ≥ 3. All reported diameters were statistically different at 95% confidence.

Consistent with other literature reports, as the pH of the starting solution of HSA/water is increased, final HSAP size decreases, as seen in Table 2.2 and Figure 2.2. Note that Figure 2.2 takes into consideration only those samples created with 20 mg HSA (see Table 2.1). The size decrease from ~248 ± 66 nm (at pH 7) to ~151± 23 nm (at pH 8) to ~140 ± 29 nm (at pH 9) is likely due to an increase in net charge of the HSA molecules, which leads to the repulsion of HSA molecules and less aggregate formation. [20, 81, 83]

At higher pH levels, the HSA became more negatively charged due to greater dissociation of protons at high pH, so smaller HSAPs were formed. The electrophoretic mobility (μE), the migration velocity per unit electric field) and the zeta potential (ζ, the electrokinetic potential of a molecule on its outer layer, slipping plane or diffuse layer), give insight into the charge and stability of the HSAPs as a colloid.[84] The larger the zeta potential value is (either positive or negative), the more stable the colloidal system. As a rule of thumb, HSAPs are generally very stable as colloids at ζ > +25 mV or ζ < -25 mV, therefore it seems that the HSAP-2 (pH8) and HSAP-3 (pH9) particles with zeta potentials of -27mV and -28mV,

respectively, are more stable that the HSAP-1 (pH7) particles that have a zeta potential of -14.[84]

This desolvation process has the potential to theoretically make trillions of particles based on the average size of the particles created and the amount of milligrams of HSA used in the batch. For example (assuming the density of the HSAP remains that of molecular HSA at 1.31 g/cm^3 and the average particle size created is 200 nm): taking into consideration the volume of the sphere, the mass per HSAP would be 5.48×10^{-12} mg. If 20 mg of HSA powder was used (and all of it goes into making HSAPs), then 3.65×10^{12} HSAPs would be produced. It should be taken into consideration however, that when any preparation parameter is changed, such as starting pH, crosslinking level or mg HSA used, the number of particles created will be affected due to the change in size outcome. Also, a gold particle is present inside of an HSAP, it takes up space and volume, leaving HSA that would normally fill that space free to make even more HSAPs. Therefore, it is possible that when gold is present, even more HSAPs are created.
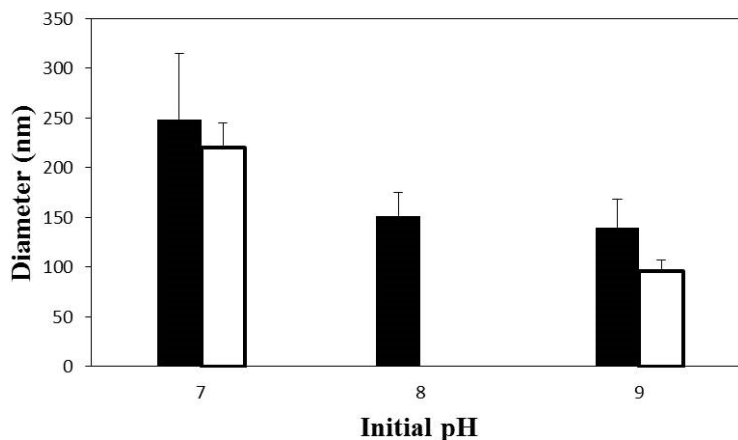
Figure 2.2. Effect of initial pH on HSAP size with 20 mg HSA and 40% theoretical crosslinking (black bars) and 80% theoretical crosslinking (white bars). Data are from HSAP-1, HSAP-2, HSAP-3, HSAP-4, and HSAP-5. Error bars represent one standard deviation with N $\geq$ 3.

After ethanol is used to denature HSA, resulting in the formation of spherical HSAPs, glutaraldehyde is used as a cross-linking reagent to covalently crosslink the HSA acervates into place after aggregation. The amine groups of the 59 lysine residues, and the 23 arginine moieties in guanidino side chains on the HSA, are crosslinked by a condensation reaction with the aldehyde groups of glutaraldehyde. [20] It has been calculated that the lowest required amount of glutaraldehyde needed to quantitatively crosslink all 59 ε-amino groups present in 100 mg of HSA is approximately 58.8 µL of 8% (V/V) glutaraldehyde in H_2O. [20] All theoretical crosslinking calculations were based on this previous work and it has been customary for groups working with this desolvation and crosslinking process to use percentage values to indicate crosslinking; even though it is essentially impossible to crosslink over 100% of the amino groups present on the HSA. [20, 85] Tables 2.2-2.5 list crosslinking percentages over 100%. This means that glutaraldehyde was added in excess as compared to the necessary theoretical amount to link all HSA amines to each other with a molecular glutaraldehyde linker.

Previous studies have found that an increase in the glutaraldehyde crosslinker used leads to more stable HSAPs [11, 13]. That increase in stability leads to particles that are not as easily digested or broken apart. Even though there is no difference in cellular uptake with a change in crosslinking, a high degree of crosslinking is not ideal for easy release of the therapeutic elements inside.[11, 13] We have found that there was a decrease in average diameter from 140 ± 29 nm to 96 ± 11 nm for particles created at pH 9 when the mole ratio of glutaraldehyde:HSA was doubled from ~12.7 to 25.4 (hallow bars in Figure 2.2). The zeta potential showed increases from -14, -27 and -28 mV (for HSAP-1, HSAP-2, and HSAP-3, respectively) to -35 and -30 mV (for HSAP-4 and HSAP-5, respectively) when the amount of crosslinking agent was increased.

2.4.2   HSAP Formation: Reagent HSA Effects

The above mentioned preparation effects on size trends are well documented, however there was one interesting experimental outcome that had not previously been found in the literature: the effects of the starting mass of HSA on the size outcome. In an effort to minimize consumption of starting materials, the amount of each reagent was cut by one-fourth: 5 mg of HSA was dissolved into 0.25 mL of water and 0.75 mL of ethanol was delivered, followed by 2.36 µL of 8% aqueous glutaraldehyde (1.9×10^{-6} moles). It was noticed that decreasing the amount of reagents used caused a change in HSAP size and zeta potential. Despite preservation of mole ratios, there was an unexpected decrease in observed HSAP size with smaller batches (compare HSAP-6 to HSAP-4 in Table 2.2). At 80% theoretical crosslinking, the average diameter of HSAPs created at pH 7 in the original 20 mg HSA batch was 220 ± 25 nm, but the average diameter of the same type of particles created in a 5 mg batch was 135 ± 3 nm.

Since the starting mass of HSA had an effect on the size of the resulting nanoparticles, careful attention must be paid to parameters during scale-up for manufacturing purposes or even for preclinical and/or clinical research[85]. This size effect may be due to changes in the number of nucleation sites.

Table 2.3. Particle size and zeta potential data for AuNR-HSAPs.

Sample	Theoretical % Crosslinked	Diameter (nm)	Zeta Potential (mV)
AuNR-HSAP-1	80	222 ± 5^a	-20
AuNR-HSAP-2	80	262 ± 20	-13
AuNR-HSAP-3	200	190 ± 1	-19
AuNR-HSAP-4	200	119 ± 4	-91
AuNR-HSAP-5	80	152 ± 20	-23

[a]Error represents one standard deviation with $N \geq 3$. All reported diameters were statistically different at 95% confidence.

2.4.3   Formation of Composite Au-HSA Particles

The aim of this project was to create Au-HSA composite particles for potential future use in photothermal therapy. We utilized three separate types of gold nanomaterials: rods, spheres and shells. Empty HSAPs created with 5 mg of HSA in 0.25 mL of H_2O with addition of 0.75 mL of EtOH and crosslinked with 9.4 μL of 2% glutaraldehyde yielded samples with a size of 135 ± 3 nm, therefore it was assumed that the AuNS-HSAPs and AuNP-HSAPs created under similar desolvation parameters would yield roughly the same particle size. That hypothesis proved correct. The protocol followed that of forming unloaded HSAPs (Section 2.4.1) however, Au nanomaterials were dispersed in aqueous albumin solutions prior to coacervation of the albumin. Because gold is readily coordinated by amines and other functional groups in the albumin, we expected the albumin to coat the surface of the gold prior to coacervation, resulting in the gold particles acting as nuclei for coacervation. We utilized several approaches to prove that the Au and HSA particles were in fact associated.

The ratio of gold particles to albumin particles was calculated for each preparation (see Table 2.1). For example, using the AuNR-HSAP-1 preparation method, if all 5 mg of HSA formed spherical particles with an average size of 200 nm, then the process was capable of creating 9.13×10^{11} HSAPs (assuming the HSAPs have a density equal to that of molecular HSA, 1.31 g/cm^3). Adding 1 mL of AuNR solution to the HSA would yield a AuNR:HSAP ratio of ~ 1:1.5. This means ~ 66% of the particles would be loaded with a gold nanorod if encapsulation were perfect.

Extensive analysis of multiple Au-HSAP samples by TEM and cryo-TEM revealed only Au-HSAP and unloaded HSAP particles; free gold particles were observed only in rare cases. (Representative figures for AuNR-HSAPs, AuNP-HSAPs and AuNS-HSAPs are shown later in this chapter.) In every case where both Au and HSA particles were co-located, the Au was fully within the outer boundary of the HSA particle; completely encapsulated into the HSA.

It is worth noting that the sample preparation is different for cryo-TEM and conventional TEM imaging. In the case of cryo-TEM, the samples are freeze dried; thus the cryo-TEM samples avoided the agglomeration that was apparent for the conventional TEM observations. In addition, heating from the intense electron beam in the conventional TEM likely cause some melding (aggregation) of the Au-HSAPs, since the proteins are highly affected by the heat. Such issues were avoided in cryo-TEM by cooling the sample during imaging.

2.4.4   Formation of Composite AuNR-HSA Particles

AuNR-HSAPs were formed using the preparation parameters in Table 2.1. In order to confirm that the AuNRs and HSA were actually encapsulated, we performed a centrifugal separation using a 1.45 g/cm^3 liquid medium (concentrated aqueous KBr). This separation resulted in two types of red materials: 1) material that precipitated (d > 1.45 g/cm^3) and 2)

material that remain suspended ($d < 1.45$ g/cm^3). The red color of these materials was due to gold. Unloaded HSAPs are white or faint yellow in color, but never red. Free gold, with a density of 19.3 g/cm^3, would have precipitated completely in this system. The suspended red material contained gold and had a density of less than 1.45 g/cm^3. The only explanation for this result is that the gold was encapsulated into an albumin particle with low density, so that the average density of the composite particle was less than 1.45 g/cm^3. For a 200 nm diameter spherical HSAP with a single 10 nm diameter × 43 nm long gold nanorod, the density would be ~1.32 g/cm^3. These composites would therefore remain suspended in the KBr solution upon centrifugation.

   We visualized the supernatant and the red precipitate from this centrifugal separation using TEM. Images of what was found in the supernatant are presented later in Figures 2.7a thru e. Although some unloaded-HSAPs were observed by TEM in the supernatant, numerous particles with nanomaterials inside them were observed. These observations are consistent with the conclusion that the gold was loaded into albumin particles. The precipitate consisted of aggregated HSAPs with multiple gold nanoparticles loaded inside of them (see Figures 2.3 a. and b.).
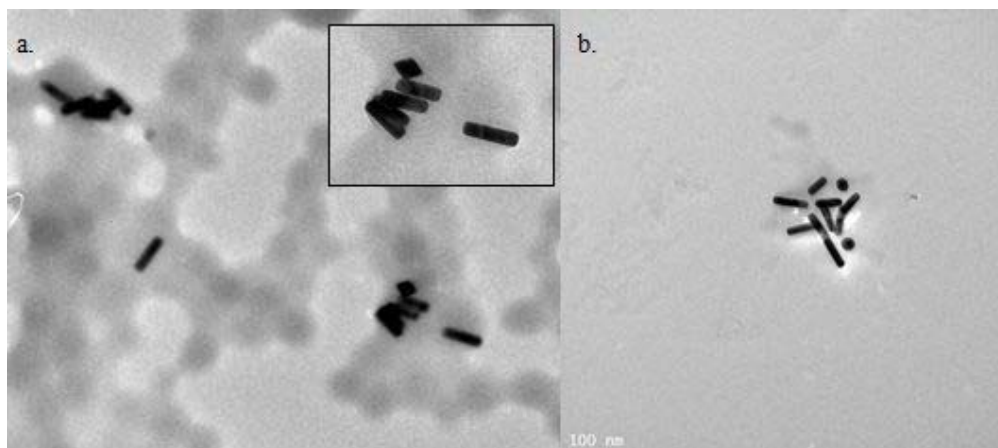
Figure 2.3. TEM images of AuNR precipitate layer after density separation for (a) AuNR-HSAP-1 (Inset: the image is further magnified) and (b) AuNR-HSAP-5.

Because of the high gold loading, these particles had a large density and were precipitated in the centrifugation. No free gold nanoparticles were observed in the precipitate, suggesting that gold particles served as nuclei for albumin coacervation. This conclusion is reasonable since free albumin is known to bind strongly to gold.[71] Further evidence that the gold was encapsulated in the albumin was provided by absorbance measurements. We collected the absorbance spectrum of the supernatant from the centrifugal separation and compared this spectrum to that of free AuNRs in aqueous solution. The spectra are presented in Figure 2.4.
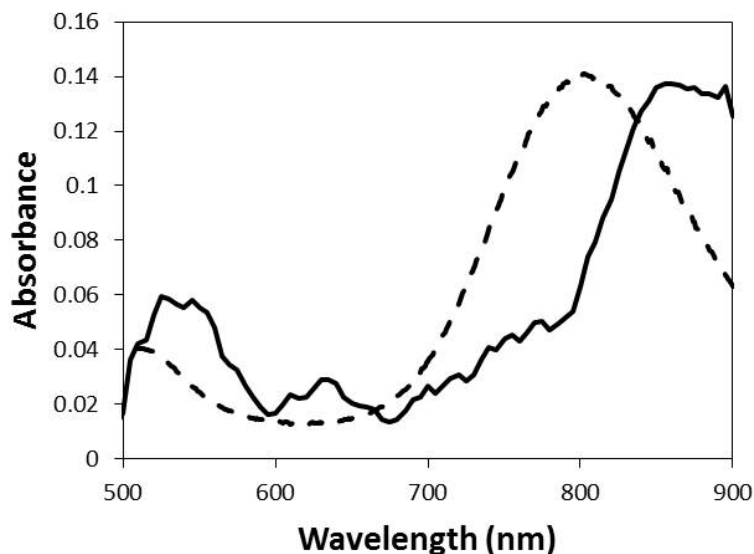
Figure 2.4. Absorbance of AuNR-HSAP-3 loaded particles (solid line) and a stock solution of free AuNRs with a concentration of 8.31 × 1010 AuNRs/mL (dashed line).

The AuNR-HSAP spectrum was background subtracted to eliminate absorbance and scattering signals from the HSAP, and considerable noise is present. Nevertheless, signals for both the transverse and longitudinal Au localized surface plasmon resonances (LSPR) are clearly visible near 540 and 850 nm. These peaks are shifted considerably from the peaks for free AuNR (520 nm for transverse axis LSPR and 800 for longitudinal LSPR). Such shifts are expected when the surface of the gold has strong interactions with other materials. [30, 66] Because of the large shifts in the LSPR and the high likelihood of concurrent changes in absorptivity, we did not perform quantitative measurements by absorbance to determine the amount of gold trapped in these particles.

A final test to prove association of the gold with the HSAPs involved measurement of particle size and zeta potential. We compared these parameters for free AuNRs, AuNR-HSAPs (as collected from the KBr supernatant) and unloaded HSAPs. The observed hydrodynamic diameters for these samples were 57 ± 7 nm, 219 ± 13 nm, and 220 ± 25 nm, respectively. The

AuNR-HSAP showed a particle size distribution similar to that of unloaded HSAP, and the

AuNR-HSAP sample had no evidence of particles with diameters corresponding to free AuNR

(see Figure 2.5).
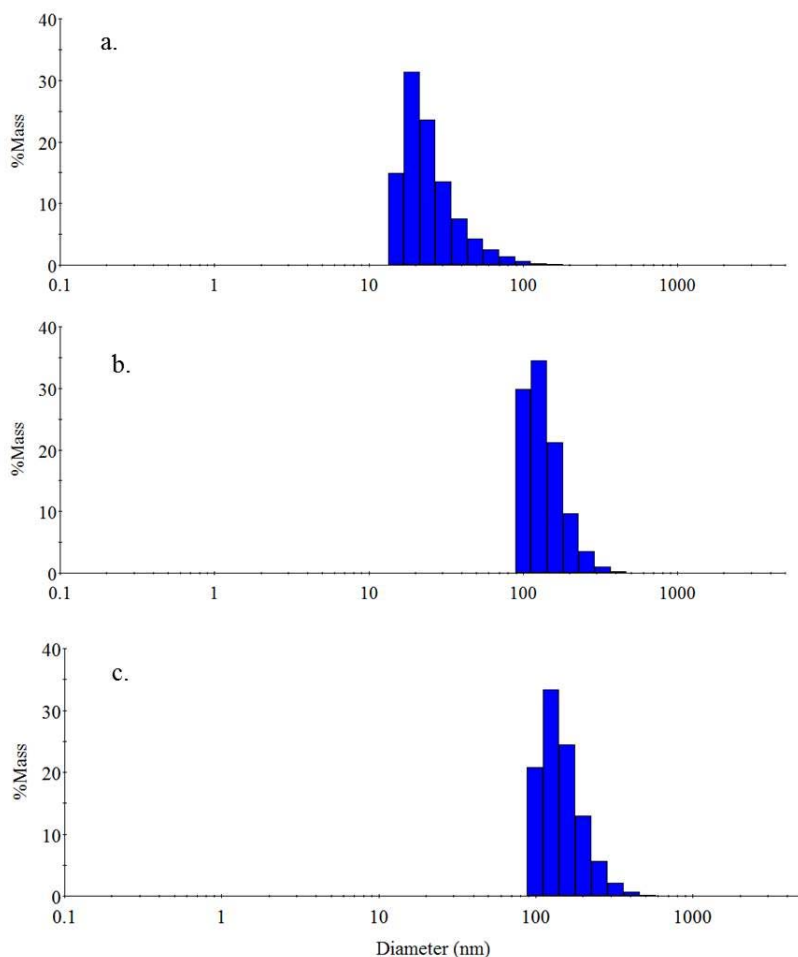
Figure 2.5. Particle size distributions for (a) free AuNRs, (b) gold-loaded HSAPs created via the AuNR-HSAP-1 method, and (c) unloaded HSAPs.

Consequently, the light scattering measurements support the conclusion that the gold in the

AuNR-HSAP sample was not free. The measured zeta potential of the free AuNRs, AuNR-

HSAPs and the unloaded HSAPs were -4.0 ± 1, -30 ± 8 and -35 mV, respectively. The gold

loaded albumin particles and unloaded albumin particles had zeta potential values that were

indistinguishable and much greater than free gold particles, suggesting that the gold particles were encapsulated in the albumin.
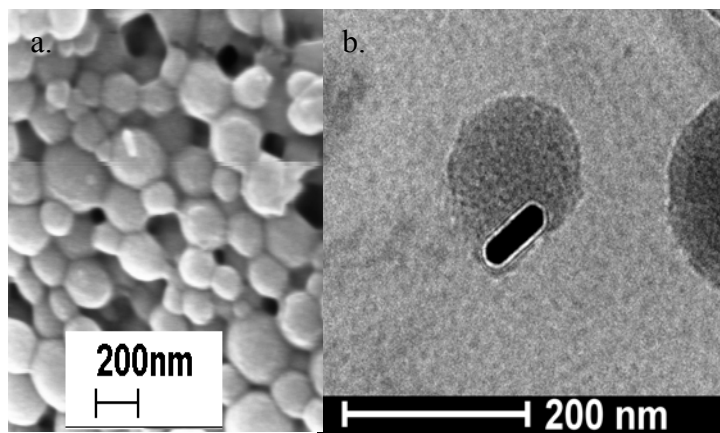
Figure 2.6. : a) FESEM image of AuNR-HSANP-1 with a gold rod visible at the surface (see arrow). Tips of other rods may also be visible (light regions on particles) and b) TEM image of AuNR-HSANP-2 particles with a gold rod visibly surrounded by a layer of albumin

Taken together with the TEM images and the absorbance data presented above, the particle size and zeta potential data further confirm that the gold was associated with albumin particles and was not present as free nanorods. Additional inspection of an FESEM image in Figure 2.6a reveals a rod apparently positioned on its axial side, protruding down into the HSAP. Evidence of HSAP particle deformation is visible in Figure 2.6b in which the HSAP shape conforms to the outline of the AuNR at the edge of the albumin particle. There is also evidence of multiple rods being loaded into one HSAP (Figure 2.8a thru e); some with nanorods apparently both parallel and perpendicular to the plane of view (Figure 2.8d and 2.8e). With a limited amount of gold nanoparticles, loading multiple gold particles into each albumin particle further decreases the chance of each albumin particle being loaded with a gold particle.
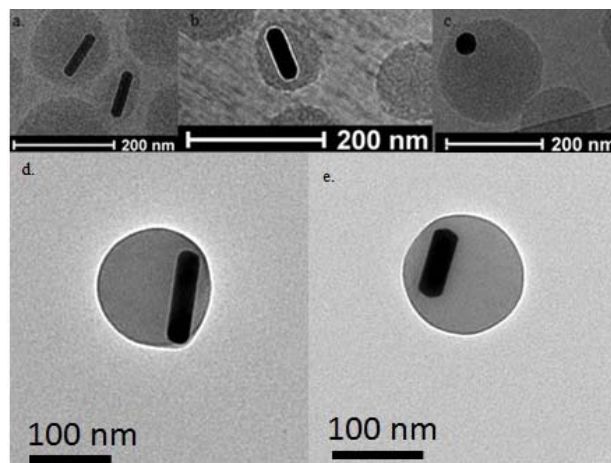
Figure 2.7. Cryo-TEM images of singly loaded AuNR-HSAPs from (a) AuNR-HSAP-1; (b and c) AuNR-HSAP-2 and (d and e) conventional TEM images of AuNR-HSAP-3.
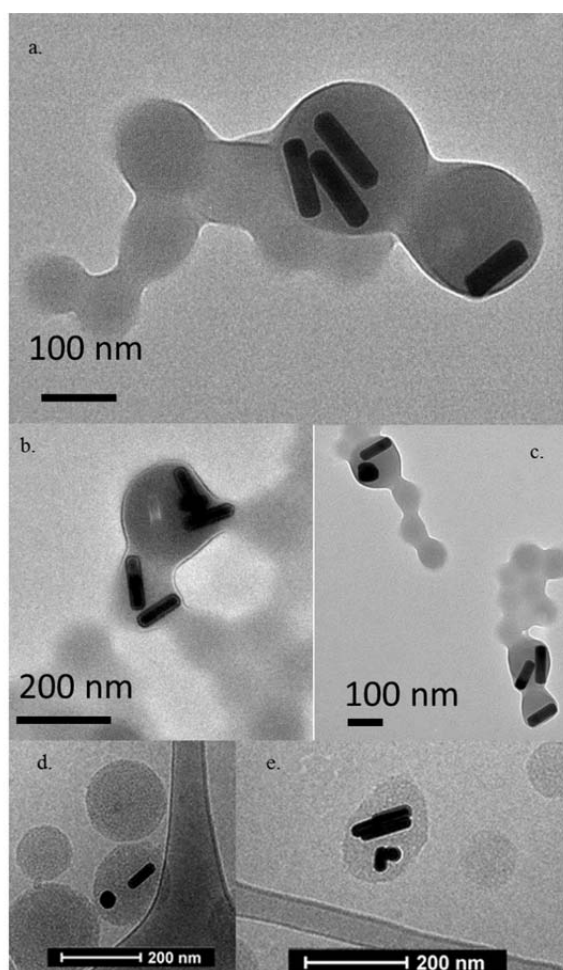
Figure 2.8. (a, b and c) Conventional TEM images of AuNR-HSAP-3; (d) cryo-TEM image of AuNR-HSAP-1 (e) and cryo-TEM image of AuNR-HSAP-2. All images show particles with multiple gold rods trapped within the HSAP.

Table 2.3 presents the particle size and zeta potential data for the AuNR-HSAPs. The observed diameters were between 119 ± 4 and 262 ± 20 nm and varied depending on the preparation parameters. As the amount of HSA decreased, the particle size decreased as well. The zeta potentials for these particles were all negative, but were slightly smaller than desired to maintain a stable colloid without aggregation. To combat this, further ultrasonication is needed to break up particle aggregation after the heavy centrifugation technique used in the density separation.

It is evident that the loading ratio of AuNRs:HSAPs determined through theoretical calculations (Table 2.1) were not represented in the ultimate formed particles. This discrepancy is partially due to the fact that HSAPs are capable of loading multiple rods, which was unexpected and opportune. In addition, loading a nanorod into an HSAP takes up a volume of space and therefore, decreases the amount of molecular HSA in that particle, freeing it for the formation of additional HSAPs. Third, the calculations were based on an average HSAP size of 200 nm, however when the average particle size decreases, many more HSAPs are formed.

The lack of gold in some of the particles did not seem to affect other characteristics of the particles, as the morphology remained spherical (aside from any slight changes to the albumin shape to accommodate encapsulated gold particles). The sizes remained within the expected range, and the zeta potentials remained negative, indicating stability. The presence of the gold did not increase aggregation of the particles. As proven via the density gradient study, free AuNRs could not be found. Every AuNR found using microscopy was in some way associated with an HSA coating, therefore the efficiency of gold incorporation can be said to be close to

100%. However, the distribution was not completely uniform. Some AuNR-HSAPs were formed with six rods encapsulated, while some HSAPs formed with no rods encapsulated.

The AuNR-HSAP-3 preparation method (containing 2 mg HSA and 2 mL AUNR stock solution) was the most successful method in this trial, yielding the greatest extent of albumin particles loaded with gold (see Figure 2.9). This result illustrates that adjusting the formation parameters can control the gold loading and particle size. However, additional work is needed to further optimize the particle characteristics.
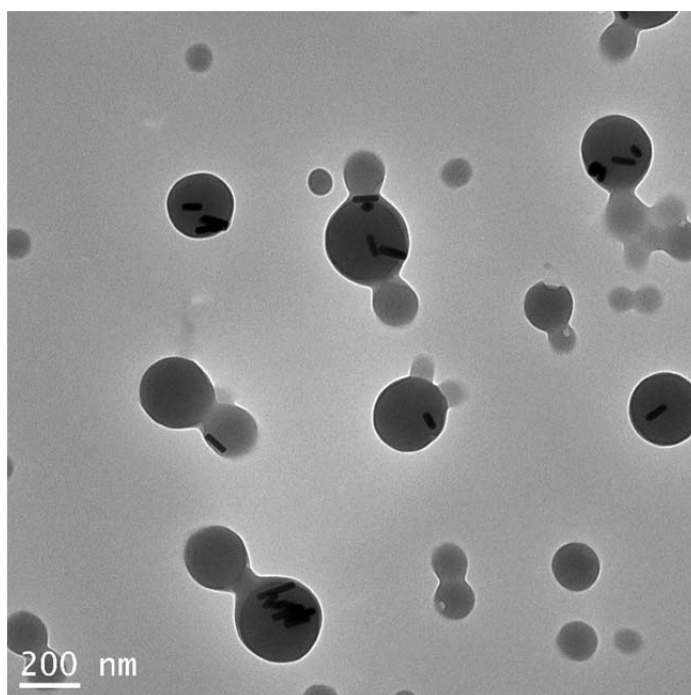
Figure 2.9. TEM image of particles created via the AuNR-HSAP-1 method with increased loading of AuNRs; illustrating the non-uniformity of loading. There is some melding of particles present due to the heating from the electron beam.

2.4.5 AuNS-HSAPs and AuNP-HSAPs Formation

Unloaded, HSAPs created with 5 mg of HSA in 0.25 mL of H_2O with addition of 0.75 mL of EtOH and crosslinked with 9.4 µL of 2% glutaraldehyde (aq.) yielded samples with a size of 135 ± 3 nm. Particle size measurements for composite particles revealed an average diameter of 156

± 15 nm for AuNS-HSAP-1 and 195 ± 9 nm for AuNP-HSAP-1. These particles remained under

200 nm in average diameter, an effective size range for use as a treatment vehicle. Tables 2.4 and

2.5 show the size and zeta potential information for the AuNS and AuNP loaded HSAPs,

respectively. These particles are slightly smaller compared to an average of 245 ± 66 nm for

unloaded HSAPs.

Table 2.4. Particle size and zeta potential data for AuNS-HSAPs.

Sample	Theoretical % Crosslinked	Diameter (nm)	Zeta Potential (mV)
AuNS-HSAP-1	80	156 ± 15^a	-26
AuNS-HSAP-2	160	102 ±1	-20
AuNS-HSAP-3	40	109 ± 4	-17
AuNS-HSAP-4	50	54 ± 2*	-26
AuNS-HSAP-5	800	51 ± 1*	-18.5

[a]Error represent one standard deviation with $N \geq 3$. All reported diameters were statistically different at 95% confidence except those noted by *.

Table 2.5. Particle size and zeta potential data for AuNP-HSAPs.

Sample	Theoretical % Crosslinked	Diameter (nm)	Zeta Potential (mV)
AuNP-HSAP-1	80	195 ± 9	-25
AuNP-HSAP-2	160	109 ± 1	-35
AuNP-HSAP-3	40	122 ± 1	-16
AuNP-HSAP-4	50	86 ± 1	-27
AuNP-HSAP-5	800	67 ± 1	-17

[a]Error represents one standard deviation with $N \geq 3$. All reported diameters were statistically different at 95% confidence.

Figure 2.10a presents a cryo-TEM image of hybrid particles from AuNS-HSAP-2, clearly

illustrating that the gold particles were encapsulated with albumin particles. There is also

evidence of individual AuNS-HSAPs incorporating more than one gold nanoshell. Figure 2.10b

presents a cryo-TEM image of AuNP-HSAP-1, where some albumin particles do not have gold inside. The ratio of AuNP to HSAP in this batch was approximately 1:1.5, indicating that the AuNP were present as a limiting reagent. Consequently, it is not surprising that we observed numerous unloaded HSAPs (not depicted) and no evidence of free AuNPs.
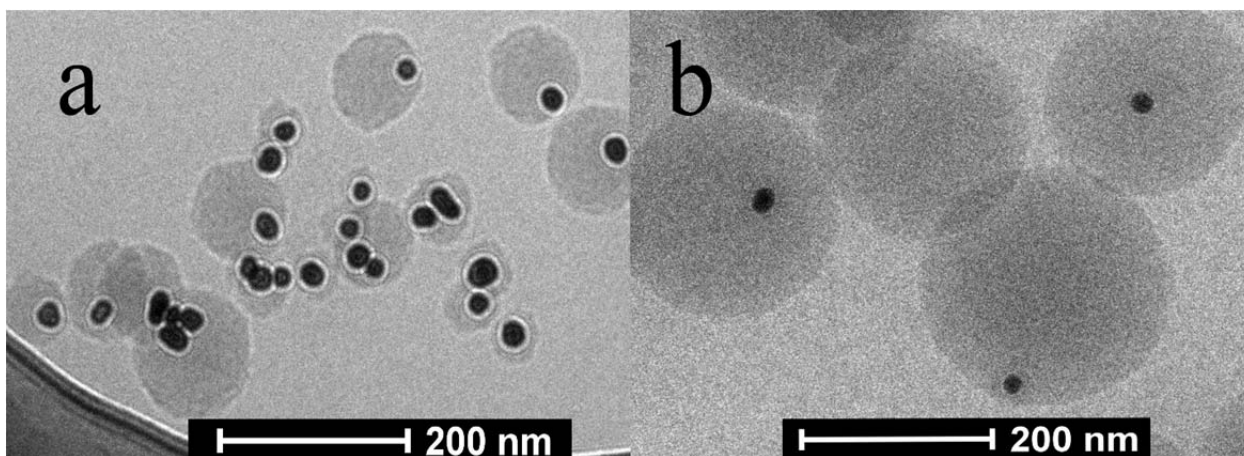
Figure 2.10. Cryo-TEM images of (a) AuNS-HSAP-2 and (b) AuNP-HSAP-1.

Figure 2.6: Cryo-TEM images of (a) AuNS-HSAP-2 and (b) AuNP-HSAP-1.

As seen in Tables 2.4 and 2.5, the average particle size and zeta potential observed for the various AuNP-HSAP and AuNS-HSAP preparations followed similar trends, suggesting that the preparation parameters can be generalized to the incorporation of any type of gold nanoparticle. For both AuNS-HSAPs and AuNP-HSAPs, increasing the extent of crosslinking resulted in smaller particles. This result is consistent with that of unloaded HSAPs, as previously discussed. For both AuNS and AuNP loading in Figures 2.10a and 2.10b, it is believed that insufficient gold particles were present to achieve complete loading of the albumin particles (due to the freeing of HSA when a gold particle takes up volume), and no evidence of free AuNPs or AuNSs was observed after extensive TEM observation.

For the purpose of creating a particle with high drug payload capacity and large ligand binding capabilities, the particle size distribution of AuNP-HSAP-5 (Figure 2.11) samples should

still prove sufficient, as it still had substantial HSAP volume around the gold and high surface area per gram due to the smaller particle size. The solid gold particles were roughly 10-30 nm, and the resulting AuNP-HSAPs were on average 67 ± 1 nm; that is a diameter increase of ~55 to 85%, which verifies the albumin coating as substantially more than a monolayer of HSA surrounding the gold. Thin HSA coatings (less than 15 nm thick) on gold nanoparticles have previously been reported as corona layers. [29, 37, 67, 68] However, those particles would not have the same drug loading capacity as those produced in this study due to the thicker coating of HSA achieved here.
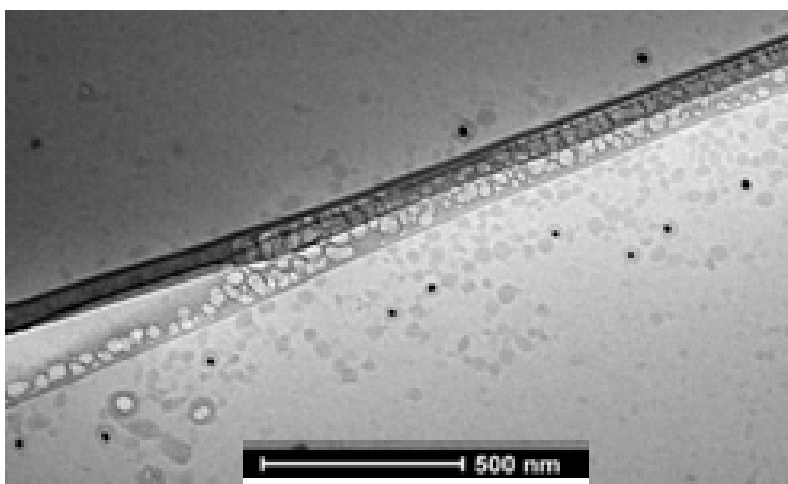
Figure 2.11. TEM image of AuNP-HSAP-5 particles created with less HSA.

2.5 Conclusions

In this study, composite AuNP-HSAPs, AuNS-HSAPs, and AuNR-HSAPs were successfully prepared as a proof of concept to show that these composite particles can serve as platforms for preparing new drug therapies. This research has shown that size-controlled encasement of these gold nanomaterials into larger (100-300 nm) HSAPs is possible via a desolvation and crosslinking process. Moreover, the same preparation parameter manipulations that allow for

36

controllable particle size of medicinally useful HSAPs are in operation when the procedure is conducted with gold nanomaterials present. One new development regarding the preparation process for making unloaded HSAPs is that the starting mass of HSA plays a role is the size outcome. Since the ultimate goal is effective treatment of cancer cells via targeted drug delivery and photothermal therapy, simultaneously loading of HSAPs with both gold nanomaterials and an appropriate drug is a future direction for these studies. The combined approach will allow killing of cancer cells by both hyperthermia and localized chemotherapy treatment and is more likely to eliminate all cancer cells.

In addition, the photothermal approach may serve as a trigger for drug release once the particles have reached their targeted tissue. Functionalizing the surface of the HSAPs with disease-specific targeting ligands may lead to even more effective delivery of cancer therapies to the site of the disease, boosting effectiveness and reducing damage to healthy tissue. [86] The optimal number of gold nanoparticles loaded into each HSAP to achieve effective hyperthermic treatment is not yet known, but is the subject of ongoing studies, as is improving the control of AuNP loading efficiency. Furthermore, the effect of radiative heating of gold nanomaterials in HSAPs on the release of simultaneously encapsulated drugs also needs additional study.

Chapter 3

Hybrid Gold Nanorod-Human Serum Albumin Nanoparticles for Simultaneous Chemotherapeutic and Photothermal Therapy Platforms

3.1 Abstract

Human serum albumin nanoparticles (HSAPs) as drug carrier systems for treatment of cancer have proven successful through current marketable clinical formulations. Despite this success, there is a lack of multi-functional HSAP that offer combinational therapies from more than one proven technique. Gold nanorods (AuNRs) have also shown medicinal promise due to their photothermal therapy capabilities. In this study, the desolvation and crosslinking approach was employed to successfully encapsulate gold nanorods into HSAPs along with incorporation of the chemotherapeutic drug paclitaxel (PAC), forming PAC-AuNR-HSAPs with desirable overall particle sizes of 299 ± 6 nm. The loading efficiency of paclitaxel into PAC-AuNR-HSAPs reached up to 3μg PAC/ mg HSA. The PAC-AuNR-HSAPs experienced photothermal heating, with bulk solution temperatures reaching up to 46 ˚C after 15 minutes of near-IR laser exposure, indicating successful attainment of the temperature necessary to cause severe cellular hyperthermia and necrosis.

This encasement strategy facilitated a colloidal hybrid treatment system capable of enhanced permeability and retention effects, photothermal ablation of cancer cells, and release of the active paclitaxel of up to 188 ng (from PAC-AuNR-HSAPs created with 30 mg HSA) in a single 15 minute irradiation session. The system also lends itself to future customizable external functionalities via conjugated targeting ligands such as antibodies. Internal entrapment of patient

tailored medication combinations are also possible with this combination treatment platform,

which may result in improved quality of life for those undergoing treatment.

3.2 Introduction

There is a current need for multi-functional, temporally active cancer treatments which maximize therapeutic effects through less invasive techniques. A hybridization of effective treatments can offer combinational therapy, which may result in higher success rates and increased quality of life for patients suffering with the disease. Gold nanorods (AuNRs) have the ability to absorb relatively harmless near infrared light, causing the subsequent release of energy via heat, which can be harnessed for use in plasmonic photothermal therapy (PPTT). [22, 34, 35, 86]

Moderate cell hyperthermia occurs at 43˚C and can cause increases in endocytosis and blood flow, resulting in not only an increase in uptake of drugs, but a breakdown in cellular structure.[26] Increasing the induced temperature to over 46˚C will cause severe hyperthermia and eventual cell death through heat ablation.[27] This dose-controllable heat therapy shows immediate anticancer effects; however, the full benefits are hindered due to the distribution of power within the beam and the gradual reduction of heat in the tissues farther from the AuNR.[28] Therefore, developing a hybrid mechanism to also carry a proven chemotherapeutic drug along with the AuNRs, with long-lasting staying power is desirable.

In a previous study, we focused on a proof-of-concept synthesis to fully encapsulate gold nanorods into HSAP spheres to harness their PPTT effects; with the goal of keeping them from being susceptible to clearing the body as fast as smaller, drug-conjugated AuNRs prepared by other researchers.[41, 87] Human serum albumin (HSA), the most abundant human blood protein, offers biocompatibility, biodegradability, and the ability to conjugate drugs and other organic and inorganic substances via covalent and non-covalent attachment to its many functional groups.[17, 3] When aggregated together via a desolvation and crosslinking technique, HSA forms nanoparticles (HSAPs).

These HSAPs have previously been surface modified for diagnostic and targeting functions and utilized in controlled release studies, due to enhanced permeability and retention effects (EPR); where particles of certain sizes accumulate at tumor sites.[5, 8, 9] Our previous approach allowed for internal binding to the HSA hydrophobic pockets as well as external surface functionalizing of the HSAPs, even with AuNRs present. The HSAPs are largely capable of binding a multitude of biomarkers, fluorophores, antibodies, etc. Because the HSAP are larger than the individual gold particles, the HSAP can bind more materials than bare AuNRs alone .[74, 75, 88, 8]

Paclitaxel (PAC) is a natural chemotherapeutic agent isolated from the bark of the western yew tree. PAC has been established as having major effectiveness in the treatment of metastatic breast cancer; however, it is dose limited because it has low water solubility and can cause neurotoxicity and myelosuppression amongst other complications.[59, 60, 61] Paclitaxel-filled HSAPs have been proven as safe medical transporters as used in the clinical formulation Abraxane[TM]; which has been successful in the treatment of lung, ovarian, breast, head and neck cancer.[63] With the FDA approval of Abraxane®, paclitaxel can be used at the most antitumor efficient doses without introducing further toxicity to the patient.[60]

In 2013, Abraxane was also approved for use in treating pancreatic cancer as a less toxic alternative to folfirinox and it is expected to become the standard of care for pancreatic cancer.[89, 90, 91] The "nab-paclitaxel" particles (nanoparticle albumin-bound) allow for transport of toxic or low solubility drugs with high loading efficiency, good storage competence, and minor leakage.[11, 15,] Our approach utilizes this up-and-coming particle formulation and improves its treatment potential with the option of controlled heating: at lower induced temperatures, drug

uptake is facilitated and at higher induced temperature, complete cancer cell ablation is possible.[92]

The goal of this study was to substantiate the theory that proven anticancer drugs, such as PAC, could also be effectively housed within the AuNR-HSAPs, with efficient loading. Subsequently, adequate PAC release via the PPTT heating of the hybrid particles was also necessary for immediate additive treatment effects. This research supplies evidence that the PAC-AuNR-HSAP hybrid delivery system offers simultaneous drug-release and PPTT as well as extended, controlled further release of the drug over time. The PAC-AuNR-HSAPs have the potential to be irradiated in the biologically safe water window (700-900 nm) *in vivo* at a tumor site up to 10 cm below the skin without affecting surrounding healthy cells. [28, 93]

This work shows drug-Au-HSAP hybrid composites with overall diameters of 299 ± 6 nm, which have a conceivable future as flexible, multimodal platforms for the targeted detection, contrast imaging and selective treatment of cancer and other diseases.[32, 77]

3.3   Experimental Methods

3.3.1 Materials and Reagents

Human serum albumin, lyophilized powder $\geq 97\%$, potassium bromide, Acrodisc® syringe filters with nylon membrane (diam. 13 mm, pore size 0.2 μm), Corning Costar cell culture plates (flat bottom, 12 well), and 8% aqueous glutaraldehyde were obtained from Sigma Aldrich (St. Louis, MO). Ethanol (200-proof, ACS/USP grade) was obtained from Pharmco-AAPER (CT, USA). Water was distilled, deionized, and then further purified with a Barnstead Nanopure system.

Bare gold nanorods (10 nm average axial diameter, 43 nm average length, surface plasmon resonance ~ 808-829 nm, OD = 1, 5.9×10^{11} AuNR/mL in water) were obtained from Nanopartz,

Inc. (Loveland, CO). The AuNRs used were advertised by the vendor as bare, but they did contain trace amounts of cetyltrimethylammonium bromide.

3.3.2 Synthesis of PAC-AuNR-HSAPs and PAC-HSAPs

The PAC-AuNR-HSAPs were prepared using a conventional desolvation technique with the addition of AuNR seeding and drug loading. [20, 81, 83] The standard method for preparation included creating an aqueous HSA stock solution (100 mg/mL). After dissolving, the pH was around 7. To a portion of the HSA stock solution, an aliquot of the AuNR stock solution was added, along with a small stir bar. From a paclitaxel stock solution (1 mg /mL ethanol), an aliquot was added drop-wise to the AuNR/HSA solution flask at a rate of 1 mL/min using a peristaltic pump. Then, additional ethanol was added to achieve a final solution containing 60% ethanol. Upon the addition of the ethanol, the solution became turbid. Finally, an aliquot of 8% glutaraldehyde (aq.) was added to crosslink the PAC-AuNR-HSAPs. After 24 h of stirring, the particles were centrifuged at 13,000 rpm (16,060 g) for 20 minutes. The supernatant was removed, filtered using a 0.2 μm syringe filter and saved for HPLC analysis. The remaining particle pellet was resuspended in a wash solution of 2:3 water:ethanol via ultrasonication. The particles were washed twice using 2:3 water:ethanol and the supernatants were saved for HPLC analysis. The washed particles were stored at 4 °C in water. The PAC-HSAPs were created by the same process as the PAC-AuNR-HSAPs, with an aliquot of pure water substituted for the AuNR stock solution.

3.3.3 HPLC

The HPLC system used to analyze the paclitaxel was an Agilent 1100 instrument (Palo Alto, CA) with a diode array absorbance detector. The column was an Agilent Eclipse XDB-C18 column (150 X 4.6 mm, particle size 5μm). The injection volume was 100 μL, and the wavelength used for quantitation was 227 nm. The solvent mobile phase was 45% acetonitrile and 55% water at a flow rate of 1 mL/min. The elution time for the PAC was approximately 3.8 minutes. Total entrapment of the drug was determined as the total mass of drug added to the particles minus the combined mass of drug in the supernatant and washes.

3.3.4 Dynamic Light Scattering

The HSAPs were characterized by measuring their diameter, mobility, and zeta potential using a Mobius dynamic light scattering (DLS) instrument (Wyatt Technology Corporation, Santa Barbara, CA). Samples were diluted with water prior to analysis.

3.3.5 Laser Irradiation of Particles

The PAC-AuNR-HSAPs and PAC-HSAPs were tested for heating ability and drug release under laser irradiation. To heat the samples, 1 mL of the sample was placed into a well of a 12-well plate. The plate was placed approximately 4 inches under a vertically mounted laser. A LabSpec 808 nm collimated diode laser system was used at a continuous wave power output of 2000 mW for 15 or 30 minutes for each sample. The size of the beam was approximately 1×1 cm. Temperature changes caused by the irradiation sessions were measured using a Spark Science Learning System™ model PS-2008A thermocouple.

After irradiation, the contents of the wells were collected and centrifuged at 13,000 RPM for 15 minutes. The resulting supernatant was collected, diluted with ethanol, filtered, and saved for HPLC analysis.

3.3.6 SEM and TEM

Particles were imaged using a field emission-scanning electron microscope FESEM, LEO 1530VP (LEO Elektronenmikroskopie GmbH, Oberkochen, Germany). HSAPs were sputtered with a thin film of gold or silver to facilitate imaging. Transmission electron microscope (TEM) images were acquired with a JEOL Model 2010 TEM.

3.4   Results and Discussion

3.4.1 Formation of PAC-HSAPs and PAC-AuNR-HSAPs

Desolvation is a simple, thermodynamically driven self-assembly process for polymeric materials by the addition of a denaturing agent, which coacervates the polypeptide molecules in the aqueous phase, thus facilitating electrostatic and hydrophobic interactions.[14] DLS confirmed that the average particle sizes for PAC-HSAPs with no AuNRs inside (using 30 mg HSA) was 158 ± 7 nm and PAC-AuNR-HSAPs were 331 ± 3, 299 ± 6 and 212 ± 28 nm when starting the preparation process with either 20, 30 or 50 mg HSA, respectively (while all other preparation parameters were held constant). When AuNRs were present, the overall average HSAP size increased; likely due to the AuNRs acting as seeds, taking up internal space in the HSAP, thus facilitating more HSA available for continued particle growth.
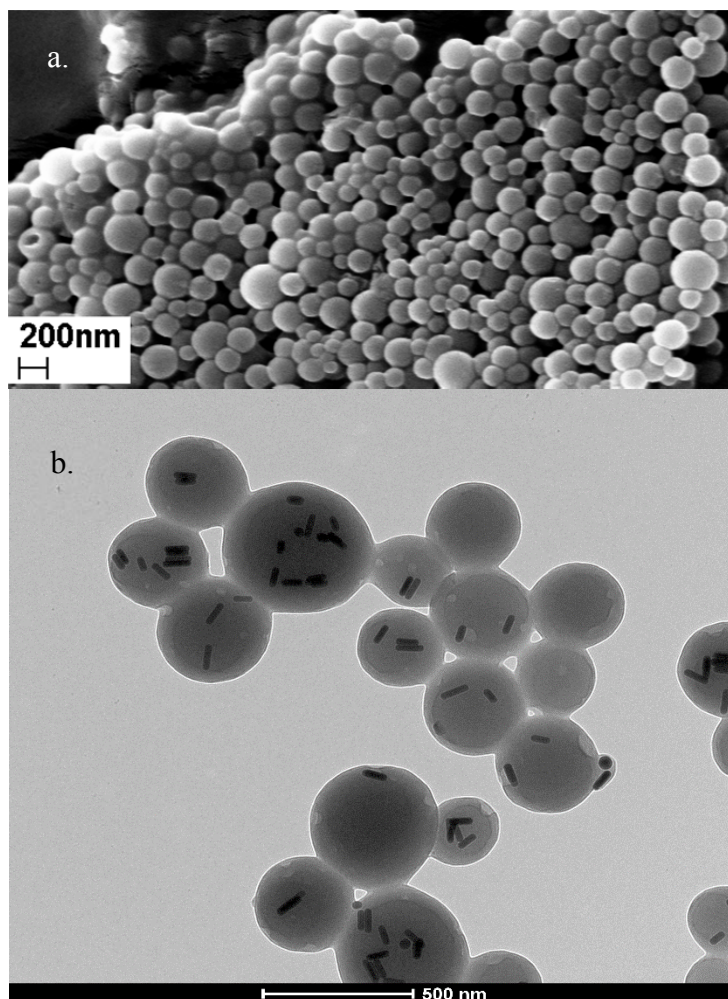
Figure 3.1. AuNR-HSAPs created with 2 mg of HSA and 2 mL of AuNR stock solution visualized via (a) FESEM image and (b) TEM image showing the AuNRs within.

There was also a trend of decreasing AuNR-HSAP size as the amount of protein available was increased from 20 to 30 to 50 mg. This size decrease is likely due to the fact that more HSA present allows for continued new particle formation after all AuNRs have been encapsulated; thus creating a greater number of smaller unloaded-HSAPs and a smaller average particle size. Therefore, the AuNR-HSAPs present are smaller overall, but with more polydispersity.

Figure 3.1 provides representational SEM and TEM images of the AuNR-HSAPs created with only 2 mg of HSA and 2 mL AuNR stock solution. (For imaging purposes, more heavily

AuNR loaded particles with larger sizes are shown here, whereas the same amount of AuNRs

loaded into 20, 30 or 50 mg of HSA would result in a TEM image of largely unloaded-HSAPs

amongst the AuNR-HSAPs.) The PAC-AuNR-HSAPs created with either 20, 30 or 50 mg of

HSA had zeta potential values of ζ = -38 ± 1, -42 ± 3 or -45 ± 3 mV, respectively; showing

highly stable particle formations; since colloids are generally very stable when ζ > +25 mV or ζ

< -25 mV.

Aside from EPR effects mentioned previously, studies have shown that albumin-bound

paclitaxel binds to the gp60 HSA receptor on the cell surface, facilitating transcytosis via the

formation of caveolae; thus causing increased uptake of PAC into diseased cells.[94] Our

formation of bio-friendly particles are not only efficiently sized for EPR effects, but they also

have the potential to mitigate damage to healthy cell membranes caused by toxic CTAB-coated

AuNRs.[95] Since any residual CTAB is hidden by the HSAP shell, the toxicity caused by CTAB

should be reduced.

3.4.2 Loading Efficiency of PAC into HSAPs and AuNR-HSAPs

The aim of this project was to create PAC-AuNR-HSAP composite particles for potential

future use in PPTT. Because gold is readily coordinated by sulfur-containing moieties in the

albumin (resulting in Au-albumin thiol bonds), we, and other researchers, have previously seen

that the albumin coats the surface of the gold.[95, 96] This protein corona layer results in the gold

particles which act as nuclei during coacervation of the AuNR-HSAPs.

To test whether the presence of AuNRs hindered the drug encapsulation ability of the

HSAPs, 0.5 mg of PAC was added to separate particle batches consisting of either 30 mg of

HSA or 30 mg HSA and 1.5 mL AuNRs solution. It was found that the PAC-HSAPs and the

PAC-AuNR-HSAPs entrapped an average of 63.3 ± 14 and 91.8 ± 9 µg of PAC, respectively.

There was a 45% increase in PAC loading when AuNRs were present in the particles. This was a surprising result and it is not fully known what caused this increase in PAC loading when AuNRs were present.

We speculate that the PAC could have adsorbed onto the AuNRs (due to a hydrophobic interaction with the trace CTAB present) prior to and during the formation of the HSA corona layer. Previous research has shown that the ammonium group of one CTAB binds to the surface of the gold and the hydrocarbon chain can interact with another CTAB's hydrocarbon chain. The second CTAB's ammonium group is positively charged and free to bind to HSA. The hydrophobic pocket created in between the two CTAB molecules is free to bind drug. Then, the amphiphilic properties of the HSA packing around the gold may have reinforced the PAC placement. [28]

To find the loading efficiency of the paclitaxel in the PAC-AuNR-HSAPs, the preparation procedure in Section 3.3.2 was followed with two distinct experimental changes: 1) the mass of HSA remained the same and the mass of PAC was varied and 2) the mass of HSA was varied and mg the mass of PAC remained constant. Figure 3.2a shows the results when 30 mg of HSA were prepared with either 0.1, 0.25 or 0.5 mg of PAC and the resulting PAC-AuNR-HSAPs were successfully loaded with 17 ± 2, 39 ± 5 and 92 ± 14 µg of PAC, respectively. The particles created with 0.5 mg PAC contained over 3 µg of drug per mg of HSA in finished particles.
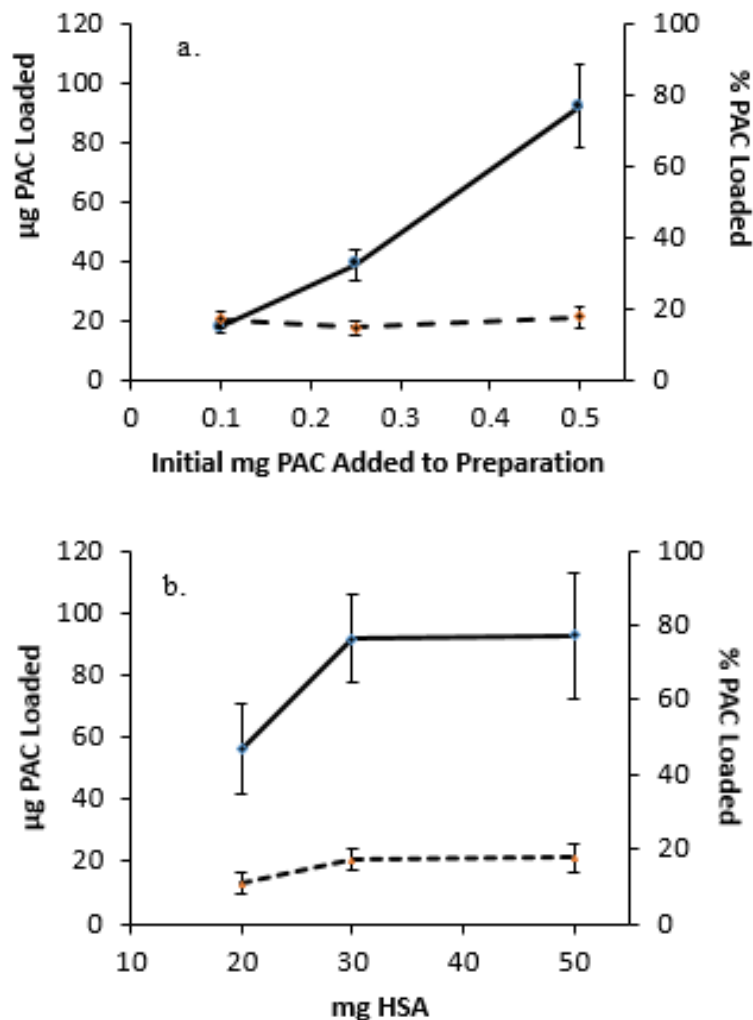
Figure 3.2. (a) 30 mg of HSA was prepared with either 0.1, 0.25 or 0.5 mg of PAC: (solid line) µg of PAC loaded into the PAC-AuNR-HSAPs vs. the mg of PAC initially added to the preparation vial and (dashed line) the percentage of loaded PAC vs. PAC added to the preparation solution. (b) 0.5 mg PAC was added to particle preparation batches containing either 20, 30 or 50 mg HSA (solid line) µg of PAC loaded into the PAC-AuNR-HSAPs vs. the mg of HSA present in the preparation vial and (dashed line) the percentage of loaded PAC vs. PAC added to the preparation solution when HSA is varied.

Since the final particle suspension was in a volume of 1 mL, the resulting concentration of drug in the suspension was 133 µM. This concentration is the amount of drug entrapped within the batch of particles and can potentially be released to the tumor site via PPTT and temporally

49

during dynamic enzymatic activity *in vivo*. That loading concentration far exceeds the *in vitro* cytotoxicity of a paclitaxel-filled lipid emulsion in a previous study, which was shown to have a paclitaxel IC_{50} value of 5.5 μM on HeLa cells.[97] The IC_{50} value is the half maximum inhibitory concentration, which is determined by a dose-response curve, and it indicates the concentration of drug that is required for 50% inhibition of the cancer cells *in vitro*.[98]

Figure 3.2b shows results when 0.5 mg PAC was added to particle preparation batches containing either 20, 30 or 50 mg HSA. The resulting drug loading was 56 ± 14, 92 ± 14 and 93 ± 20 μg PAC, respectively. There was a larger increase in drug loading when increasing mass of HSA in the sample from 20 to 30 mg HSA; followed by a plateu in PAC loading when using 30 or 50 mg HSA. The 30 mg HSA sample was still able to hold the most drug per mg of HSA: 3 μg PAC/mg HSA.

The % PAC loading data shown in Figures 2a and 2b confirm the particles do not entrap more than roughly 17% of the 0.5 mg PAC added to the preparation solution, even when more HSA is available. This result was not fully understood, except for the hypothesis that the crosslinking of these particles might be playing a role in the effective drug entrapment as both the 30 mg and 50 mg particle batches were theoretically crosslinked at 40%.

3.4.3   Effect of Crosslinking on Drug Loading

The amine groups on the HSA are crosslinked by a condensation reaction with the aldehyde groups of glutaraldehyde.[20] It has been calculated that the lowest required amount of glutaraldehyde needed to quantitatively crosslink all 59 ε-amino groups present in 100 mg of HSA is approximately 58.8 μL of 8% (V/V) glutaraldehyde (4.7×10^{-5} moles) in H_2O. [20] All theoretical crosslinking calculations were based on this previous work and it has been customary

for groups working with this desolvation and crosslinking process to use percentage values to indicate the expected degree of crosslinking.[85]
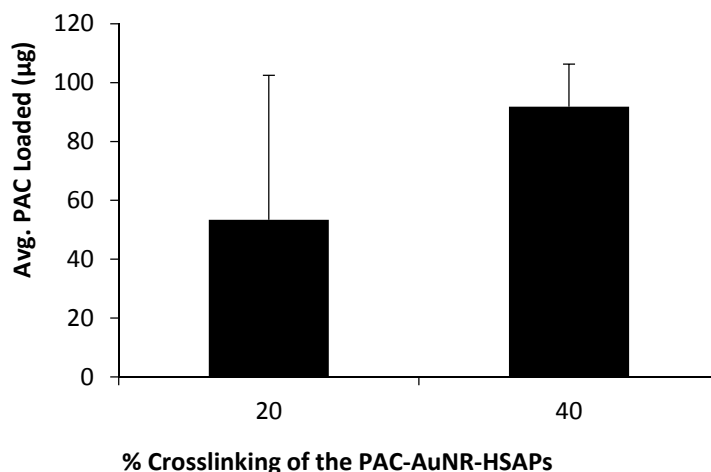
Figure 3.3. Average μg of PAC loaded into PAC-AuNR-HSAPs vs. the % of theoretical crosslinking of the particles. Error bars represent standard deviations of measurements (n > 3).

To test whether the crosslinking played a major role in drug loading, two sample preparations of PAC-AuNR-HSAPs were created with 30 mg HSA and 0.5 mg PAC; one batch was theoretically crosslinked at 20% (2.87×10^{-6} moles glutaraldehyde) and the other at 40% (5.73×10^{-6} moles glutaraldehyde). As shown in Figure 3.3, the 40% crosslinked PAC-AuNR-HSAPs had more drug loading (92 ± 14 μg) with less deviation, while the 20% crosslinked particles had less consistent drug loading (53 ± 49 μg). Although, some batches of the 20% crosslinked particles were capable of loading up to 102 μg of PAC, there was a large error associated with the loading. Therefor crosslinking definitely plays a role in keeping the paclitaxel locked into the particles until it is provoked for release.

3.4.4 PAC-AuNR-HSAP and AuNR-HSAP Heating Capabilities

It has previously been discovered that when AuNR induced PPTT is used to create hyperthermia in human prostate tumor bearing mice, maintaining temperatures of 42-43˚C for 10

minutes showed an increase of macromolecular delivery into the tumor site. [99] In a separate study, when using paclitaxel-conjugated 11-mercaptoundecanoic acid-linked polyethylene glycol coated AuNRs, a combination of the drug and heating to 58°C left absolutely no viable A549 breast cancer cells. [28] Our approach allows for heating via selective temperature ranges, depending on the dosage of the PAC-AuNR-HSAPs delivered and the NIR treatment time.
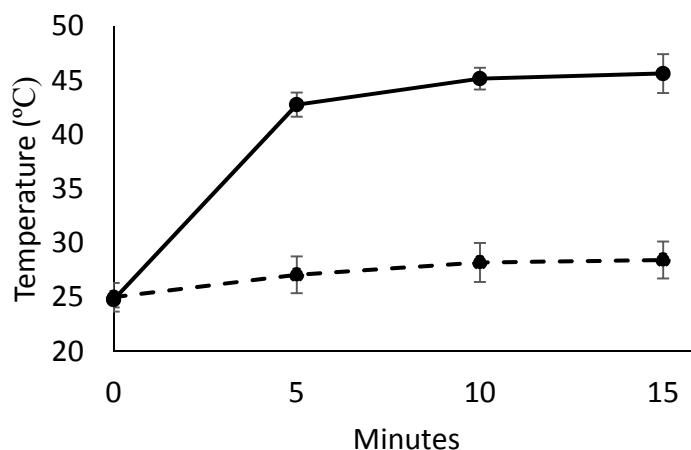
Figure 3.4. Heating trend in °C of (solid line) PAC-AuNR-HSAPs and (dashed line) PAC-HSAPs

A cell well-plate was placed under the vertically mounted laser and particle batches suspended in water and ethanol were placed in the wells. The 808 nm laser was turned on at 2 W of power for up to 15 minutes while a thermocouple, placed on the side of the well, recorded the temperature continuously. The particle solution was then collected via a pipette, centrifuged and the supernatant was saved for drug content analysis. Figure 3.4 shows the heating trend (solid line) for PAC-AuNR-HSAPs created with 30 mg of HSA, 1.5 mL AuNR stock and 0.5 mg of PAC. The particles experience a sharp increase to 43°C in roughly 5 minutes and continue to 46° within 15 minutes.

The dashed line in Figure 3.4 represents the heating ability PAC-HSAPs with no AuNRs inside; it is shown that these particles never reached a temperature over normal body temperature. The graph clearly shows that the AuNRs are necessary to cause substantial heating. Consequently, only cells with HASP-AuNR and exposure to laser radiation would experience hyperthermia.

3.4.5 Drug Release via Photothermal Irradiation

Literature reports state that paclitaxel has cytotoxic activity at concentrations as low as 50 nM, and it was evident that the PAC-AuNR-HSAP delivery system was capable of loading far more paclitaxel than that (up to 133 μM in a 1 mL sample, shown in Section 3.4.2), while still maintaining heating abilities.[100] The PAC-AuNR-HSAPs we created are true hybrids, where the anticancer functions of PPTT aided-uptake, heat ablation, EPR and drug release coexist, so it was important to know the heat-induced drug release. Our method must prove drug release of at least the minimum cytotoxic dose via PPTT and temporal release in order to be a viable treatment vehicle

In this study, the PAC-AuNR-HSAPs initially created with 0.1, 0.25 or 0.5 mg PAC (created with 30 mg HSA and crosslinked 40%) were irradiated with 808 nm NIR light for 15 minutes to monitor PAC release. These particles contained on average 56.1 ± 14, 91.8 ± 14 and 92.7 ± 20 μg PAC and after only 15 minutes, they released 189 ± 108, 111 ± 33 and 124 ± 70 ng, respectively. In each case, a slight burst of release less than 1% of the loaded PAC was shown. Although a small percentage, the induced release would be considered an effective dose, with the lowest average concentration of 145 nM released into the 1 mL of irradiated solution. This is actually a desirable outcome, as a quick complete release of the drug payload can result in lower antitumor efficacy due to the subsequently quick drug clearance from the body.[60] The ideal

antitumor treatment would be to harness the initial shock of the heat ablation and paclitaxel dose in a localized area, followed by the slower, continued release of the drug penetrating further into the tumor site via the leaky vasculature and heightened metabolism of the site.

It is also worth noting that the particles which were created with different crosslinking percentages showed differences in drug release as well. The PAC-AuNR-HSAPs created with 20% theoretical crosslinking released over 4% of the entrapped drug; an average of 932 ng PAC released vs. 124 ng (less than 1%) released by the 40% crosslinked particles. As found with the loading, there is a large statistical error for the drug release associated with the lesser crosslinked particles: 932 ± 646 ng. The amount of drug that remains in the less tightly locked particles has a better chance of being released.

Conversely, greater crosslinking allows for increased loading and the opportunity for prolonged release as well as decreased chances of drug release in areas other than the tumor site. These release results were compared to two control scenarios, where release was tested on irradiated PAC-HSAPs containing drug, but no AuNRs and on PAC-AuNR-HSAPs which were not irradiated. In both cases, the drug in the measured particle supernatant was below the detection limit of 0.00001 mg PAC/ mL using HPLC analysis.

3.4.6 Temporal Drug Release

Finally, to show that the paclitaxel was indeed released continually from the PAC-AuNR-HSAPs after the initial irradiation period, three separate batches of PAC-AuNR-HSAPs samples (batches A, B and C) were created (each with 0.5 mg PAC and 40% crosslinking preparation parameters) and irradiated for 15 minutes. For each batch, the sample suspensions were centrifuged and the supernatants were removed for initial, laser provoked drug release

analysis. Just as in Section 3.4.5, the initial burst of drug release for each sample batch was below 1% of the total loaded drug.

The particle batches were then stored at 4 ºC for a certain amount of time: batch A was stored for 7 days, batch B for 14 days and batch C for 21 days in order to monitor subsequent drug release when no further irradiation is performed past the initial laser session. Figure 3.5 shows the release trend for the post-irradiated particles. Total drug released after 7, 14, and 21 days was 136 ± 22, 193 ± 36 and 224 ± 68 ng, respectively, for batches A, B and C. For example, this means that after 7 days, samples in batch A experienced a further drug release of 136 ± 22 ng in addition to the initial drug release the samples had already experienced during the irradiation session. Therefore, Figure 3.5 is not a cumulative representation of drug release including the irradiation-provoked release, but rather it is a representation of how the PAC-AuNR-HSAPs are capable of extended drug release post initial PPTT treatment.
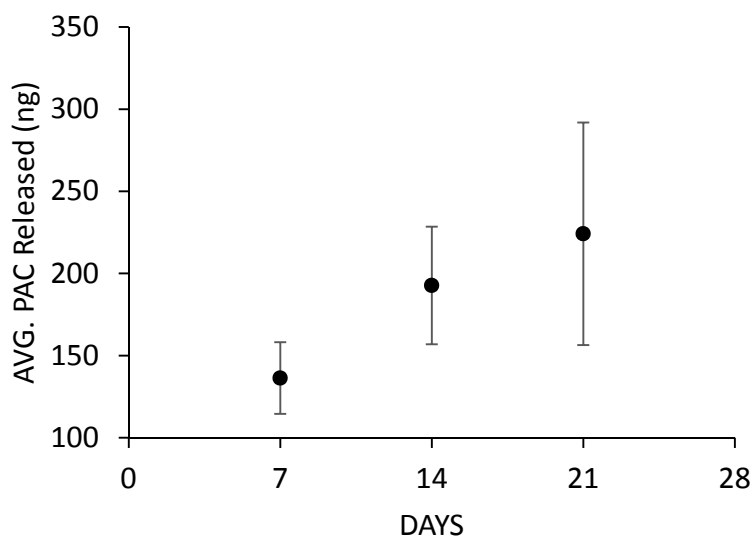
Figure 3.5. Average ng of unprovoked PAC released vs. Time in days. Error bars represent standard deviations of measurements (n > 3).

This release was in water at a low temperature without irradiation, so it should be noted that the dynamic activity of a tumor at normal body temperature and a slightly acidic pH (as seen in tumor sites) will enhance the release rate. Even though PAC-HSAPs with no gold nanorods inside did not experience an initial irradiation-provoked burst of drug release because of their inability to sufficiently heat, the PAC-HSAPs did release 104 ± 22 ng over a 7 day period, compared to 136 ± 22 for PAC-AuNR-HSAPs. This confirms that any particles which do not end up with a gold nanorod inside will still complete the function of controlled drug release over time.

What makes this even more promising is that PAC-HSAPs without AuNRs inside would travel alongside the PAC-AuNR-HSAPs *in vivo* and they may still experience the heating effects of the neighboring gold-filled particles. So, under biological conditions, the PAC-HSAPs may still experience the initial burst of drug release during irradiation as well as undergo their temporal chemotherapeutic function.

3.5 Conclusions

In this study, hybrid PAC-AuNR-HSAPs were successfully prepared with simultaneously loaded drug and encapsulated AuNRs to show that these composite particles can serve as platforms for preparing new drug therapies. The combined approach will allow killing of cancer cells by both hyperthermia and localized chemotherapy treatment and is more likely to eliminate all cancer cells. The photothermal approach not only results in hyperthermic treatment, but it also serves as a trigger for drug release once the particles have reached their targeted tissue and may aid in controlled release only at the tumor site. Functionalizing the surface of the HSAPs with disease-specific targeting ligands may lead to even more effective delivery of cancer

therapies to the site of the disease, boosting effectiveness and reducing damage to healthy

tissue.[42]

Chapter 4

Hybrid Gold Nanorod Human Serum Albumin Nanoparticles for Photothermal Therapy of Renal Cell Carcinoma

4.1 Abstract

In this study, the desolvation and crosslinking approach was employed to successfully encapsulate gold nanorods into HSAPs, forming AuNR-HSAPs (in accordance with Chapter 2) for *in vitro* studies. For particles created with the same amount of AuNRs, but varying amounts of HSA (1, 5 and 20 mg), the overall particle diameters were 409 ± 224, 294 ± 83 and 167 ± 4 nm, respectively. It was found that particles created with more protein result in a smaller, but more controllable, desirable average diameter size. The particular AuNR-HSAPs in this chapter were synthesized for specific use in the plasmonic photothermal therapy (PPTT) of renal cell carcinoma (cell line 786-O), using 808 nm near-infrared laser irradiation. Dosing experiments were done *in vitro* to determine the appropriate amount of unloaded-HSAPs and AuNR-HSAPs which can be delivered to the cells with limited inherent toxicity when no laser treatment was inflicted (dark treatments).

Irradiation treatments were also completed to test the dosing amount of AuNR-HSAPs needed to facilitate sufficient temperatures for PPTT of the cancer cells. We found that even though an increase in the relative amount of HSA present during preparation leads to more unloaded-HSAPs present alongside the AuNR-HSAPs in the final particle suspension, it also leads to an increase in heating capabilities. An increase in HSAPs delivered also leads to more toxicity under dark treatment conditions. A dose of HSAPs/AuNR-HSAPs created with 20 mg versus 5 mg of HSA caused dark cell viability percentages of 64.5% and 87%, respectively. All

of the AuNR-HSAPs batches experienced photothermal heating of above 42 ˚C (sufficient for moderate hyperthermia) when delivered to the cells in a 1 mL dose (all particles created in a given batch). After the full irradiation time, an MTT assay showed the AuNR-HSAPs PPTT effects: the strategy facilitated a significant decrease in cell viability to 0%.

An imaging dye, coumarin-6, was used to visualize the cell uptake of the AuNR-HSAPs via fluorescence microscopy. The particles did become fluorescently labeled and the cells showed signs of endocytosis when in contact with the AuNR-HSAPs. The system also lends itself to future customizable external functionalities such as stealth travel throughout the body and increased tumor uptake via conjugated targeting ligands. Internal entrapment of the chemotherapeutic medication sorafenib is currently being tested and optimized for tandem chemotherapeutic and photothermal therapies during a given treatment time. Animal models for *in vivo* testing are also being arranged in the near future for more dynamic treatment experiments.

4.2 Introduction

Renal cell carcinoma (RCC) is the most common kidney-based malignant tumor and it does not respond to traditional chemotherapy and radiotherapy to the same extent as some other tumor types.[96] The most used method of treatment has been partial nephrectomy, where the diseased portion of the kidney is removed.[92] This method is, of course, invasive and is especially dangerous for elderly and health-compromised patients. Diagnostic advancements of early-stage RCC have allowed for non-invasive treatments which spare much of the healthy kidney tissue.[99]

One such treatment is radiofrequency ablation, which uses a probe to inflict an alternating electrical current that induces heating of greater than 60°C, with optimal temperatures between 50-100°C.[99,101] If temperatures are too high (> 105°C), the tissue can be charred; resulting in reduced dissemination and tissue resistance. Uncontrolled heating can also result in reduced renal function over time or uneven heating, nullifying the use of an alternative treatment. Therefore, tumor recurrences after heating are a problem, especially in larger tumors and radiofrequency ablation tends to require repeated ablations.[92, 101]

Despite the successes of thermal ablation on RCC, uncontrolled or incomplete heating, coupled with RCC's increased drug resistance, calls for a better treatment method which delivers the best of both therapy options. Human serum albumin nanoparticles (HSAPs) filled with gold nanorods (AuNRs) form composite AuNR-HSAPs which offer a combative approach to solving both treatment problems. The AuNR-HSAPs can offer biocompatible, controlled heating in a specific location and the release of an increased dose of an otherwise dose-limiting chemotherapeutic drug.

In a previous study in Chapter 2, we focused on a proof-of-concept synthesis to fully encapsulate gold nanorods into size-controlled HSAP spheres with the future goal of taking advantage of the plasmonic photothermal therapy (PPTT) effects of the AuNRs without having them susceptible to clearing the body as fast as drug-conjugated AuNRs.[41] The hybrid particles are drug-loading powerhouses capable of enhanced permeability and retention effects within a tumor site. [8, 9, 10] In Chapter 3, we reached the goal of successfully encapsulating the anticancer drug paclitaxel within the AuNR-HSAPs simultaneously with the AuNRs; with efficient loading. That research supplied evidence that the PAC-AuNR-HSAP hybrid delivery system offered simultaneous drug-release and PPTT as well as extended, controlled release of the drug over time.

The work in this chapter aimed to prove that the AuNR-HSAP hybrid composites actually work to effectively kill cancer cells, without inherent toxicity, thus giving future purpose and promise to our former successes of being able to create and load drugs into the particles. Through fluorescence microscopy cell uptake studies and MTT cell assays, we show a definite increase in cell death with the use of the AuNR-HSAPs as a PPTT vessel. Current studies on loading AuNR-HSAPs with sorafenib, an angiogenesis inhibiting antitumor agent, are ongoing and hold much promise for a complete hybrid SRF-AuNR-HSAP in the near future for use in the RCC treatment of animal models. [60]

4.3 Experimental Methods

4.3.1 Materials and Reagents

Human serum albumin, lyophilized powder ≥ 97%, potassium bromide, Acrodisc® syringe filters with nylon membrane, diam. 13 mm, pore size 0.2 μm, Corning Costar cell culture plates, 12 well, flat bottom and 8% aqueous glutaraldehyde were obtained from Sigma Aldrich (St.

Louis, MO). Ethanol, 200-proof, ACS/USP grade was obtained from Pharmco-AAPER (CT, USA). Water was distilled, deionized, and then further purified with a Barnstead Nanopure system. The renal cell carcinoma cell line, RPMI media, coumarin-6, and materials for the MTT assay were supplied by Tulane University Medical Center.

Bare gold nanorods (10 nm average axial diameter, 43 nm average length, surface plasmon resonance ~ 808-829 nm, OD = 1, 5.9×10^{11} AuNR/mL in water) were obtained from Nanopartz, Inc. (Loveland, CO). The AuNRs used were advertised by the vendor as "bare", but they did contain trace amounts of cetyltrimethylammonium bromide.

4.3.2 Synthesis of AuNR-HSAPs

The AuNR-HSAPs were prepared using a conventional desolvation technique from Chapter 2 with the addition of AuNRs for seeding.[20, 81, 83] The standard method for preparation included creating an HSA stock solution of 100 mg HSA/ 1 mL of water. After dissolving, the pH was around 7. To an aliquot of the HSA stock solution (containing 1, 5 or 20 mg of HSA), 2 mL (1.18×10^{12} AuNRs) of the AuNR stock solution was added, along with a small stir bar. Then, 100% ethanol was added to a known volume to denature the protein and facilitate aggregation. Upon addition of the ethanol, the solution became turbid. Finally, an aliquot of 8% glutaraldehyde (aq.) was added to crosslink the AuNR-HSAPs. After 24 h of stirring, the particles were centrifuged at 13,000 rpm (16,060 g) for 20 minutes. The supernatant was removed and the remaining particle pellet was washed twice by resuspending AuNR-HSAPs in water via ultrasonication. The final particles were redispersed and stored at 4 °C in water. The final particle suspensions were named by the amount of HSA in mg used in the preparation process: 1-AuNR-HSAPs, 5-AuNR-HSAPs and 20-AuNR-HSAPs for 1, 5, and 20 mg HSA, respectively.

4.3.3 Dynamic Light Scattering

The completed HSAPs were characterized by measuring the diameter, mobility, and zeta potential using a Mobius dynamic light scattering (DLS) instrument (Wyatt Technology Corporation, Santa Barbara, CA). Samples were diluted with water prior to analysis.

4.3.4 SEM and TEM

Particles were imaged using a field emission-scanning electron microscope FESEM, LEO 1530VP (LEO Elektronenmikroskopie GmbH, Oberkochen, Germany). HSAPs were sputtered with a thin film of gold or silver to facilitate imaging. Transmission electron microscope (TEM) images were acquired with a JEOL Model 2010 TEM.

4.3.5 Cell Line

 RCC 786-O were incubated in 30, 1cm diameter wells. They were grown to approximately 70-80% confluence in 1mL of RPMI media at a temperature of 37° Celsius and at 5.0% CO2, using Forma Scientific^{TM} CO_2 Water Jacketed Incubator Model 3110 (115V, 3.6A, 50/60Hz).

4.3.6 Laser Irradiation of Particles

The final, washed AuNR-HSAPs and HSAPs were tested for heating ability and cell death via laser irradiation. To heat the samples, an aliquot of the particle sample was placed into a well of a 28-well plate containing renal cell carcinoma. The plate was placed approximately 4 to 6 inches under a vertically mounted laser. A LabSpec 808 nm collimated diode laser system was used at a continuous wave power output of 2000mW for 30 minutes (irradiated) or zero minutes (dark)for each sample. The size of the beam was approximately 1×1 cm. Temperature changes caused by the irradiation sessions were measured using a Spark Science Learning System™ model PS-2008A thermocouple.

The cells received a total of 1 mL of liquid: an aliquot of media and a dose of the Au-HSAP suspension (50 μL, 0.5 mL or 1.0 mL) that contained either a control condition containing no particles, unloaded-HSAPs, bare AuNRs or 1-, 5- or 20-AuNR-HSAPs. Every batch of AuNR-HSAPs contained some HSAPs that formed with no gold nanorods within them; therefore there is always a certain ratio of unloaded-HSAPs to AuNR-HSAPs in a batch. For the preparation methods 1-AuNR-HSAPs, 5-AuNR-HSAPs and 20-AuNR-HSAPs (all with 1.18×10^{12} AuNRs), the resulting finished particle batches contained varying ratios of unloaded-HSAPs and AuNR-HSAPs. All samples were kept out of the incubator for the same amount of time to ensure that no cells were protected from the effects of the environment any more than cells currently being irradiated. After irradiation, the contents of the wells were assayed via an MTT assay for cell viability testing.

4.3.6 MTT Assay

Cell viability after AuNR-HSAPs and HSAPs treatment was measured by MTT assay. The assay used a tetrazolium compound (Sigma Aldrich, St. Louis, MO), which when reduced by intracellular mitochondrial dehydrogenase enzyme, converts tetrazolium into purple formazan indicating the magnitude of cell viability. The viability of cells post treatment was measured by the quantification of purple formazan by colorimetric method using a spectrophotometer (Beckman Coulter, Inc., Schaumburg, IL).

4.3.7 Cell Uptake Studies via Fluorescence Microscopy

RCC 786-O were incubated in 3 separate plates of 10mL of RPMI media at a temperature of 37° Celsius and at 5.0% CO_2. An aliquot of 0.5 mL of unloaded-HSAPs, coumarin-6 loaded AuNR-HSAPs was added and incubated for 24 hours before images were taken using an Olympus IX70-S1F2 fluorescence microscope (220-240V, 1.8/0.8A, 50/60Hz) with an Olympus

DP71 camera (12.5 megapixel) and Olympus BH2 RFL- T3 Power Supply (100-120V, ~2.8 A, 50-60Hz).

4.4 Results and Discussion

4.4.1 Formation of AuNR-HSAPs

Using the desolvation and crosslinking process discussed in Chapter 2 to create thiol bonds between the AuNRs and the HSAPs, a self-assembly process facilitated the formation of a spherical HSAPs (see Table 4.1) around the AuNRs with average particle size diameters of 409 ± 224, 294 ± 83 and 167 ± 4 nm when using 1-AuNR-HSAPs, 5-AuNR-HSAPs and 20-AuNR-HSAPs, respectively. [14] The zeta potential values for those AuNR-HSAPs were -39 ± 3, -35 ± 4 and -33 ± 3 mV, respectively.   It is evident from the size information that as the mass of HSA increased, the average particle size became smaller, with less deviation. Since the zeta potential values for these size distributions reflect stable particles, we are confident that these fluctuations are actually large distributions in size and not reflections of sizable aggregates.

When using 1-HSAPs, 5-HSAPs and 20-HSAPs without gold nanorods (see Table 4.1), unloaded-HSAPs were created with average diameters of 400 ± 160, 182 ± 46 and 174 ± 3 nm, respectively. The zeta potential values for the particles were -26 ± 8, -22 ± 8 and -35 ± 3 mV, respectively. This size and zeta potential information for unloaded-HSAPs depict a trend of smaller particle sizes for a given amount of protein when no Au rods are present, with the exception of the particles created via 20-HSAPs. The deviations in size also decreased. The zeta potential values continued to reflect stability of the particles, however the AuNR-HSAPs showed greater stability than the unloaded-HSAPs. This stability increase was a desirable result; as it reflects another benefit of the hybrid particle.

Table 4.1. Particle sizes and zeta potential data for AuNP-HSAPs and Unloaded-HSAPs used on RCC.

mg HSA in Preparation Method	AuNR-HSAPs		Unloaded-HSAPs	
	Avg. Diameter (nm)	Zeta Potential (mV)	Avg. Diameter (nm)	Zeta Potential (mV)
1	409 ± 224	-39 ± 3	400 ± 160	-26 ± 8
5	294 ± 83	-35 ± 4	182 ± 46	-22 ± 8
20	167 ± 4	-33 ± 3	174 ± 3	-35 ± 3

[a]Error represents one standard deviation with N ≥ 3.

When comparing this data to the initial size values obtained for AuNR-HSAPs in Chapter 2, there are some size difference due to differences in crosslinking, ethanol volumes, mass of HSA used and volume of stock AuNR solution used.

4.4.2 Unloaded-HSAP and AuNR-HSAP Dark Effects on Renal Cell Carcinoma

Upon dispersion of a prepared sample into water, the final volume was 1 mL of suspension. In an attempt to find any inherent toxicity caused by the particles, dark experiments were performed on the RCC using either 50 µL, 0.5 ml or 1.0 mL doses of the finished particle batches. Table 4.2 displays the viability data for the 'dark' treatment for both Unloaded-HSAPs and AuNR-HSAPs created with varying amounts of HSA. There is a definite correlation between the number of particles placed onto the cells and cell death.

For the Unloaded-HSAPs, it is theorized that 20-HSAPs creates far more particles due to the increase in protein available for particle formation, thus the cells may become overwhelmed by the 1.0 mL full batch dose and the cell viability is only 13%. However, when the 20-HSAP prepared particles were dosed with only 0.2 or 0.05 mL of the originally prepared 1 mL particle suspension, the cell viability was 70 and 80%, respectively. This viability increase proves that it is not the 20-HSAPs themselves that are toxic to the RCC, but it is the amount of particles delivered which causes some toxicity.

The 1-AuNR-HSAPs, 5-AuNR-HSAPs and 20-AuNR-HSAPs also caused a decrease in cell viability with a 0.5 mL dose, with the 5-AuNR-HSAPs causing the least amount of cell death at 87%. It is interesting that the viability does not change much from the 50 µL dose when using the 5-AuNR-HSAPs preparation type. It is clear that using the entire batch of particles, a 1.0 mL dose, is too much for the RCC to handle and nearly all cells are killed without irradiation.

Table 4.2. 'Dark' Treatment: Cell Viability Data for RCC Dosed with 0.05, 0.5 or 1.0 mL of Unloaded-HSAPs or AuNR-HSAPs of Varying HSA Amounts

% Cell Viability After 'Dark' Treatment			
mg HSA in Sample Preparation	Amount of Unloaded-HSAPs or AuNR-HSAPs Sample Added to the RCC		
	50 µL	0.5 mL	1 mL
0 (Control)	100%	100%	100%
5-HSAPs	94%	-	-
20-HSAPs	-	-	13%
1-AuNR-HSAPs	86%	53%	0.6%
5-AuNR-HSAPs	84%	87%	2.9%
20-AuNR-HSAPs	-	65%	4.5%

Hash mark indicates no data available for a particular study.

4.4.3 Photothermal Irradiation Effects on Renal Cell Carcinoma

Understanding that the dose should be 0.5 mL or lower for a particular preparation method, irradiation studies were still done with 50 µL, 0.5 mL and 1.0 mL doses. Initially, when 50 µL of 1-AuNR-HSAPs, 5-AuNR-HSAPs and 20-AuNR-HSAPs were added to the cell wells, none of the trials were able to decrease cell viabilities to below 37% or final temperatures above 44°C when irradiated for 30 minutes. While that temperature may cause moderate hyperthermia, temperatures above 46°C are needed to induce coagulative necrosis. [45, 93] It became evident that the number of AuNRs had to be increased in order to reach sufficient heating, therefore the number of AuNR-HSAPs had to be increased.

An interesting trend as seen in Figure 4.1 was, despite the samples having equal amounts of AuNRs present within the particles, the 20-AuNR-HSAPs samples were able to heat the cells to the highest temperature. The reason for this phenomena is not exactly known, however it is speculated that the HSAP acts as some sort of spacer for the rods, thus allowing them to be more individually effected by the light. One study found that increased amount of AuNRs past 0.5 nM has an adverse effect on heating because of increased light absorption and decreased photothermal conversion. [45] When delivered in a 1.0 mL dose, the 20-AuNR-HSAPs experienced heating up to 51°C after only 5 minutes a temperature necessary to cause severe cellular hyperthermia and necrosis.
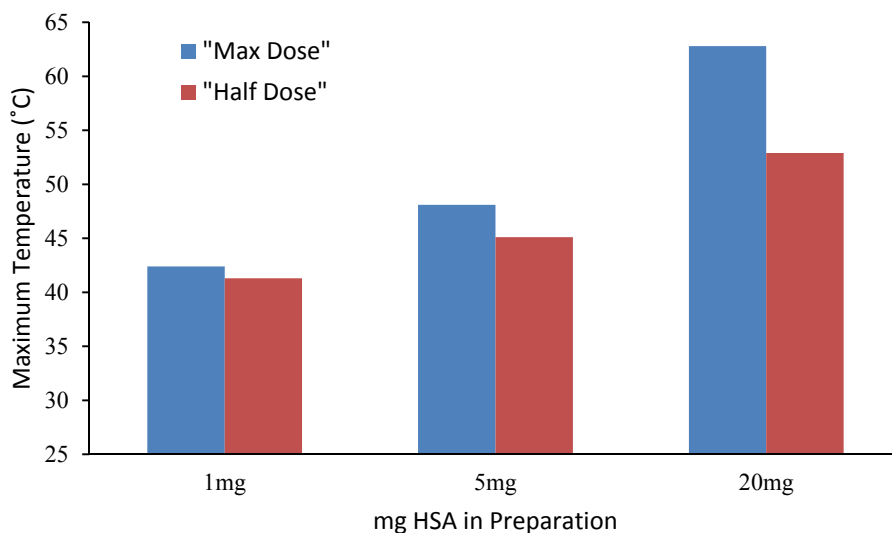
Figure 4.1. Heating Capabilities of AuNR-HSAP batches made with varying mg HSA and heated in either 0.5 or 1.0 mL doses.

Table 4.3 displays the cell viability information for the irradiated cells treated with particles. Minimal warming was experienced when the laser was directed at RCC that were not treated with particles (control). The Unloaded-HSAPs also experienced minimal warming, with cell

viability dropping to 92% for the irradiated study from 94% during the dark study. The 1.0 mL

dose of particles had already experienced almost complete cell death during the dark study, so

the increase in necrosis after irradiation was not surprising.

The true testament to the effectiveness of the irradiation on the AuNR-HSAPs was the 0.5

mL dose of all three sample preparation types. The 1-AuNR-HSAPs, 5-AuNR-HSAPs and 20-

AuNR-HSAPs all experienced decreases in the percentage of viable cells, as seen in Figure 4.2.

Table 4.3. 'Irradiated' Treatment: Cell Viability Data for RCC Dosed with 0.05, 0.5 or 1.0 mL of Unloaded-HSAPs or AuNR-HSAPs of Varying HSA Amounts

% Cell Viability After 'Irradiated' Treatment			
mg HSA in Sample Preparation	Amount of Unloaded-HSAPs or AuNR-HSAPs Sample Added to the RCC		
	50 μL	0.5 mL	1 mL
0 (Control)	99.5%	99.5%	99.5%
5-HSAPs	92%	-	-
1-AuNR-HSAPs	86%	36%	0.2%
5-AuNR-HSAPs	68%	25%	1.6%
20-AuNR-HSAPs	-	3.6	0%

Hash mark indicates no data available for a particular study.
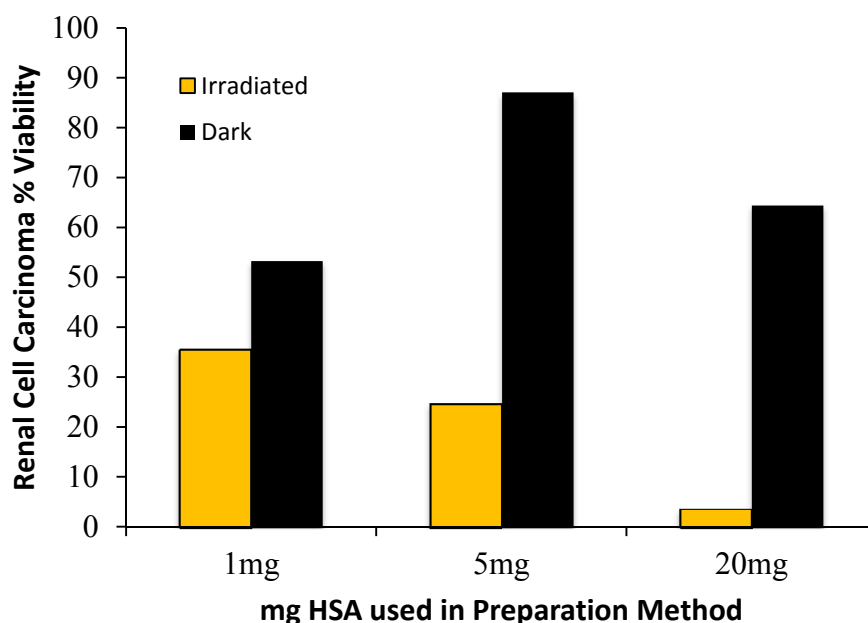
Figure 4.2. Percent viability of Renal Cell Carcinoma after 'dark' (red bars) or 'irradiated' (blue bars) treatment using AuNR-HSAPs made with varying mg HSA: 1, 5 or 20 mg.

It is worth noting that bare AuNRs killed of over 35% of the cancer cells without irradiation. Even though the nanorods are marketed as "bare", with almost all CTAB washed off, there are still some residual amounts which has been shown to exhibit cytotoxicity unless properly encapsulated.[80] A proof of concept trial using only the bare AuNRs reached 59.7°C with 100% cell kill. AuNRs produced both the highest temperatures and the highest rate of cell kill, but also demonstrated cytotoxicity in the absence of irradiation, whereas 1-AuNR-HSAPs showed less cell kill but also demonstrated less cytotoxicity. HSAPs alone and 1-AuNR-HSAPs did not produce cell kill rates higher than 15%. Low doses (0.5 mL or less) of 20-AuNR-HSAPs seem the best therapeutic option moving forward.

4.4.4 Fluorescence Cell Uptake Studies

In order to determine whether the HSAPs were indeed being taken into the RCCs, a fluorescence uptake study was performed using coumarin-6 dye as a label. Particles created via

5-AuNR-HSAP were prepared in the presence of the dye. Figure 4.3 shows the fluorescence microscopy of the coumarin-6 labeled AuNR-HSAPs after incubation with the renal cell carcinoma. The particles are underwent endocytosis but were taken up into the cell nucleus. Coupled with the irradiation data, these results are promising and display sufficient evidence that the AuNR-HSAPs will be in close enough proximity to diseased cells to cause necessary temperature increases upon irradiation *in vivo*.
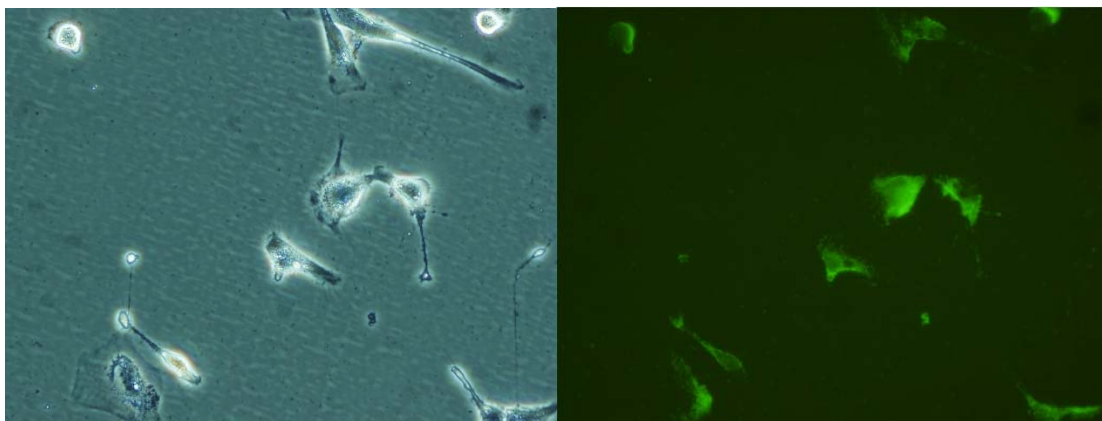
Figure 4.3. (a) Confocal Microscope image of Renal Cell Carcinoma Treated with coumarin-6 labeled AuNR-HSAP-5 and (b) the fluorescence emission of the same cells.

4.5 Conclusions

In this study, hybrid AuNR-HSAPs were successfully prepared and showed more controllable size distributions when more protein is added to the preparation vial. The particles were able to heat to necessary temperatures in order to cause renal cell carcinoma death, but careful consideration of the particle dose has to be maintained in order to not overwhelm the cells without irradiation. This incidence of dark condition cell death may not matter very much in a tumor site, however necrosis of healthy cells surrounding the tumor site must be avoided during the time it takes for all of the AuNR-HSAPs to become trapped in the tumor vasculature.

Since, fluorescence microscopy showed that the cells were taking up the AuNR-HSAPS, functionalizing the surface of the HSAPs with disease-specific targeting ligands may lead to even more effective delivery of cancer therapies to the site of the disease, boosting effectiveness and reducing damage to healthy tissue. [42]

Chapter 5

Loading CPT (camptothecin) and BACPT (7-butyl-10-aminocamptothecin) Into Human Serum Albumin Nanoparticles for use as a Targeted Therapy Platform

5.1 Abstract

Camptothecin, a natural antineoplastic agent, and BACPT (7-butyl-10-aminocamptothecin), an analogue of camptothecin (CPT), have garnered attention in the medical field due to their high effectiveness against pancreatic, lung and ovarian cancers, however due to their water insolubility, they has been lacking in fulfilling their potential as major anti-cancer pharmaceuticals unless they have been manipulated in some way. Manipulations such as creation of a prodrug or attachment of solubility ligands cause a decrease in the effectiveness of the drugs and there is still a problem of toxicity. Camptothecin and BACPT also possess a propensity to open their lactone rings in the presence of water forming a carboxylated version of the drug, which some research suggests, causes some loss in effectiveness. Carboxylated camptothecins also possess a high binding affinity for HSA, so are susceptible to being carried away from the tumor site prematurely by molecular HSA, causing reduced efficacy.

However, there is evidence that, when in high enough concentrations, the carboxylate form of camptothecins have the ability to effectively kill or slow the growth of cancer cells as well as the lactone form. By taking advantage of the CPT's and BACPT's affinities to HSA and entrapping the BACPT within human serum albumin nanoparticles (HSAPs), which have had success as a colloidal carrier system for targeted treatment of cancer, the amount of drug that reaches the cancer site can be greatly enhanced. This enhancement can potentially increase

efficacy, safety and treatment success. HPLC and fluorescence spectroscopy were used to determine drug loading efficiency.

Both the CPT-HSAPs and the BACPT-HSAPs showed toxicity to human sarcoma cells *in vitro*. However, finding the drug loading amounts that caused the desirable toxicity was a challenge. HPLC proved unreliable as an analytical technique for CPT and BACPT due to inconsistent results from lactone conversion during the mobile phase. CPT could not be determined via fluorescence spectroscopy as well due to sporadic, uncontrollable changes in the fluorescence emission. The loading of BACPT into BACPT-HSAPs was determined via HPLC and fluorescence spectroscopy and compared.

This research reports an efficient strategy for preparing 200-300 nm, size-controlled BACPT-HSAPs with up to 5.25 micrograms of BACPT/ mg of HSA, as determined by fluorescence spectroscopy. The BACPT-HSAPs showed evidence of cell necrosis for human sarcoma cancer cells during *in vitro* studies. This proof of concept research shows that BACPT-HSAPs are effective at killing cancer cells when the BACPT is present in both carboxylate and lactone forms. The strategy also enables maximum external surface area for future functionalization of targeting ligands for stealth-like disease detection.

5.2 Introduction

Camptothecins are used on primary and metastatic colon carcinoma, platinum-refractory ovarian cancer, and small cell lung carcinoma. It acts by poisoning the DNA target enzyme topoisomerase I (top I) during its catalytic cycle of DNA relaxation, leading to the generation of DNA double-strand breaks and cell death by apoptosis.[46,48,49,50] BACPT, 7-butyl-10-aminocamptothecin (Figure 5.1), was developed in an effort to improve potency and cross-resistance profiles of camptothecins.[54] BACPT is promising because it has been found that a

substitution at the C-10 position (See Figure 5.1) increases lipophilicity while substitution at the C-7 position enhances potency *in vitro*. When binding to DNA, BACPT intercalates at the site of DNA cleavage and is stabilized by an E-ring hydrogen bond contact with an aspartic acid. [54,55] The A-ring's amine at the C-10 position also forms a hydrogen bond to an oxygen atom of the side chain of a glutamine moiety. The C7- butyl moiety causes a very good steric fit of BACPT with the top I enzyme, and the planar ring system of the drug mimics a DNA base-pair.[54,55]

These effects correlate with increasing persistence of the DNA cleavage complex created by BACPT.[54,55] Hiding the highly effective BACPT and CPT in a biocompatible protein sheild in concentrations high enough to overcome the effects of the reduced lactone version will accomplish the task of maximizing efficiency while minimizing harmful effects.
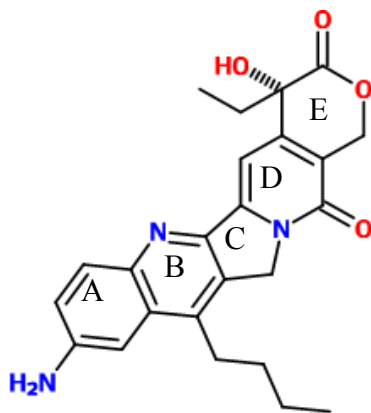
Figure 5.1. BACPT

There has been some debate as to whether the antitumor activity is fully lost when a camptothecins undergo a transforation to the carboxylate verion after they come into contact with physiological pH and the structure of a blood protein such as HSA or if the process is indeed a reversible process (Figure 5.2). [102] However, studies have shown evidence to suggest that a significant amount (33% at pH 7.4, 66% at pH 6.8) of uncharged carboxylated BACPT

could enter tumor cells at acidic pH and accumulate in mitochondria to inhibit mitochondrial top I. [58] This is compared to the lactone form where 83-100% of the BACPT remains uncharged. [58] It has also been demonstrated that the carboxylate version of camptothecin sodium has been effective against L1210 leukemia and carboxylate topotecan can bind to top I. [103, 104] A recent study proved that the inhibitory rate of tumor percent caused by 9-nitrocamptothecin was significant down to 25% lactone (vs. carboxylate) in tumor bearing mice. [105] The pH sensitive antitumor drug is desirable because it can exploit the pH gradient which exists in solid tumors but not in normal tissues [106].
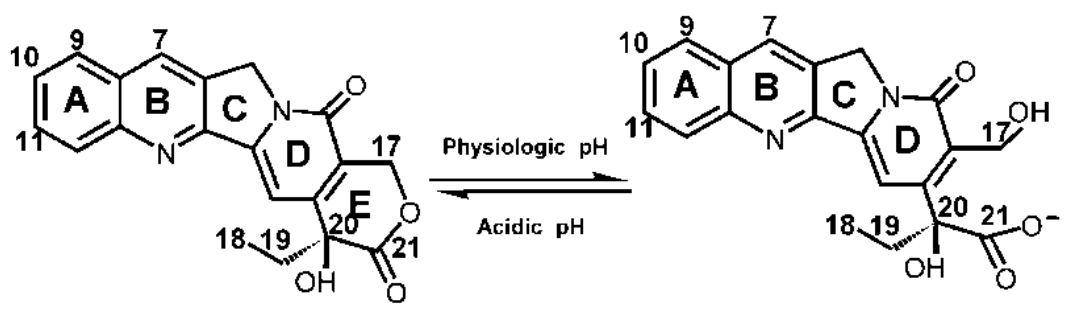
Figure 5.2. Structure of CPT at physiological versus acidic pH.

The innovation of this project is the strategic use of HSAP's enhanced permeation and retention effects to entrap the aggressive, insoluble CPT and BACPT for more concentrated release at a tumor site; increasing the dosage safely. The CPT/BACPT must be in continuous contact with replicating cancer cells to be optimally therapeutic, therefore keeping the drug in constant release, even in carboxylate form, in the acidic tumor is desirable. [105, 107] In this study, a desolvation and crosslinking entrapment method facilitated size-controlled HSAP shells for efficient internal enclosure of BACPT and CPT, as well as maximum external surface area for future functionalizing of targeting ligands for disease detection. We have used an *in vitro* human

sarcoma cell culture as a preliminary study of the effectiveness of BACPT-HSAPs for cancer treatment. [108]

5.3 Experimental Methods

5.3.1 Materials and Reagents

Human serum albumin, lyophilized powder ≥ 97%, 8% aqueous glutaraldehyde, RPMI 1640, porcine trypsin - 1X Solution, fetal bovine serum, streptomycin and amphotericin, were obtained from Sigma Aldrich (St. Louis, MO). Ethanol, 200-proof, ACS/USP grade was obtained from Pharmco-AAPER (CT, USA), Phosphate buffer (pH 7.2) and a Mini-Pump Variable Flow peristaltic pump were obtained from VWR International (Radnor, PA). An AccuSpin Micro centrifuge was obtained from Fisher Scientific (Pittsburg, PA). Water was distilled, deionized, and then further purified with a Barnstead Nanopure system. Camptothecin (S) (+) was obtained from VWR and BACPT was obtained from Dekk-Tec, Inc. (New Orleans, LA). Cells: "CL" Human Sarcoma, cultured from a patient; Brain Dekk-Tec. Inc., 725 Topaz St, New Orleans, LA)

5.3.2 Synthesis of Unloaded HSAPs

The HSAPs were prepared using a conventional desolvation technique.[6, 15, 82, 81, 83] The standard method for preparation included addition of 20 mg of solid HSA to 1 mL of water . After dissolving, the pH was around 7. A small stir bar was added to the solution, and 3 mL of 100% ethanol was added at a rate of 1 mL/min using a peristaltic pump. Upon addition of the ethanol, the solution became turbid. Finally, 4.7 μL of 8% glutaraldehyde (aq.) was added to crosslink the HSA within the particles. After 24 h of stirring at room temperature, the particles were centrifuged at 13,000 rpm (16,060 g) for 30 minutes to 1 hour. The supernatant was removed and the remaining pellet was ultrasonicated and resuspended. The suspension was

washed twice with water with intervening centrifugation steps. The washed particles were ultrasonicated in water and stored at 4 °C.

5.3.3 Synthesis of BACPT-HSAPs

The procedure for preparing the drug-loaded particles followed section 5.3.2 with a modification to the ethanol addition step and final volume. To create the BACPT loaded HSAPs, a stock solution of the BACPT was first created: 1 mg BACPT/mL ethanol. Then, an aliquot of the drug stock solution was added to more ethanol. The BACPT/EtOH solution was added to an HSA sample solution drop-wise. The overall parameters used for preparing HSAPs loaded with varying amounts of BACPT are provided in Table 5.1 (all samples contained 4.7 μL of 8% glutaraldehyde; causing 40% theoretical crosslinking). The washes for the drug-loaded particles were done with a solution of 1:3 water:ethanol.

Table 5.1. Preparation Parameters for all BACPT-loaded HSAPs

Sample Preparation Type	Drug Stock Solution (mL)	EtOH (~mL)	Drug Added (mg)
BACPT-HSAP-1	0.01	3.99	0.01
BACPT-HSAP-2	0.1	3.9	0.1
BACPT-HSAP-3	0.25	3.75	0.25
BACPT-HSAP-4	0.5	3.5	0.5
BACPT-HSAP-5	1	3.0	1

5.3.4 Synthesis of CPT-HSAPs

The procedure for preparing the drug-loaded particles followed section 5.3.2 with a modification to the ethanol addition step and final volume. To create the CPT loaded HSAPs, a

stock solution of the CPT was first created: 1 mg CPT/mL in 2:3 chloroform:ethanol. Then, an

aliquot of the drug stock solution was added to more ethanol. The CPT/EtOH solution was

added to an HSA sample solution drop-wise. The overall parameters used for preparing HSAPs

loaded with varying amounts of CPT are provided in Table 5.2 (all samples contained 4.7 µL

of 8% glutaraldehyde; causing 40% theoretical crosslinking). The washes for the drug-loaded

particles were done with a solution of 1:3 water:ethanol.

Table 5.2. Preparation Parameters for all CPT-loaded HSAPs

Sample Preparation Type	Drug Stock Solution (mL)	EtOH (~mL)	Drug Added (mg)
CPT-HSAP-1	0.1	3.9	0.1
CPT-HSAP-2	0.25	3.75	0.25
CPT-HSAP-3	0.5	3.5	0.5

5.3.5   Absorbance

Absorbance measurements of the BACPT-HSAPs were performed with a Cary 60

absorbance spectrometer (Agilent Technologies).

5.3.6 HPLC

The HPLC system used was an Agilent 1100 instrument (Palo Alto, CA) with a diode array

absorbance detector. The column was an Agilent Eclipse XDB-C18 column (150 X 4.6 mm,

particle size 5µm). The injection volume was 200 µL, and the absorbance wavelength used for

quantitation of BACPT was 227 nm and for CPT it was 254 nm. The mobile phase was 60%

acetonitrile: 40% water at a flow rate of 1 mL/minute.

5.3.7 Fluorescence

Fluorescence was measured with a Cary Eclipse fluorometer with excitation for BACPT at 403 nm and emission scanned from 413-600 nm. For CPT, the excitation wavelength was 358 nm and the emission was scanned from 368-550 nm. Excitation and emission slits were 2.5 nm.

5.3.8 Dynamic Light Scattering

The completed HSAPs were characterized by measuring the diameter, mobility, and zeta potential using a Mobius dynamic light scattering (DLS) instrument (Wyatt Technology Corporation, Santa Barbara, CA). Samples were diluted with water prior to analysis.

5.3.9 Microscopy

Particles were imaged using a field emission-scanning electron microscope FESEM, LEO 1530VP (LEO Elektronenmikroskopie GmbH, Oberkochen, Germany). HSAPs were sputtered with a thin film of gold or silver to facilitate imaging. To check cell vitality after the addition of nanoparticles to the cancer cells, a compound microscope was used; Meiji Techno, TC5300, Compound - 100x on large view, 200x in zoom view, (Meiji Techno America, San Jose, CA)

5.3.10 Cell Cultures

Cell vitality studies were performed by two different methods.

CELL METHOD 1. For visual cytotoxicity studies without washing off unloaded-HSAPs, CPT-HSAPs or BACPT-HSAPs: On a 12-well cell plate, to the each well, 1 mL of sterile RPMI media was added, then, 1-drop aliquots of diluted (with RPMI) or undiluted harvested cell solutions were placed into every well. The well plates were incubated at 37°C for 24 hours to facilitate cell growth. After the 24 hour period, addition of the nanoparticles was accomplished by adding 0.5 ml of the particle solution being tested; either unloaded-HSAPs or a particular concentration of CPT-HSAPs or BACPT-HSAPs. The control was a well containing only cells

and no nanoparticles. After the plates were incubated again with the particles at 37°C for 24 hours, the cells were visually checked for blebbing and necrosis on the compound microscope; with the nanoparticles still present.

CELL METHOD 2. For visual cytotoxicity studies involving field of view differences after washing the wells of nanoparticles and dead cells: the well plates were prepared as they were in cell method 1, but after the initial incubation period, only 0.1 mL of particle solution being tested was added. A control of cells only was prepared a well. After 24 hours of incubation, the wells were removed of all particles and dead cells by pipetting off all media in which they were incubated. The wells were washed twice with 1 mL of fresh RPMI. Any remaining cells were viable and stuck to the well plate. Dead cells were washed away. A visual inspection on the compound microscope showed differences in the live cell population of the control and the treated wells.

5.4 Results and Discussion

5.4.1 Formation and Characterization of BACPT-HSANPs

The same thermodynamically driven self-assembly process for polymeric materials was used in this chapter and proceeded by the addition of a denaturing agent to denature HSA in the aqueous phase, causing aggregation, thus facilitating electrostatic and hydrophobic interactions.[14,18]
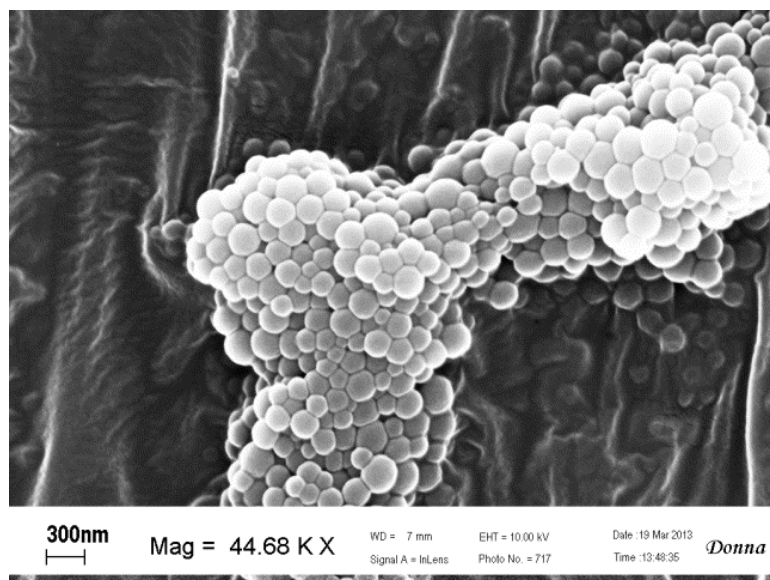
Figure 5.3. FESEM images of BACPT-HSANPs.

This process yielded samples with a size of 248 ± 66 nm, therefore it was assumed that the

BACPT-HSAPs created under similar desolvation parameters would yield roughly the same

particle size. That hypothesis proved correct. All five BACPT-HSAP preparation methods

yielded average size measurements within 227 ± 19 and 247 ± 30 nm. Figure 5.3 is an FESEM

image of BACPT-HSAPs showing that particles created in the presence of BACPT do not lose

their characteristic spherical shape or size. These BACPT-HSAPs created were still in a proven

effective size range for use as a targeted treatment vehicle.

BACPT-HSAPs created were still in a proven effective size range for use as a targeted

treatment vehicle.

Table 5.3. Preparation Type vs. Overall size of Completed BACPT-HSAPs

Sample Preparation Type	Drug Added (mg)	Average BACPT-HSAP Size (nm)
BACPT-HSAP-1	0.01	234 ± 42
BACPT-HSAP-2	0.1	235 ± 20
BACPT-HSAP-3	0.25	242 ± 5
BACPT-HSAP-4	0.5	227 ± 19
BACPT-HSAP-5	1	247 ± 30

The overall average particle sizes for loading scenarios 1 thru 5 do not vary drastically, as seen in Table 5.3. This research focuses on entrapping the BACPT described above into a shell of HSAP big enough to also bind and hold an extremely high, maximum payload of drug while succumbing to the EPR effects that will cause it to be trapped in a cancerous matrix, so the consistent particle size is desirable.

5.4.2 Determination of Loading Efficiency of BACPT via HPLC

It was a concern that using HPLC as a quantitation method would not be an accurate representation of the amount of drug washed off of the particles because the HPLC mobile phase contains water. As discussed previously, water (at neutral pH) has the ability to open the BACPT's lactone ring (as seen in Figure 5.3), thus causing the structure of the BACPT to change, potentially resulting in a shift of the characteristic peak. Figure 5.4 shows absorbance spectra of 0.5 mg/mL solutions of a BACPT. The dashed line represents the absorbance of a solution of BACPT in 1:4 water: ethanol; consistent with the solvent matrix in the particle preparation supernatant. The solid line represents the absorbance of BACPT in 50:50 water: ethanol; consistent with a "wash". It is clear that there is absorbance spectrum shift with the addition of more water in the BACPT matrix. This could affect the HPLC results, along with the conformational change in the BACPT molecule which is responsible for the shift.
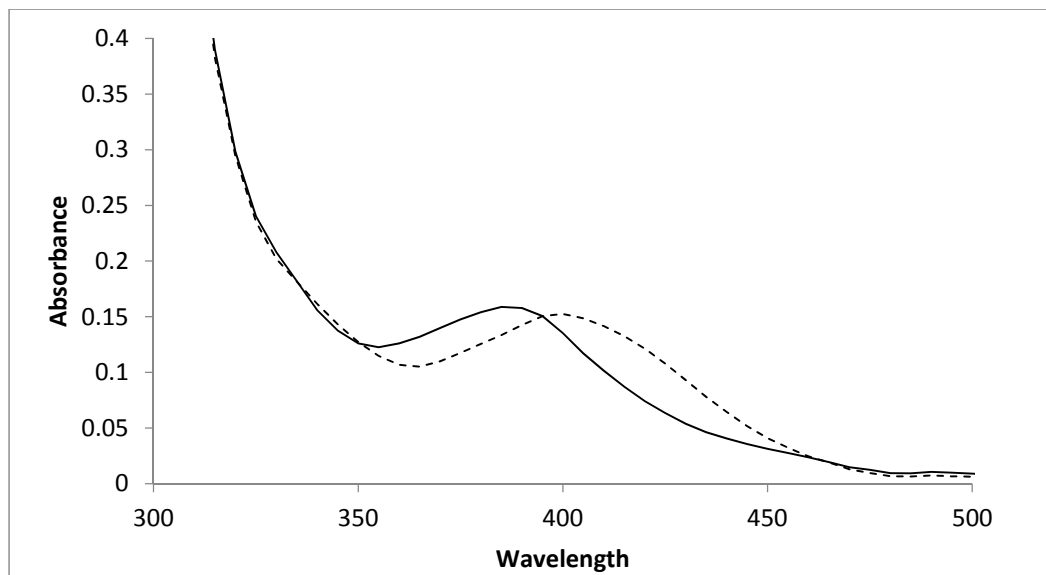
Figure 5.4. Absorbance spectra of (solid line) 0.5 mg/mL BACPT in 50:50 water:ethanol and (dashed line) 0.5 mg/mL BACPT in 1:4 water:ethanol.

Despite the shift, we sought to find out if HPLC could achieve drug quantitation in the initial supernatant and subsequent particle washes. HPLC analysis of the particle preparation supernatant and wash solutions were compared to a set of drug solution standards in 1:3 water:ethanol to mimic the matrix of the preparation solution. Figure 5.5 shows an HPLC spectrum for a sample created with the BACPT-HSAP-4 preparation parameters (0.5 mg of

BACPT added) and revealing a BACPT peak at 5.3 minutes.
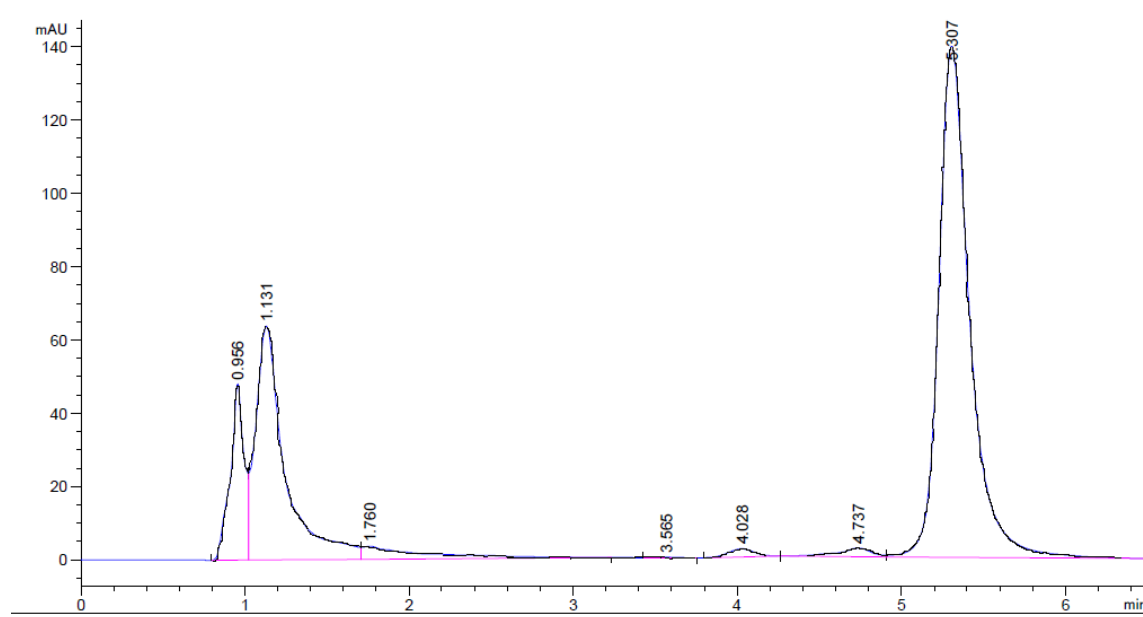
Figure 5.5. HPLC spectrum of the initial centrifugal supernatant from a sample created with 0.5 mg BACPT. The BACPT manifests a peak at 5.3 minutes.

As discussed previously, water and its neutral pH has the ability to open the BACPT's lactone ring, thus causing the structure of the BACPT to change, potentially resulting in a shift of the characteristic peak. It was indeed noted that the longer the samples (and standards) were allowed to sit (even refrigerated), there was a reduction of the ~ 5 minute peak area. When samples were compared to older standards, there was an undesirable finding of the calculated drug washed off of the particles being higher than the amount of drug actually added to the sample during preparation.

Given the impossibility of this result being accurate, all samples had to be analyzed within 48 hours of preparation and again, the washes could not be done with water alone but with an ethanol mixture. Upon HPLC analysis of BACPT-HSAPs prepared by either, BACPT-HSAP-1, BACPT-HSAP-4 or BACPT-HSAP-5, there was an increase in drug loading.
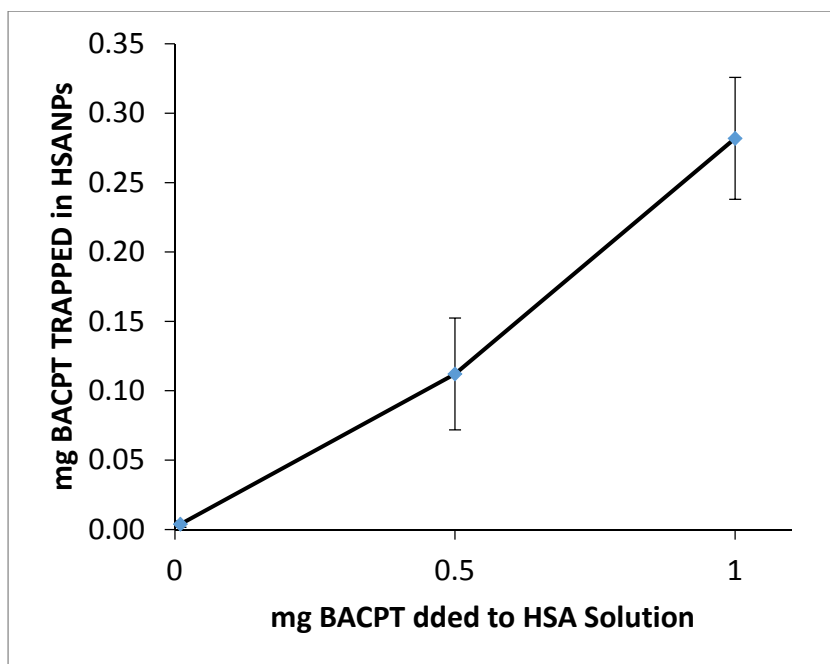
Figure 5.6. Relationship of starting mg BACPT added to a particle batch compared to the mg BACPT trapped within the particles in that batch. The measurements shown are the average calculated values of drug trapped for the preparation types BACPT-HSAP-1, BACPT-HSAP-4 and BACPT-HSAP-5.

Figure 5.6 shows the relationship created by comparing the mg of BACPT added to the initial formation solution and the calculated mg of BACPT trapped within the HSAPs, as determined via HPLC. The average loading of BACPT into HSAPs when 0.01, 0.5 and 1.0 mg of BACPT was added to a preparation solution was 3.8, 112.1 and 281.8 mg BACPT, respectively. This is a final average drug concentration range of 3.8 to 281.8 μg/mL if the particles are resuspended in 1 mL of water. The particle solutions had resulting BACPT concentrations ranging 9.1 to 671 nM.

In each batch, the amount of HSA remained unchanged at 20 mg, therefore, there is clear evidence that the HSAPs can hold an increasing amount of BACPT, but never all of the BACPT added. There is a loading factor taking place here that is not clearly known. What is clear however, is that further increasing the amount of BACPT into the preparation solution should continue to increase the amount of BACPT capable of being trapped within 20 mg of HSAP until

86

a plateau is reached at max loading capacity. In an effort to spare resources, we did not investigate this loading maximum, as it has been shown that BACPT concentrations in the µmol/L range have been sufficient for cell death. [52, 55]
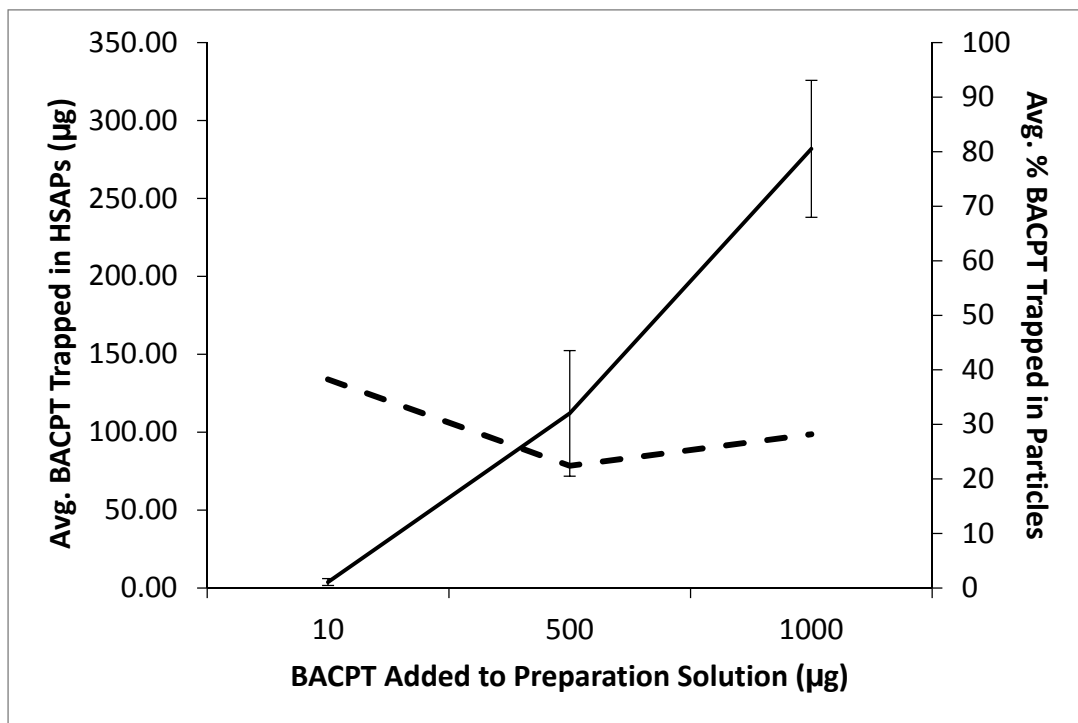
Figure 5.7. Relationship between mg BACPT added to formation solution and (solid line) mg BACPT trapped in the particle batch and (dashed line) % of BACPT loading efficiency. The measurements shown are the average calculated values for the preparation types BACPT-HSAP-1, BACPT-HSAP-4 and BACPT-HSAP-5.

Figure 4.7 further illustrates the loading dynamics by showing that although the amount of drug increases with increased mg BACPT added to the formation solution (which might be expected), the percentage of drug loaded does not increase; decreasing from roughly 38-22% loading. This decrease confirms the idea of a loading plateau for 20 mg of HSAPs and may indicate some kind of binding competition or other kinetic influence. It was initially thought that as the amount of BACPT added to the formation solution decreased, the percentage of drug loaded should increase until all of the available drug was trapped inside, but the results dictated

that only a percentage of the available drug is binding to the HSA during BACPT-HSAP formation.
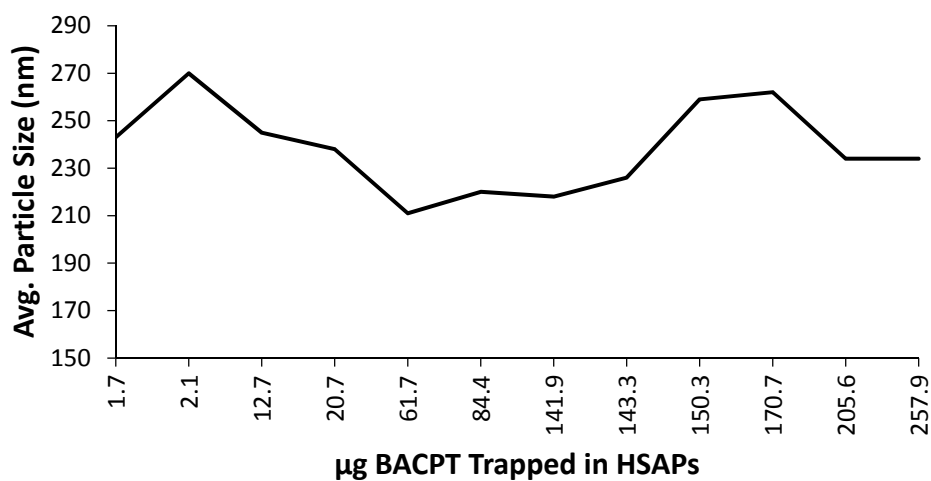
Figure 5.8. Final BACPT-HSAP size compared to the amount of BACPT μg added to the preparation solution for individual samples.

It is speculated that particle formation dynamics may play a role in loading. More evidence that the particles size did not change in correlation to increasing amounts of BACPT present is shown in Figure 5.8; where the size consistency of BACPT-HSAPs is not effected by the drug mass trapped inside them, with all particles remaining within 211 to 270 nm diameter when loaded with 1.7 to 258 μg of BACPT. Taking that into consideration, one explanation for the percentage-based loading of the particles could be that some geographical section of the formed HSAP contains HSA which is available for drug binding and another portion of the HSAP contains HSA which is less capable of drug binding due to conformational changes responsible for the consistent sizing. That theory would have to be explored further to indicate a definitive answer.

Some researchers have concluded that fluorescence should be used for quantitation of camptothecins, especially after exposure to HSA.[109] Our own experience using HPLC for

BACPT analysis corroborated with this conclusion that intricate methodology is necessary for precise analysis.

5.4.3 Determination of Loading Efficiency of BACPT via Fluorescence Spectroscopy

In an effort to see how the structure of BACPT might be changing over time and to better quantitate loading efficiency, the sample supernatants and washes were analyzed by fluorescence spectroscopy and compared to a set of standards that were created at the same time. In an effort to spare resources, we did not investigate this loading maximum, as it has been shown that BACPT concentrations in the μmol/L range have been sufficient for cell death. [52, 55]

Previous literature has shown that the fluorescence of BACPT does change over time, with conversion to the carboxylate form capable of happening in as little as 30 minutes in water. Since the particle solution we have used is 80% ethanol, the conversion was expected to happen more slowly, however it would still likely take place. A standard solution of 0.001 mg/mL BACPT in 50:50 water:ethanol was created and fluorescence spectroscopy was done with excitation at 403 nm with emission collected at 500 nm to monitor fluorescence changes. Twenty four hours later, the same standard solution was analyzed with fluorescence spectroscopy again.
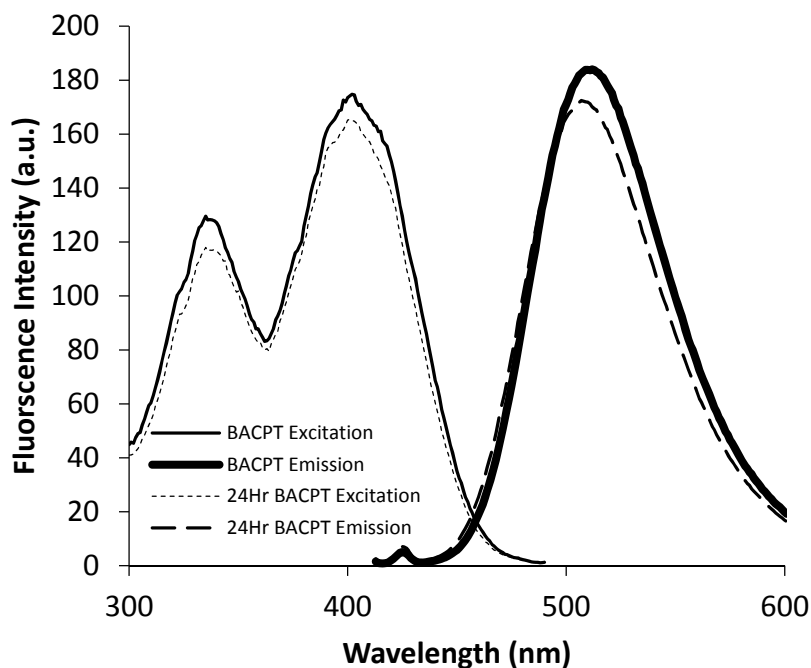
Figure 5.9. Excitation and emission of 0.001 mg/mL solution of BACPT in 1:3 water:ethanol (solid lines) 30 minutes after creation and (dashed lines) 24 hours later.

Figure 5.9 shows the excitation and emission spectrum of the BACPT standard within 30 minutes after creation (solid lines) and 24 hours later (dashed lines). It is evident in the graph that there exists some decrease and shift in the fluorescence emission of the BACPT standard after only 24 hours in 50:50 water:ethanol. This would make it difficult to compare a sample supernatant to a standard of known concentration if the age of the solutions are different. In order to find out if the fluorescence change was concentration dependent, we prepared a set of standards of equal volume (all in 50:50 water:ethanol), but of varying concentrations of BACPT and measured the fluorescence intensity. Then, the standards were allowed to sit in the dark for 24 hours and fluorescence intensity measurements were taken again. The fluorescence intensity of the standards measured within 30 minutes of creation and 24 hours later changed at the same rate.
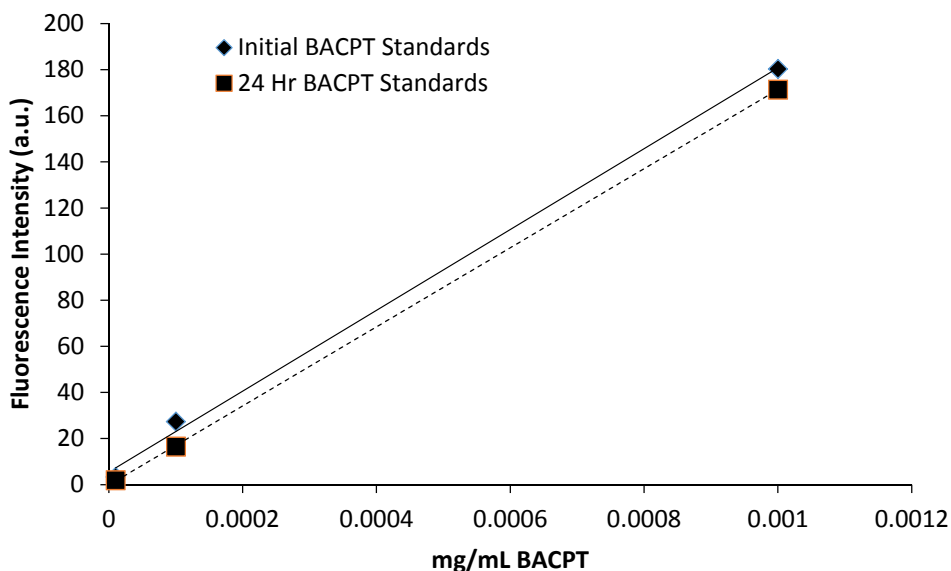
Figure 5.10. Fluorescence Emission points for a series of 3 standard solutions (0.00001, 0.0001 and 0.001 mg/mL) of BACPT in 1:3 water ethanol solvent (Solid trend line and diamond data point markers) within 30 minutes after creation and (Dashed lines) 24 hours later.

Figure 5.10 represents calibration curves for the standards within 30 minutes (solid trend line) of creation and 24 hours later (dashed trend line). As seen in the graph, the standards change at the same rate, as shown by the linearity of the points. This means that the BACPT may in fact be changing to the carboxylate form (assuming this isn't just representative of a loss of fluorescence in general), however the change is not dependent on drug concentration. Therefore, we can use fluorescence to analyze total BACPT present in the sample supernatant and washes, regardless of which form the BACPT is in, as long as the standards are created at the same time as the samples.

Of course, sample analysis sooner rather than later post preparation is preferred. However with the preparation process calling for at least 12 hours of formation and cross-linking time, there must be some lag in analysis time. The emission spectra for carboxylate and lactone forms of BACPT are so similar, that it can be difficult to tell them apart, as they both excite at 403 nm.

91
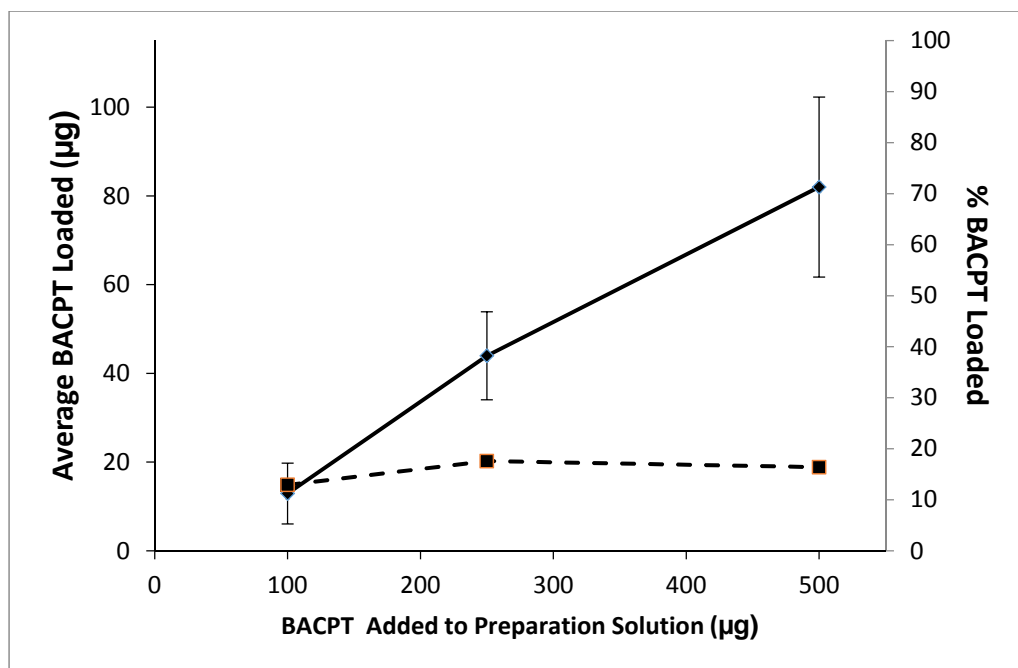
Figure 5.11. Relationship between mg BACPT added to formation solution and (solid line) μg BACPT trapped in the particle batch and (dashed line) % of BACPT loading efficiency. The measurements shown are the average calculated values for the preparation types BACPT-HSAP-2, BACPT-HSAP-3 and BACPT-HSAP-4.

Upon fluorescence analysis of BACPT-HSAPs prepared by either, BACPT-HSAP-2, BACPT-HSAP-3 or BACPT-HSAP-4, it can be seen in Figure 5.11 that there is a relationship between μg of BACPT added to the preparation solution and μg of BACPT that becomes encased in the HSAPs, just as in the case of HPLC analysis.

Upon investigation of the percent of BACPT trapped versus the μg of BACPT added to the preparation solution, a discrepancy from HPLC becomes evident. When utilizing fluorescence for quantitation, the calculated average loading is reduced to 82 μg from 112 μg (as determined via HPLC) for a sample created with 500 μg of BACPT added to initial preparation (method BACPT-HSAP-4) While 82 μg mg is inside of the calculated error for the BACPT-HSAP-4 created batches, it is still worth considering that the HPLC method separated the carboxylate and lactone forms of BACPT differently in the standard solutions due to the water in the mobile

phase; possibly causing it to appear as though there was more BACPT present in the samples when compared to the peak areas of older standard solutions.

Regardless of the quantitation method, there is evidence in both cases that BACPT is indeed becoming trapped within the HSAPs. The real test of whether or not the encapsulated BACPT is still effective at killing cancer cells was yet to be seen, therefore cell studies were done to determine that the combative properties of the BACPT had not been lost.

This means that the BACPT may in fact be changing to the carboxylate form (assuming this isn't just representative of a loss of fluorescence in general), however the change is not dependent on drug concentration. Therefore, fluorescence could be used to analyze total BACPT present in the sample supernatants and washes, regardless of which form the BACPT is in, as long as the standards are created at the same time as the samples. Of course, sample analysis sooner rather than later post preparation is preferred. However with the preparation process calling for at least 12 hours of formation and cross-linking time, there must be some lag in analysis time.
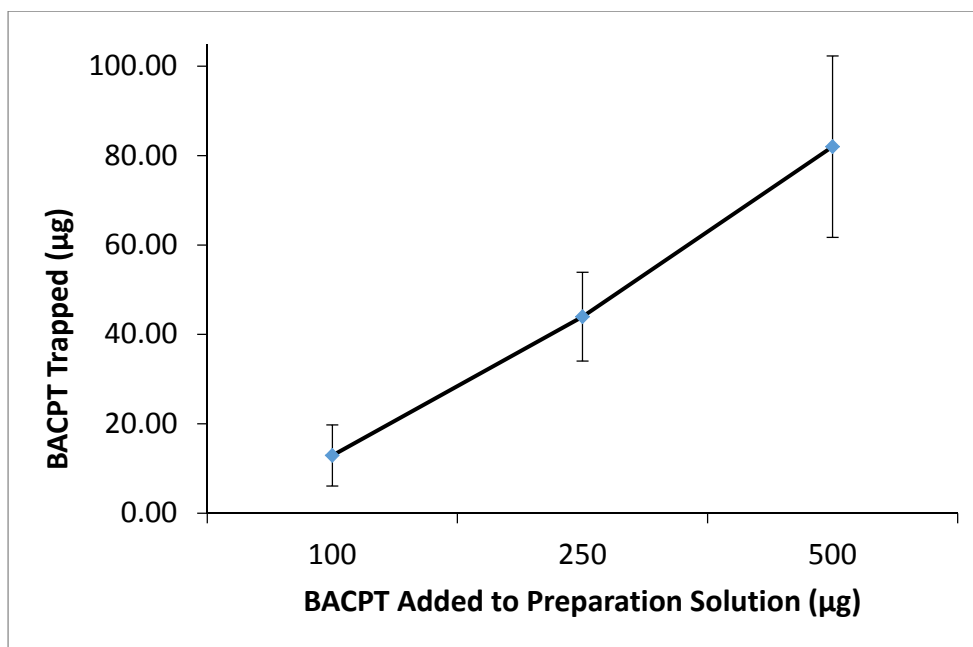
Figure 5.12. Relationship between μg BACPT added to the sample formation solution and the average μg BACPT trapped in the BACPT-HSAPs.

Upon analysis of BACPT-HSAPs prepared with either, 100, 250 or 500 μg BACPT, it can be seen in Figure 5.12 that 13 ± 7, 44 ± 10 and 82 ± 20 μg BACPT is entrapped, respectively. There is a linear relationship between μg of BACPT added to the preparation solution and μg of BACPT that becomes encased in the HSAPs. There is evidence that BACPT is indeed becoming trapped within the HSAPs. The real test of whether or not the encapsulated BACPT is still effective at killing cancer cells was yet to be seen, therefore cell studies were done to determine that the combative properties of the BACPT had not been lost.

5.4.4 Human Sarcoma (CL) in vitro Cytotoxicity of Unloaded-HSAPs & BACPT-HSAPs

Using untreated human sarcoma cancer cells (CL) as a cell control and Unloaded-HSAPs as a particle control, the BACPT-HSAPs were tested for visual cytotoxicity. In order to test the cytotoxicity of the unloaded-HSAPs, they were delivered at a concentration of $\sim 9.1 \times 10^{11}$ HSAPs/ mL to the cells (theoretical particle creation calculation based on all 20 mg of HSA

94

forming 200 nm diameter spherical particles with density of 1.3 g/cm^3). Figure 5.13a shows the CL cell control with no particles added, where cells are vital and continuing to grow and multiply. Figure 5.13b shows some inhibition of cell growth when unloaded HSAPs were added where most cells were inhibited to a rounded state without much multiplication, however some cells were still growing. With this high HSAP concentration, there is an increase in what seems to be aggregation of the particles around the cancer cells, causing the growth inhibition, however there doesn't appear to be any cell death.

This inhibition could be considered a positive result as it would confirm that the HSA particles are indeed attracted to and attaching themselves onto human cancer cells. This growth inhibition may not be an accurate reflection of what would happen in an *in vivo* scenario, when the HSAPs are not simply deposited on top of a few cells, but are allowed to distribute through a tumor site.
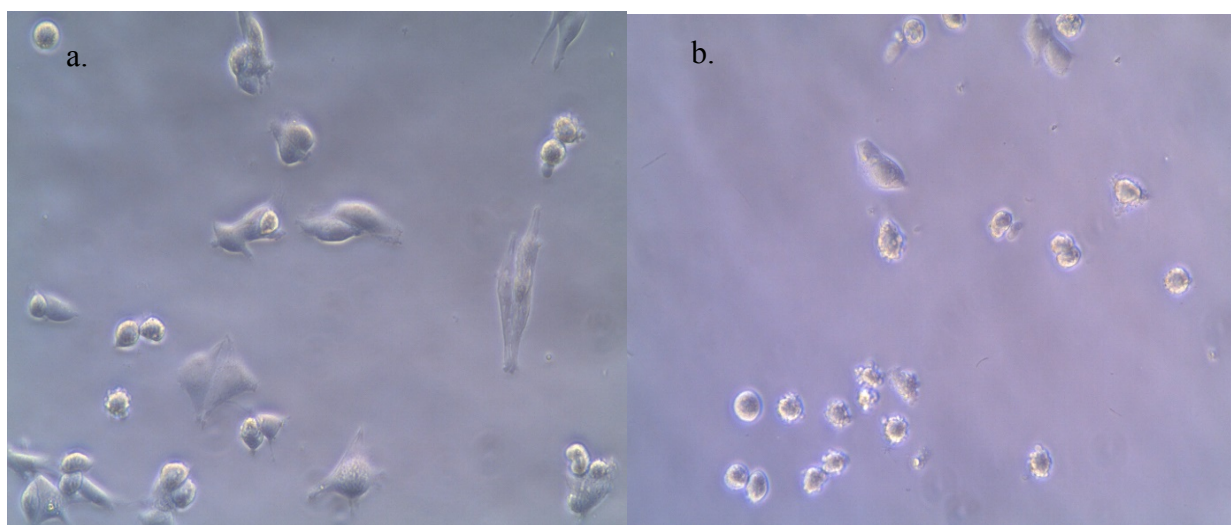
Figure 5.13. Optical Image of Human Sarcoma Cells (CL) with A) no nanoparticles added. B) unloaded-HSAPs added

BACPT-HSAPs were tested for visual cytotoxicity as well using CELL METHOD 1. A BACPT-HSAP-4 preparation method yielded a particle batch with ~124 µg of BACPT trapped within 20 mg of HSAPs; the entire batch was dispersed into 4 mL of water and ultrasonicated. A BACPT-HSAP solution was diluted further in RPMI, yielding an effective BACPT drug dose delivered to the cell of approximately 15.5 ng. Decreased BACPT-HSAP amounts were initially chosen in order to not overwhelm the cells with particles, but to test the combative properties of the drug. Notably, in Figure 5.14, the lesser dose condition shows growth inhibition, cell blebbing and signs of apoptosis.
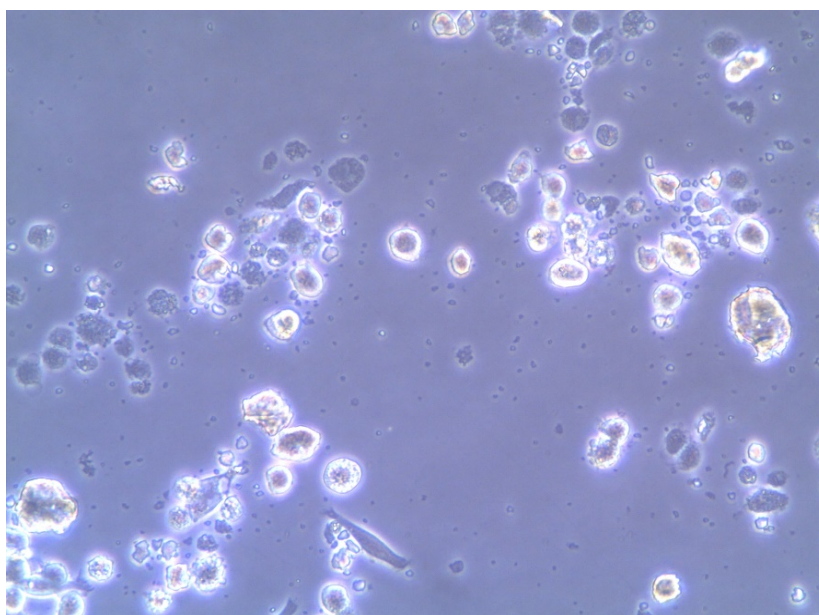
Figure 5.14. Optical image of Human Sarcoma Cells (CL) with a diluted dose of BACPT-HSANPs. Approximately 15.5 ng BACPT delivered.

This low-dose anticancer activity was an extremely hopeful result. It is in-line with previous studies which have found that at low concentrations, J-type aggregates are formed by stacking of the BACPT rings, resulting in self- aggregation which prevents hydrolysis of the lactone ring at neutral pH, assuming they have come completely away from the HSA. [102]   In one

study, BACPT showed the most potency when compared to six other classes of cancer drugs, including gemcitabine, the current gold standard for treatment of pancreatic cancer. BACPT was sixfold more potent than the gemcitabine and two to four logs more active than the other five drugs: vinorelbine, etoposide, dasatinib, 5-flurouracil and 5-azacytidine. [55]

5.4.5 Cytotoxicity of BACPT-HSAPs of Varying Concentrations on Human Sarcoma (CL)

Using CELL METHOD 2, BACPT-HSAPs were delivered to the CL cells without dilution, but with varying concentrations of drug loaded within; with overall higher drug dosages. Since the BACPT-HSAP solution aliquot delivered to the cells theoretically contains upwards of 100 billion particles, it could be hard to see the resulting vital state of the cells. It was decided that the cytotoxicity test would include incubating the cells which were stuck to the well plates with the particles, then removing the RPMI media, along with the particles and dead cells.

Three samples of BACPT-HSAPs were created via preparation methods BACPT-HSAP-2, BACPT-HSAP-3 and BACPT-HSAP-4 with varying amounts of BACPT encapsulated within them (as determined via fluorescence): ~20, 37 and 74 μg, respectively. Without dilution, 0.1 mL of the BACPT-HSAPs were each delivered to separate CL cell samples in replicate, resulting in ~2, 3.7 or 7.4 μg of encapsulated BACPT actually delivered to the cell well. No particles were added to the cell control.

Figure 5.15 shows the cell plates after the particles and dead cells were removed. Figure 5.15a shows that the untreated cells were able to thrive and continue to grow, even after washing. Cells treated with ~2, 3.7 and 7.4 μg (Figures 5.15b, 5.15c and 5.15d, respectively) show progressively less viable cells after treatment and washing; with Figure 5.15d having no cells

visible in the center of the well. This indicates that as the dosage of BACPT increased, more CL

cells were killed, became unstuck from the plate, and were washed away.
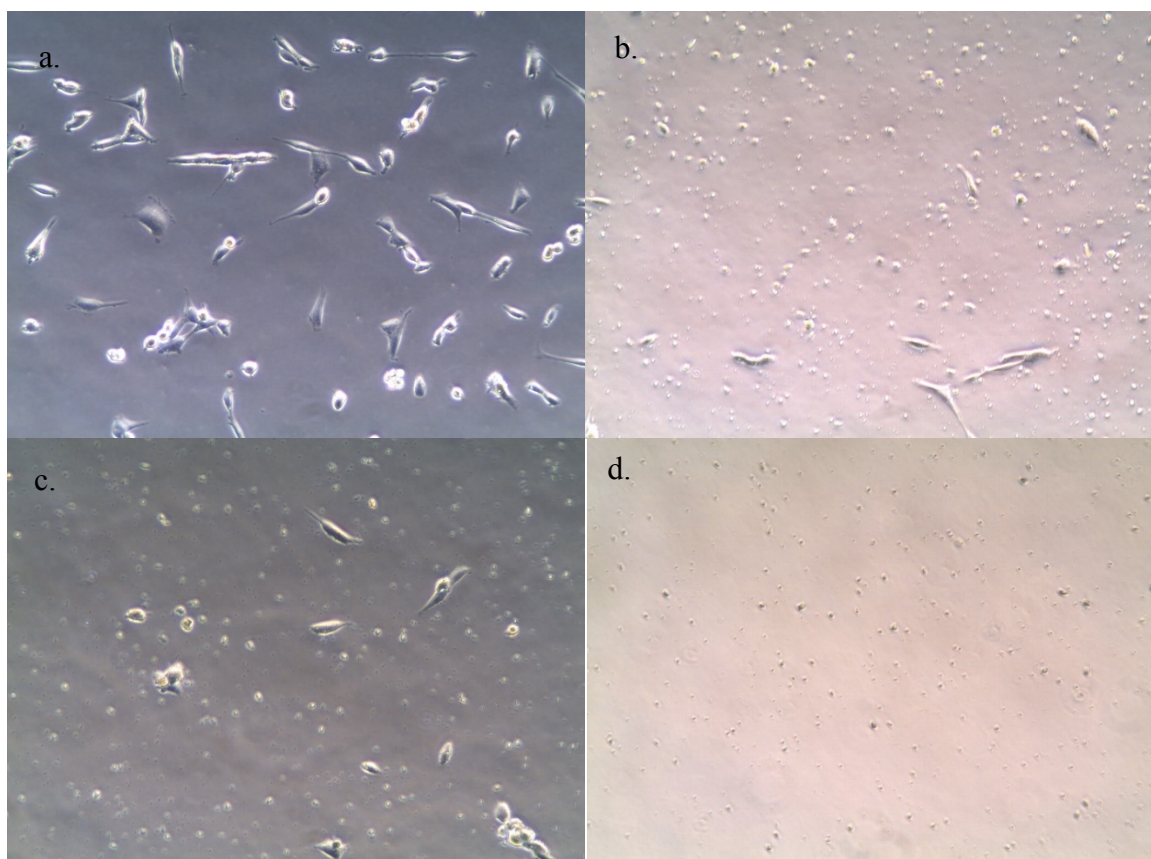
Figure 5.15. Optical image of Human Sarcoma Cells (CL) with (a) non-treated control cells and cells treated with a dose of BACPT-HSAPs containing (b) 2 µg, (c) 3.7 µg and (d) 7.4 µg of BACPT.

It becomes obvious that these doses of BACPT are in fact effective for killing human

sarcoma cancer cells *in vitro*. This proves that the amount of BACPT-HSAPs is not responsible

for overwhelming the cells and killing them, but it is the concentration of the BACPT which is

responsible for cell death. According to these findings that BACPT-HSAPs (likely with BACPT

present in the carboxylate form) are effective at killing human sarcoma cancer cells.

Decidedly, *in vivo* work on an active animal model will give further insight into the effectiveness of BACPT-HSAPs under dynamic, realistic tumor conditions. Such *in vivo* experiments must be done to confirm cell growth and complete cytotoxicity. Also, the atmospherically oxygenated environment (20-21% oxygen) of the *in vitro* cell work presented here is not reflective of the hypoxic environment of a tumor site (1-2% oxygen), which causes the acidic extracellular environment. Since the cytotoxicity of most anticancer drugs is extremely pH dependent both *in vitro* and *in vivo*, a dynamic *in vivo* experiment is vital for further studies.[58]

5.4.6 Formation and Characterization of CPT-HSANPs

In an effort to compare the HSAP loading efficiency of the 7 and 10 carbon substituted BACPT with the parent drug camptothecin, CPT-HSAPs were prepared and analyzed. The CPT has a low solubility of < 1mg/ mL in ethanol. [110] Therefore, the camptothecin was dissolved in a mixture of 50:50 chloroform: ethanol. Subsequent dilutions for the preparation of standards were done with 3:2 ethanol: water. Via dynamic light scattering, the CPT-HSAPs were found to have an average diameter of 475 ± 15 nm. These particles are larger than the BACPT-HSAPs, however they may have just been more susceptible to aggregation, due to the average zeta potential value being -12 ± 4 mV. Either the CPT facilitates larger particle formation or it causes more attractive interactions between particles.

5.4.7 Determination of Loading Efficiency of CPT

To determine the loading efficiency of CPT into the CPT-HSAPs, HPLC was chosen first again as a quantitative method of analysis. Using a 40: 60 acetonitrile: water mobile phase, the CPT standards produced an analyte peak at 3.1 minutes. A standard solution of 0.01 mg CPT/ ml solvent (1:3 water: ethanol) was analyzed within 30 minutes of preparation and found to have a

peak area of 683 at 3.1 minutes. The same standards was analyzed 24 hours later on HPLC and found to have a significantly reduced peak area at 3.1 minutes. Aside from the decrease at 3.1 minutes, the aged standard showed new peaks at 0.9 minutes and 6.2 minutes.

It was thought that peaks appearing at 0.9 to 1.2 min could be the open ringed, carboxylate version of the camptothecin molecules eluting from the column quickly in the mobile phase. The peak appearing at roughly 6.2 minutes was actually thought to be a lower concentration of the lactone version of the CPT. This is thought to be the portion of the lactone-CPT that is in water, thus lingering on the column longer; with only 40% acetonitrile not having the solvency strength to push it thought the column as quickly. Interestingly enough, the remaining peak at 3.1 minutes, which is the time at which the CPT elutes in a freshly made CPT solution is thought to be the lactone-CPT stacking upon itself in the ethanol present in the solvent. [102] The stacking of the molecules cause an elution time slower than that of the carboxylate version being pulled off by the acetonitrile, but slower than the lactone version in water.

When a solution of 0.001 mg of CPT in 1 mL of ethanol only was created and analyzed on HPLC, the analyte eluted at ~3.0 minutes with a peak area of 350 mA.U. Twenty four hours later, the standard solution eluted at the same time, but with a peak area of only 72 mA.U. There was not a large peak increase at 0.9 or 6.2 minutes to account for this elution loss at 3.0 minutes. Therefore, the molecule was likely sticking to the column, as the acetonitrile concentration was not strong enough to elute the CPT as it had when the sample was fresh.

More experimentation would need to be done to confirm the sample breakdown hypothesis, proving information about the change in conformational states of the CPT over time. However, for our purposes in this project, HPLC would not serve as an efficient method of analysis, as the solvent was playing too big of a role in the temporal integrity of the sample.

Again, fluorescence was chosen as the secondary means of quantitative analysis of the CPT washed off of the CPT-HSAPs. Although, contrary to the case of BACPT, fluorescence measurements for CPT quantitation turned out to be even more elusive and sporadic. Samples of CPT-HSAPs were created for dosing the CL human sarcoma cell line, so the loading quantitation was attempted. The initial sample preparation solution for the treatment batch was made with 0.5 mg of CPT, so batches of CPT-HSAPs were created with 0.1, 0.25 and 0.5 mg CPT in order to find a loading trend.

Upon fluorescence spectroscopy, with excitation maximum at 358 nm and emission at 428 nm, it was found that every batch of CPT-HSAPs created with carrying starting masses of CPT gave loading efficiencies of over 100%, despite have linear calibration curves for reference. This is not possible, so further fluorescence studies on standard solutions of CPT were performed.

First, standards of 0.0005 mg CPT/ mL solvent were created in chloroform and ethanol only and in chloroform, ethanol and water (to more closely mimic the particle preparation matrix). The CPT solutions in chloroform and ethanol showed a decrease in fluorescence intensity over 72 hours, as shown by Figure 5.16.
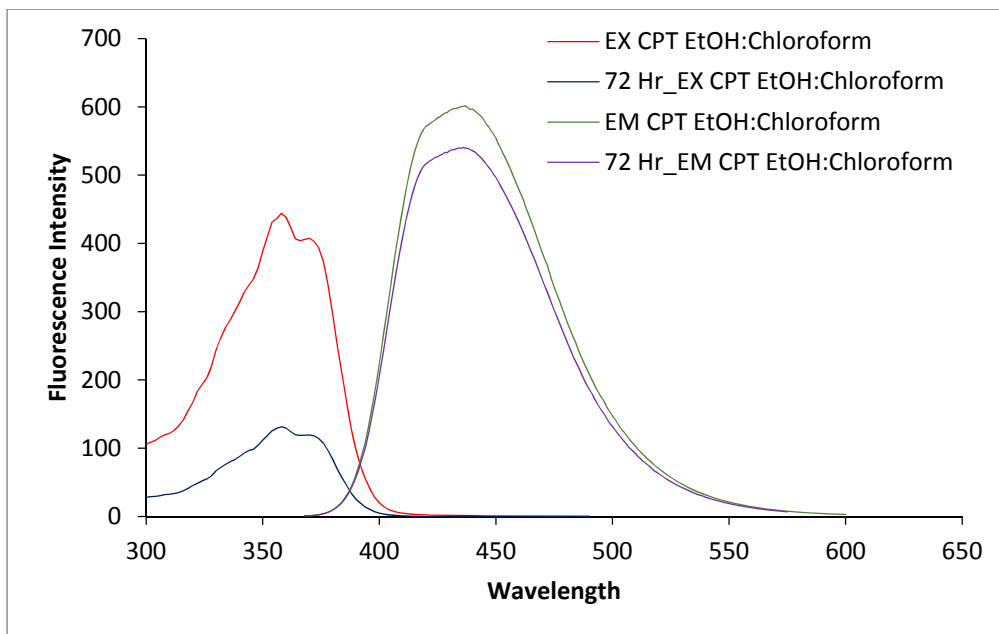
Figure 5.16. Fluorescence excitation and emission spectra of 0.005 mg CPT/ mL in ethanol and chloroform, immediately after preparation and 72 hours later.

Notably, when less than 1% water was present in the solvent matrix, the CPT fluorescence intensity remained the same for 72 hours (as did the excitation intensity), as seen in Figure 4.17.
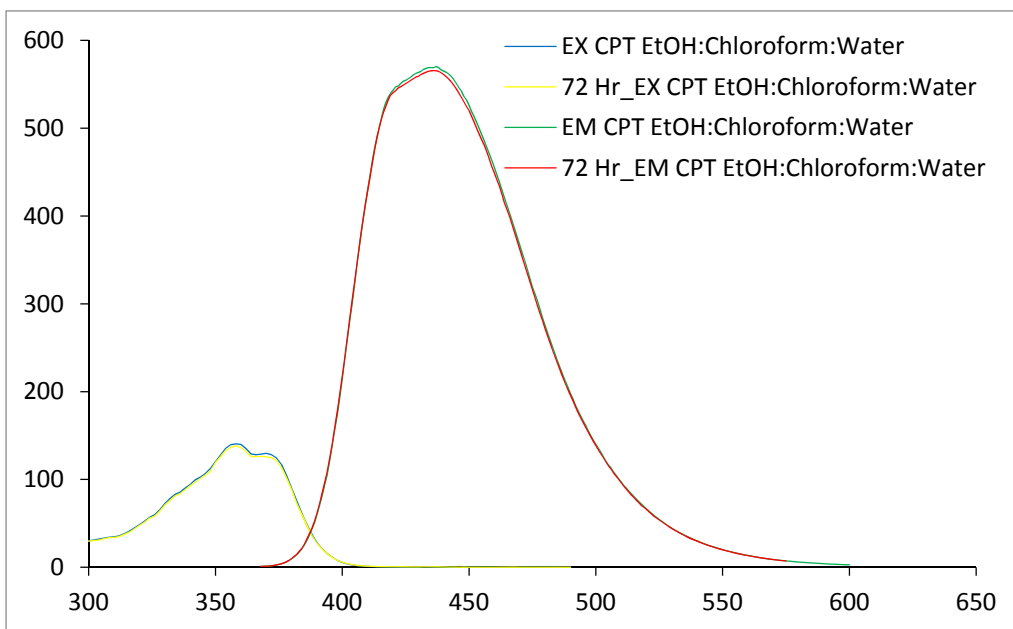
Figure 5.17. Fluorescence excitation and emission spectra of 0.005 mg CPT/ mL in ethanol, chloroform and 0.27% water, immediately after preparation and 72 hours later.

The reason the fluorescence intensity was not effected over 72 hours when water was present is not known. What is noticeable is that the solvent effects caused a difference in initial fluorescence intensity of roughly 598 for the chloroform:ethanol standard and roughly 558 for the standard containing as little as less than 1% water in the solvent matrix.

Because the sample matrix never contains that little water (and initial supernatants and subsequent washes even contain varying amount of water), another solution of 0.0005 mg CPT/ mL solvent was created with 25 % water present along with the ethanol:chloroform matrix. As seen in Figure 5.18, this time, the fluorescence intensity of the solution did decrease over 24 hours and continued to decrease as far as 9 days later.
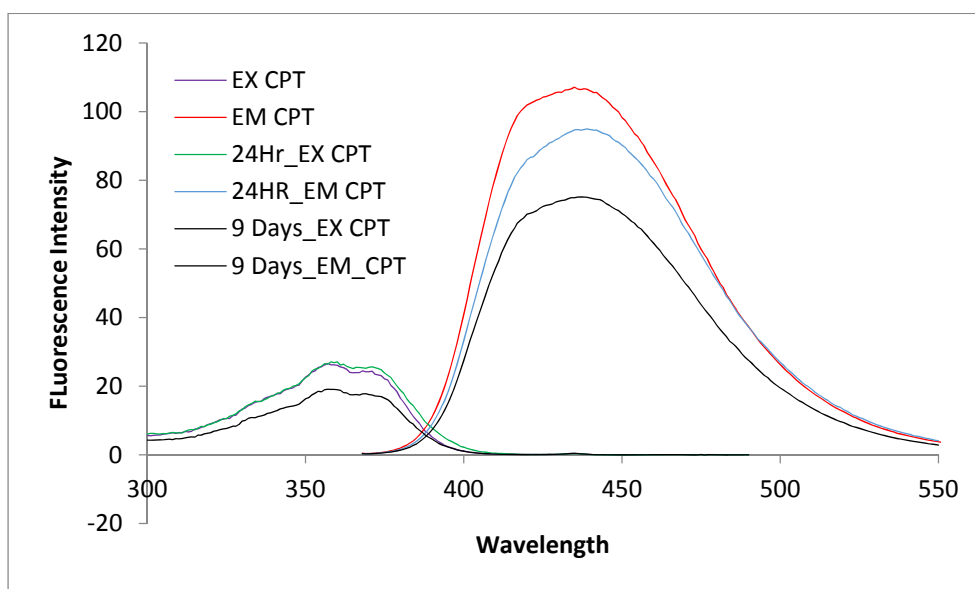
Figure 5.18. Fluorescence excitation and emission spectra of 0.005 mg CPT/ mL in ethanol, chloroform and 25% water, immediately after preparation, 24 hours later and 9 Days later.

To see whether this decrease was concentration dependent, a set of standards of varying concentrations were made with the more realistic solvent matrix of 25% water and 75% ethanol:chloroform to study the fluorescence intensity change over 24 hours. Figure 5.19 shows the decline in CPT fluorescence intensity over 24 hours.
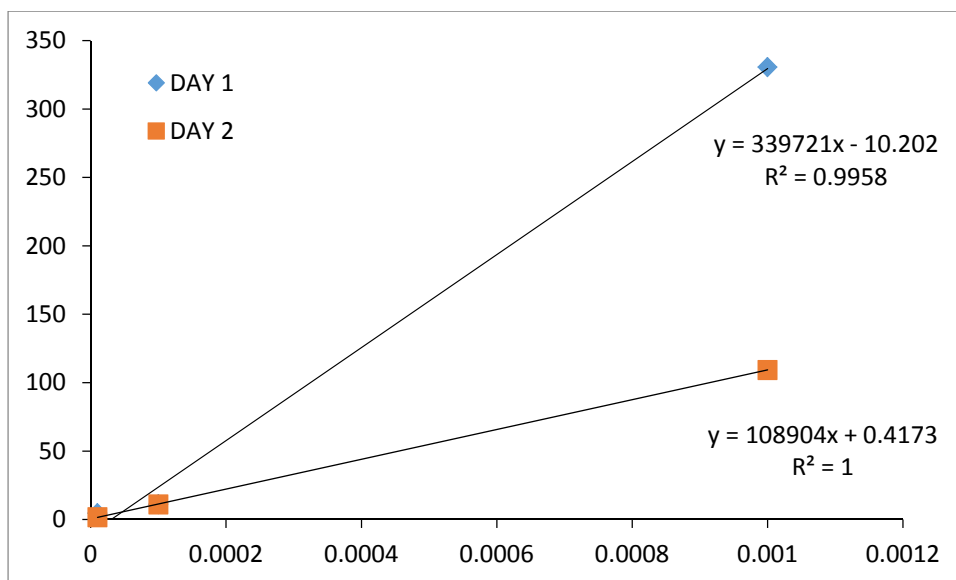
Figure 5.19. Fluorescence emission calibration curves for CPT standards with concentrations of 0.00001, 0.0001 and 0.001 mg CPT/ mL in ethanol, chloroform and 25% water, immediately after preparation and 24 hours later.

Although on first glance, the loss of fluorescence intensity does not seem to be concentration dependent, as noted by the linearity of the standards' fluorescence change over time, Observing the actual fluorescence intensity values versus the concentration values (in Table 5.4) of the solutions gives another perspective:

Table 5.4. Max fluorescence intensity for CPT solutions upon creation and 24 hours later.

Concentration of CPT (mg/mL)	MAX Fluorescence Intensity on DAY 1	MAX Fluorescence Intensity on DAY 2
0.00001	4.6	1.7
0.0001	11.2	11.1
0.001	330.7	109.3

At the lowest concentration of 0.00001 mg/mL, the CPT fluorescence intensity decreased by 36%, but remained constant for the 0.0001 mg/mL CPT standard. Finally, the 0.001 mg/mL experienced a 33% decreased in fluorescence intensity. Either the 0.0001 mg/mL CPT solution

104

was an anomaly and kept its quantum efficiency or there was some error in the analysis. Regardless, the fluorescence intensity changes for the camptothecin are difficult to fully assess and would require more time and effort to comprehensively explain the kinetics of the opening of the lactone ring based on varying concentrations and solvent effects.

Finally, the loss in fluorescence intensity is greater for CPT than BACPT over a twenty four hour period and is likely causing the sample supernatants to seem as though they contain more CPT than what was originally added to the preparation solution when compared to a decaying set of standards. It is a possibility that the HSA could be protecting the CPT from decaying s fast in the sample matrix in some way, but more studies would have to be performed to prove that theory.

5.4.8 Cytotoxicity of CPT-HSAPs of Varying Concentrations on Human Sarcoma (CL)

Despite the trouble with completely and accurately quantifying the amount of CPT trapped within the CPT-HSAPs, the particles were still tested for cytotoxicity against the human sarcoma "CL" cell line. A 20 μL aliquot of the final particle sample was added to a well containing the CL cells and termed a "high dose" of the particles. Figure 5.20 shows the cytotoxic effects of the particles. When compared to the human sarcoma CL control from Figure 5.13a and the HSAP control from Figure 5.13b, it is evident that these CPT-HSAPs cause cell death.
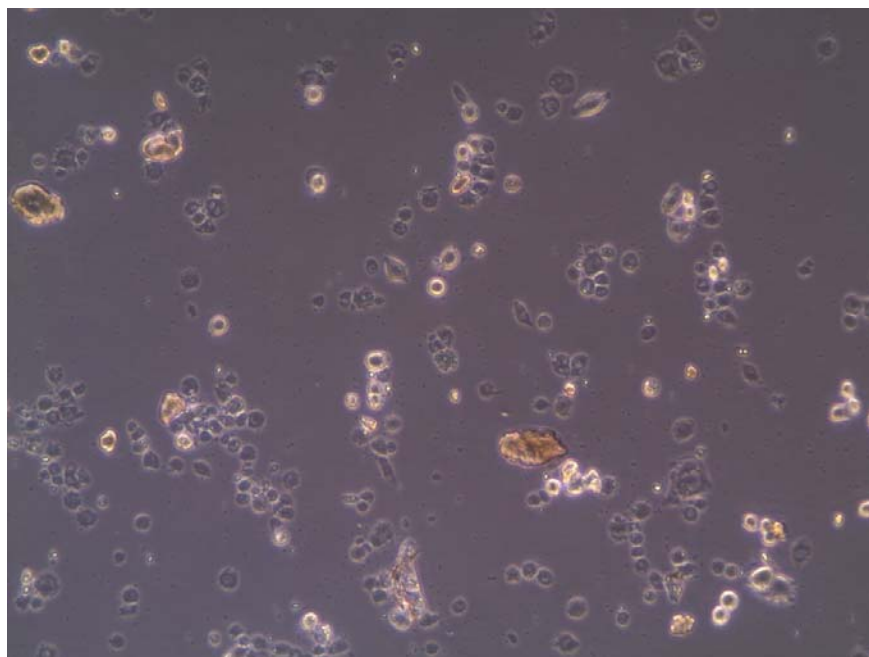
Figure 5.20. Optical Image of Human Sarcoma Cells (CL) treated with a "low dose" of CPT-HSANPs.

When a 20 µL aliquot of 25% diluted CPT-HSAPs was added to the CL cells, the trial was termed a "low dose" particle delivery. Figure 5.21 shows the human sarcoma CL cells after incubation with a low dose of the CPT particles. Again, even when the particles were diluted, they still caused cell death. Unfortunately, due to the quantitation issues surrounding the CPT, it is not known what the actual mass of drug present in the particle sample was. Without that knowledge and a valid method to continue quantitation, subsequent release studies could not be performed to try to determine what mass of camptothecin was responsible for causing this successful cytotoxicity result.
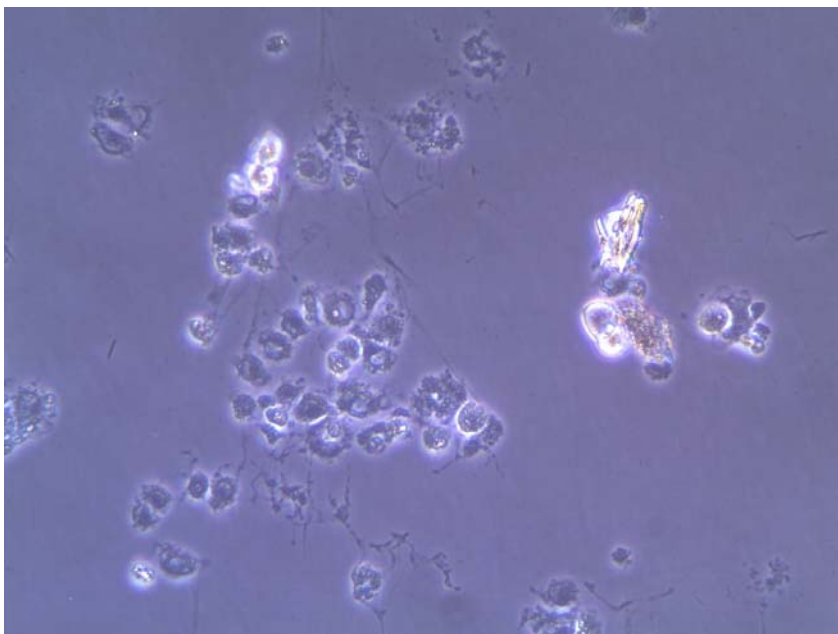
Figure 5.21. Optical image of Human Sarcoma Cells (CL) treated with a "low dose" of CPT-HSANPs.

5.5 Conclusions

This research has shown that the loading BACPT and CPT into HSAPs is possible with controlled particle size within 200-300 nm for the BACPT-HSAPs and 400-500 nm for the CPT-HSAPs. The resulting BACPT-HSAPs are capable of encapsulation efficiency of at least up to 21%. Moreover, the BACPT-HSAPs are visually cytotoxic to human sarcoma cancer cells down to a 15 ng dose, despite ideas that BACPT becomes irreversibly bound to HSA and subsequently medicinally inactive. Further *in vivo* experiments need to be done to determine whether BACPT-HSAPs are an effective delivery mechanism for BACPT in an active tumor site and to determine whether there is a concentration of BACPT-HSAPs that is effective at delivering the drug in low enough concentrations that a patient's organs and healthy cells are not at risk.

Unfortunately, the CPT loading quantitation could not be determined with either HPLC or fluorescence spectroscopy due to the water in the mobile phase during HPLC analysis and the erratic effects of the water in the sample preparation on the fluorescence emission of CPT.

Chapter 6 Summary and Conclusions

In Chapter 2, composite AuNP-HSAPs, AuNS-HSAPs, and AuNR-HSAPs were successfully prepared as a proof of concept to show that these composite particles can serve as platforms for preparing new drug therapies. This research has shown that size-controlled encasement of these gold nanomaterials into larger (100-300 nm) HSAPs is possible via a desolvation and crosslinking process. This study served as the basis for the rest of the work. Proving gold nanomaterials could be encased in a bio-friendly protein shell which is large enough to load sufficient drug was important. Moreover, the same preparation parameter manipulations that allow for controllable particle size of medicinally useful HSAPs are in operation when the procedure is conducted with gold nanomaterials present. What we were left with was a template for future custom loading and surface functionalization.

In Chapter 3, the first assessment of simultaneous loading of gold nanomaterials and proven chemotherapeutic drug proved successful with the formation of PAC-AuNR-HSAPs. In addition to the loading capabilities, the photothermally active function of the gold was not lost after forming thiol bonds with the HSA or with any interaction with the drug. The combined approach will allow killing of cancer cells by both hyperthermia and localized chemotherapy treatment and is more likely to eliminate all cancer cells.

We saw that the level of heating could be controlled with the amount of gold present in the particles and the 'doses' of each preparation type. This is important because it allows for controlled heating, where a tumor in a particularly fragile site may not be able to receive complete ablation, however slight heating of the particles may result in an increase in drug uptake over time. The exact number of gold nanoparticles loaded into each HSAP to achieve

effective hyperthermic treatment safe enough for *in vivo* treatment is not yet known, but is the subject of ongoing studies, as is a step-wise increase in heating temperatures.

In Chapter 4, hybrid AuNR-HSAPs were successfully prepared for *in vitro* studies and showed more controllable size distributions when more protein is added to the preparation vial. The particles were able to heat to necessary temperatures in order to cause renal cell carcinoma death, but careful consideration of the particle dose has to be maintained in order to not overwhelm the cells without irradiation. Fluorescence uptake studies confirmed that the AuNR-HSAPs are being taken up into the cancer cells, but are not entering the cell nuclei. Functionalizing the surface of the HSAPs with disease-specific targeting ligands may lead to even more effective delivery of cancer therapies to the site of the disease, boosting effectiveness and reducing damage to healthy tissue [42]

Finally, in Chapter 5, the research has shown that the loading BACPT and CPT into HSAPs is possible with controlled particle size and resulting BACPT-HSAPs are capable of encapsulation efficiency of at least up to 21%. Moreover, the BACPT-HSAPs are visually cytotoxic to human sarcoma cancer cells down to a 15 ng dose, despite ideas that BACPT becomes irreversibly bound to HSA and subsequently medicinally inactive. CPT is also toxic to human sarcoma cells but the necessary loaded drug amount is not known. HPLC analysis proved unhelpful in assessing loading efficiency of the drugs due to the impeding mobile phase on the stability of the drug structure.

Further *in vivo* experiments need to be done to determine whether BACPT-HSAPs are an effective delivery mechanism for BACPT in an active tumor site and to determine whether there is a concentration of BACPT-HSAPs that is effective at delivering the drug in low enough concentrations that a patient's organs and healthy cells are not at risk.

Currently on-going studies include the loading of sorafenib (SRF), an angiogenesis inhibitor, into AuNR-HSAPs for use on renal cell carcinoma *in vitro*. Animal studies are currently being arranged with our Tulane collaboration to assess the photothermal therapy capabilities of the AuNR-HSAPs as well as the hybrid effects of the sorafenib-loaded SRF-AuNR-HSAPs. Future studies will also include surface functionalization of targeting ligands to direct the hybrid particles to the tumor site as well as increase particle uptake.

6.2 References

1.   Society, A. C. Cancer Facts & Figures 2013.

2.   Dreis, S., Rothweiler F., Michaelis M., Cinatl Jr. J., Kreuter, J., Langer, K. , Preparation, characteristics and maintenance of drug efficacy of doxorubicin-loaded human serum albumin (HSA) nanoparticles. *International Journal of Pharmaceutics* **2007,** *341*, 207-214.

3.   Fanali, G., di Masi, A., Trezza, V., Marino, M., Fasano, M., Ascenzi, P., Human serum albumin: from bench to bedside. *Molecular Aspects of Medicine* **2012,** *33* (3), 209-290.

4.   Kufleitner, J., Worek, F, Kreuter, J., Incorporation of obidoxime into human serum albumin nanoparticles: optimisation of preparation parameters for the development of a stable formulation. *Journal of microencapsulation* **2010,** *27* (7), 594-601.

5.   von Storp, B., Engel, A., Boeker, A., Ploeger, M., Langer, K., Albumin nanoparticles with predictable size by desolvation procedure. *Journal of microencapsulation* **2012,** *29* (2), 138-146.

6.   Langer, K., Balthasar, S., Vogel, V., Dinauer, N., von Briesen, H., Schubert, D., Optimization of the preparation process for human serum albumin (HSA) nanoparticles. *International Journal of Pharmaceutics* **2003,** *257* (1-2), 169-180.

7.   Kufleitner, J., Wagner, S., Worek, F., von Briesen, H., Kreuter, J., Adsorption of obidoxime onto human serum albumin nanoparticles: drug loading, particle size and drug release. *Journal of microencapsulation* **2010,** *27* (6), 506-13.

8.   Ulbrich, K.; Michaelis, M.; Rothweiler, F.; Knobloch, T.; Sithisarn, P.; Cinatl, J.; Kreuter, J., Interaction of folate-conjugated human serum albumin (HSA) nanoparticles with tumour cells. *Int J Pharm* **2011,** *406* (1-2), 128-34.

9.   Jithan, A., Madhavi, K., Madhavi, M., Prabhakar, K., Preparation and characterization of albumin nanoparticles encapsulating curcumin intended for the treatment of breast cancer. *Int J Pharm Investig* **2011,** *1* (2), 119-25.

10.   Gupta, P. K., Hung, C.T., Albumin microspheres II: applications in drug delivery. *J. Microencapsulation* **1989,** *6* (4), 463-472.

11.   Anhorn, M. G., Wagner, S., Kreuter, J., Langer, K., von Briesen, H., Specific Targeting of HER2 Overexpressing Breast Cancer Cells with Doxorubicin-Loaded Trastuzumab-Modified Human Serum Albumin Nanoparticles. *Bioconjugate Chem* **2008,** *19* (12), 10.

12.   Maeda, H., Wu, J., Sawa, T., Matsumura, Y., Hori, K., Tumor vascular permeability and the EPR effect in macromolecular therapeutics: a review. *Journal of controlled release : official journal of the Controlled Release Society* **2000,** *65* (1-2), 271-84.

13.   Wartlick, H.; Spänkuch-Schmitt, B.; Strebhardt, K.; Kreuter, J.; Langer, K., Tumour cell delivery of antisense oligonuclceotides by human serum albumin nanoparticles. *Journal of Controlled Release* **2004,** *96* (3), 483-495.

14.   Lin, W., Coombes, A.G.A, Davies, M.C., Schacht, E., Davis, S.S., IIIum, L., Preparation of sub-100 nm human serum albumin nanospheres using a pH-coacervation method. *Journal of Drug Targeting* **1993,** *1*, 237-243.

15.   Sebak, S., Mirzaei, M., Malhotra, M., Kulamarva, A., Human serum albumin nanoparticles as an efficient noscapine drug delivery system for potential use in breast cancer: preparation and in vitro analysis. *International Journal of Nanomedicine* **2010**, 525.

16.   Gradishar, W. J., Albumin bound nanoparticle paclitaxel. *Clinical Advances in Hematology and Oncology* **2005,** *3* (5), 348-349.

17.   Fasano, M.; Curry, S.; Terreno, E.; Galliano, M.; Fanali, G.; Narciso, P.; Notari, S.; Ascenzi, P., The extraordinary ligand binding properties of human serum albumin. *IUBMB Life* **2005,** *57* (12), 787-96.

18.   Jun, J. Y., Nguyen, Hoang Hai, Paik, Sae-Yeol-Rim, Chun, Hyang Sook, Kang, Byeong-Cheol, Ko, Sanghoon, Preparation of size-controlled bovine serum albumin (BSA) nanoparticles by a modified desolvation method. *Food Chemistry* **2011,** *127* (4), 1892-1898.

19.   Webb, B. A., Chimenti, M., Jacobson, M.P., Barber, D.L., Dysregulated pH: a perfect storm for cancer progression. *Nature Reviews Cancer* **2011,** *11* (9), 671-677.

20.   Langer, K., Anhorn, M. G., Steinhauser, I., Dreis, S., Celebi, D., Schrickel, N., Faust, S., Vogel, V., Human serum albumin (HSA) nanoparticles: reproducibility of preparation process and kinetics of enzymatic degradation. *Int J Pharm* **2008,** *347* (1-2), 109-17.

21.   Cole, J. R., Mirin, N.A., Knight, M.W., Goodrich, G.P., Halas, N.J., Photothermal efficiencies of nanoshells and nanorods for clinical therapeutic applications. *J.Phys. Chem.* **2009,** *113*, 12090–12094.

22.   Huschka, R., Zuloaga, J., Knight, M. W., Brown, L. V., Nordlander, P., Halas, N. J., Light-induced release of DNA from gold nanoparticles: nanoshells and nanorods. *J Am Chem Soc* **2011,** *133* (31), 12247-55.

23.   Huang, X. J., P.K.; El-Sayed, I.H.; El-Sayed, M.A., Plasmonic photothermal therapy (PPTT) using gold nanoparticles. *Lasers Med Sci* **2008,** *23*, 217-228.

24.   Morton, J. G., Day, E.S., Halas, N.J., West, J.L., Nanoshells for photothermal cancer therapy. In *Cancer Nanotechnology; Methods and Protocols*, Humana Press: New York, 2010; Vol. 624, pp 101-117.

25.   Choi, W. I., Kim, Ja-Young, Kang, Chul, Byeon, Clare C., Kim, Young Ha, Tae, Giyoong, Tumor Regression In Vivo by Photothermal Therapy Based on Gold-Nanorod-Loaded, Functional Nanocarriers. *ACS Nano* **2011,** *5* (3), 1995-2003.

26.   van der Zee, J., Heating the patient: a promising approach? *Annals of oncology : official journal of the European Society for Medical Oncology / ESMO* **2002,** *13* (8), 1173-84.

27.   Gormley, A. J.; Larson, N.; Banisadr, A.; Robinson, R.; Frazier, N.; Ray, A.; Ghandehari, H., Plasmonic photothermal therapy increases the tumor mass penetration of HPMA copolymers. *Journal of Controlled Release* **2013,** *166* (2), 130-138.

28.   Ren, F.; Bhana, S.; Norman, D. D.; Johnson, J.; Xu, L.; Baker, D. L.; Parrill, A. L.; Huang, X., Gold nanorods carrying paclitaxel for photothermal-chemotherapy of cancer. *Bioconjugate chemistry* **2013,** *24* (3), 376-86.

29.   Nayak, N. C.; Shin, K., Human serum albumin mediated self-assembly of gold nanoparticles into hollow spheres. *Nanotechnology* **2008,** *19* (26), 265603.

30.   Bardhan, R., Grady, N.K., Cole, J.R., Joshi, A., Halas, N.J., Fluorescence enhancement by Au nanostructures: nanoshells and nanorods. *ACS Nano* **2009,** *3* (3), 744–752.

31.   You, J., Zhang, G., Li, C., Exceptionally high payload of doxorubicin in hollow gold nanospheres for near-infrared light-triggered drug release. *ACS Nano* **2010,** *4* (2), 8.

32.   Stone, J.; Jackson, S.; Wright, D., Biological applications of gold nanorods. *Wiley Interdiscip Rev Nanomed Nanobiotechnol* **2011,** *3* (1), 100-9.

33.   Choi, J., Yang, J., Jang, E., Suh, J., Huh, Y., Lee, K., Haam, S., Gold nanostructures as photothermal therapy agent for cancer. *Anti-Cancer Agents in Medicinal Chemistry* **2011,** *11*, 953-964.

34.   Jang, B., Park, J., Tung, C., Kim, I., Choi, Y., Gold nanorod-photosensitizer complex for near-infrared fluorescence imaging and photodynamic/photothermal therapy *in vivo*. *ACS Nano* **2011,** *5* (2), 1086–1094.

35.   Terentyuk, G. S., Ivanov, A.V., Polyanskaya, N.I., Maksimova, I.L., Skaptsov, A.A., Chumakov, D.S., Khlebtsov, B.N., Khlebtsov, N.G., Photothermal effects induced by laser heating of gold nanorods in suspensions and inoculated tumours during in vivo experiments. *Quantum Electronics* **2012,** *42* (5), 380-389.

36.   Huang, X., El-Sayed, Ivan H., Qian, Wei, El-Sayed, Mostafa A., Cancer Cell Imaging and Photothermal Therapy in the Near-Infrared Region by Using Gold Nanorods. *Journal of the American Chemical Society* **2006,** *128* (6), 2115-2120.

37.   Kannan, R., Nune, Satish, Chanda, Nripen, Zambre, Ajit, Shukla, Ravi, Novel nanochemistry toward generation and stabilization of gold nanoparticles in human serum albumin matrix. *Pure and Applied Chemistry* **2011,** *83* (11), 2055-2062.

38.   Zhang, S.; Li, J.; Lykotrafitis, G.; Bao, G.; Suresh, S., Size-Dependent Endocytosis of Nanoparticles. *Advanced Materials* **2009,** *21* (4), 419-424.

39.   Kou, L.; Sun, J.; Zhai, Y.; He, Z., The endocytosis and intracellular fate of nanomedicines: Implication for rational design. *Asian Journal of Pharmaceutical Sciences* **2013,** *8* (1), 1-10.

40.   Duncan, R.; Richardson, S. C., Endocytosis and intracellular trafficking as gateways for nanomedicine delivery: opportunities and challenges. *Molecular pharmaceutics* **2012,** *9* (9), 2380-402.

41.   Charan, S., Sanjiv, Kumar, Singh, Narendra, Chien, Fan-Ching, Chen, Yi-Fan, Nergui, Navchtsetseg Navchaa, Huang, Shih-Hsin, Kuo, Chiung Wen, Lee, Te-Chang, Chen, Peilin, Development of Chitosan Oligosaccharide-Modified Gold Nanorods for in Vivo Targeted Delivery and Noninvasive Imaging by NIR Irradiation. *Bioconjugate chemistry* **2012,** *23* (11), 2173-2182.

42.   Alkilany, A. M.; Murphy, C. J., Toxicity and cellular uptake of gold nanoparticles: what we have learned so far? *J Nanopart Res* **2010,** *12* (7), 2313-2333.

43.   Jain, R. K.; Stylianopoulos, T., Delivering nanomedicine to solid tumors. *Nature reviews. Clinical oncology* **2010,** *7* (11), 653-64.

44.   Bertrand, N.; Wu, J.; Xu, X.; Kamaly, N.; Farokhzad, O. C., Cancer nanotechnology: the impact of passive and active targeting in the era of modern cancer biology. *Advanced drug delivery reviews* **2014,** *66*, 2-25.

45.   Jang, B.; Kim, Y. S.; Choi, Y., Effects of gold nanorod concentration on the depth-related temperature increase during hyperthermic ablation. *Small (Weinheim an der Bergstrasse, Germany)* **2011,** *7* (2), 265-70.

46.   Zu, Y.; Meng, L.; Zhao, X.; Ge, Y.; Yu, X.; Zhang, Y.; Deng, Y., Preparation of 10-hydroxycamptothecin-loaded glycyrrhizic acid-conjugated bovine serum albumin nanoparticles for hepatocellular carcinoma-targeted drug delivery. *Int. J. Nanomed.* **2013,** *8*, 1207-1222.

47.   Wall, M. E.; Wani, M. C.; Cook, C. E.; Palmer, K. H.; McPhail, A. T.; Sim, G. A., Plant Antitumor Agents. I. The Isolation and Structure of Camptothecin, a Novel Alkaloidal Leukemia and Tumor Inhibitor from Camptotheca acuminata1,2. *Journal of the American Chemical Society* **1966,** *88* (16), 3888-3890.

48.   Vassal, G.; Pondarre, C.; Cappelli, C.; Terrier-Lacombe, M. J.; Boland, I.; Morizet, J.; Benard, J.; Venuat, A. M.; Ardouin, P.; Hartmann, O.; Gouyette, A., DNA-topoisomerase I, a new target for the treatment of neuroblastoma. *Eur J Cancer* **1997,** *33* (12), 2011-5.

49.   Pommier, Y.; Pourquier, P.; Fan, Y.; Strumberg, D., Mechanism of action of eukaryotic DNA topoisomerase I and drugs targeted to the enzyme. *Biochimica et biophysica acta* **1998,** *1400* (1-3), 83-105.

50.   Kohn, K. W.; Shao, R. G.; Pommier, Y., How do drug-induced topoisomerase I-DNA lesions signal to the molecular interaction network that regulates cell cycle checkpoints, DNA replication, and DNA repair? *Cell Biochem Biophys* **2000,** *33* (2), 175-80.

51.   Warnecke, A.; Kratz, F., Maleimide-oligo(ethylene glycol) derivatives of camptothecin as albumin-binding prodrugs: synthesis and antitumor efficacy. *Bioconjugate chemistry* **2003,** *14* (2), 377-87.

52.   Morgan, M. T. W., M.; Nakanishi, Y.; Oberlies, N.H.; Grinstaff, M.W.; Kroll, D.J.; Griset, A.P.; Manikumar, G.; Carnahan, M.A.; Wani, M.C., Dendrimer-encapsulated camptothecins: increased solubility, cellular uptake, and cellular retention affords enhanced anticancer activity *in vitro*. *Cancer Res* **2006,** *66* (24), 11913-11921.

53.   Hu, X.; Tian, J.; Liu, T.; Zhang, G.; Liu, S., Photo-Triggered Release of Caged Camptothecin Prodrugs from Dually Responsive Shell Cross-Linked Micelles. *Macromolecules* **2013,** *46* (15), 6243-6256.

54.   Adams, D. J.; da Silva, M. W.; Flowers, J. L.; Kohlhagen, G.; Pommier, Y.; Colvin, O. M.; Manikumar, G.; Wani, M. C., Camptothecin analogs with enhanced activity against human breast cancer cells. I. Correlation of potency with lipophilicity and persistence in the cleavage complex. *Cancer Chemother Pharmacol* **2006,** *57* (2), 135-44.

55.   Adams, D. J.; Waud, W. R.; Wani, M. C.; Manikumar, G.; Flowers, J. L.; Driscoll, T. A.; Morgan, L. R., BACPTDP: a water-soluble camptothecin pro-drug with enhanced activity in hypoxic/acidic tumors. *Cancer Chemother Pharmacol* **2011,** *67* (4), 855-65.

56.   Wachsberger, P. R.; Landry, J.; Storck, C.; Davis, K.; O'Hara, M. D.; Owen, C. S.; Leeper, D. B.; Coss, R. A., Mammalian cells adapted to growth at pH 6.7 have elevated HSP27 levels and are resistant to cisplatin. *International journal of hyperthermia : the official journal of European Society for Hyperthermic Oncology, North American Hyperthermia Group* **1997,** *13* (3), 251-5; discussion 257-9.

57.   Tomida, A.; Tsuruo, T., Drug resistance mediated by cellular stress response to the microenvironment of solid tumors. *Anticancer Drug Des* **1999,** *14* (2), 169-77.

58.   Adams, D. J.; Morgan, L. R., Tumor physiology and charge dynamics of anticancer drugs: implications for camptothecin-based drug development. *Curr Med Chem* **2011,** *18* (9), 1367-72.

59.   Surapaneni, M. S.; Das, S. K.; Das, N. G., Designing Paclitaxel drug delivery systems aimed at improved patient outcomes: current status and challenges. *ISRN Pharmacol* **2012,** *2012*, 623139.

60.   Zhang, J. Y.; He, B.; Qu, W.; Cui, Z.; Wang, Y. B.; Zhang, H.; Wang, J. C.; Zhang, Q., Preparation of the albumin nanoparticle system loaded with both paclitaxel and sorafenib and its evaluation in vitro and in vivo. *Journal of microencapsulation* **2011,** *28* (6), 528-36.

61.   Montana, M. D., C.; Verhaeghe, P.; Terme, T.; Vanelle, P.; Rathelot, P., Albumin-bound paclitaxel: the benefit of this new formulation in the treatment of various cancers. *Journal of Chemotherapy* **2011,** *23* (2), 59-66.

62.   Deepa, G.; Ashwanikumar, N.; Pillai, J. J.; Kumar, G. S., Polymer nanoparticles--a novel strategy for administration of Paclitaxel in cancer chemotherapy. *Curr Med Chem* **2012,** *19* (36), 6207-13.

63.   Yardley, D. A., nab-Paclitaxel mechanisms of action and delivery. *Journal of controlled release : official journal of the Controlled Release Society* **2013,** *170* (3), 365-72.

64.   Ljungberg, B.; Cowan, N. C.; Hanbury, D. C.; Hora, M.; Kuczyk, M. A.; Merseburger, A. S.; Patard, J. J.; Mulders, P. F.; Sinescu, I. C., EAU guidelines on renal cell carcinoma: the 2010 update. *European urology* **2010,** *58* (3), 398-406.

65.   Park, S. Y.; Park, B. K.; Kim, C. K., Thermal ablation in renal cell carcinoma: what affects renal function? *International journal of hyperthermia : the official journal of European Society for Hyperthermic Oncology, North American Hyperthermia Group* **2012,** *28* (8), 729-34.

66.   Cañaveras, F., Madueño, Rafael, Sevilla, José M., Blázquez, Manuel, Pineda, Teresa, Role of the Functionalization of the Gold Nanoparticle Surface on the Formation of Bioconjugates with Human Serum Albumin. *The Journal of Physical Chemistry C* **2012,** *116* (18), 10430-10437.

67.   Sen, T.; Mandal, S.; Haldar, S.; Chattopadhyay, K.; Patra, A., Interaction of Gold Nanoparticle with Human Serum Albumin (HSA) Protein Using Surface Energy Transfer. *The Journal of Physical Chemistry C* **2011,** *115* (49), 24037-24044.

68.   Naveenraj, S., Anandan, S., Kathiravan, A., Renganathan, R., Ashokkumar, M., The interaction of sonochemically synthesized gold nanoparticles with serum albumins. *Journal of pharmaceutical and biomedical analysis* **2010,** *53* (3), 804-10.

69.   Cedervall, T.; Lynch, I.; Lindman, S.; Berggard, T.; Thulin, E.; Nilsson, H.; Dawson, K. A.; Linse, S., Understanding the nanoparticle-protein corona using methods to quantify exchange rates and affinities of proteins for nanoparticles. *Proceedings of the National Academy of Sciences of the United States of America* **2007,** *104* (7), 2050-5.

70.   Mahmoudi, M.; Lynch, I.; Ejtehadi, M. R.; Monopoli, M. P.; Bombelli, F. B.; Laurent, S., Protein-nanoparticle interactions: opportunities and challenges. *Chemical reviews* **2011,** *111* (9), 5610-37.

71.   Tsai, D. H.; Delrio, F. W.; Keene, A. M.; Tyner, K. M.; Maccuspie, R. I.; Cho, T. J.; Zachariah, M. R.; Hackley, V. A., Adsorption and Conformation of Serum Albumin Protein on Gold Nanoparticles Investigated Using Dimensional Measurements and in Situ Spectroscopic Methods. *Langmuir* **2011**.

72.   Kah, J. C. Y. C., J.; Zubieta, A.; Hamad-Schifferli, K., Exploiting the protein corona around gold nanorods for loading and triggered release. *ACS Nano* **2012,** *6* (8), 6730–6740.

73.   Casals, E.; Pfaller, T.; Duschl, A.; Oostingh, G. J.; Puntes, V., Time Evolution of the Nanoparticle Protein Corona. *ACS Nano* **2010,** *4* (7), 3623-3632.

74.   Wagner, S.; Rothweiler, F.; Anhorn, M. G.; Sauer, D.; Riemann, I.; Weiss, E. C.; Katsen-Globa, A.; Michaelis, M.; Cinatl Jr, J.; Schwartz, D.; Kreuter, J.; von Briesen, H.; Langer, K., Enhanced drug targeting by attachment of an anti αv integrin antibody to doxorubicin loaded human serum albumin nanoparticles. *Biomaterials* **2010,** *31* (8), 2388-2398.

75.   Kim, T. H., Jiang, H. H., Youn, Y. S., Park, C. W., Lim, S. M., Jin, C. H., Tak, K. K., Lee, H. S., Lee, K. C., Preparation and characterization of Apo2L/TNF-related apoptosis-inducing ligand-loaded human serum albumin nanoparticles with improved stability and tumor distribution. *J Pharm Sci* **2011,** *100* (2), 482-91.

76.   Stankus, D. P.; Lohse, S. E.; Hutchison, J. E.; Nason, J. A., Interactions between natural organic matter and gold nanoparticles stabilized with different organic capping agents. *Environ Sci Technol* **2011,** *45* (8), 3238-44.

77.   Warner, S., Diagnostics plus therapy = theranostics. *Scientist* **2004,** *18* (16), 38-39.

78.   Xia, Y., Li, W., Cobley, C.M., Chen, J., Xia, X., Zhang, Q., Yang, M., Cho, E., Brown, P.K., Gold nanocages: from synthesis to theranostic applications. *Account of Chemical Research* **2011,** *44* (10), 10.

79.   Bardhan, R., Lal, S., Joshi, A., Halas, N.J., Theranostic nanoshells: From probe design to imaging and treatment of cancer. *Accounts of Chemical Research* **2011,** *44* (10), 936-946.

80.   Preciado-Flores, S.; Wang, D.; Wheeler, D. A.; Newhouse, R.; Hensel, J. K.; Schwartzberg, A.; Wang, L.; Zhu, J.; Barboza-Flores, M.; Zhang, J. Z., Highly reproducible synthesis of hollow gold nanospheres with near infrared surface plasmon absorption using PVP as stabilizing agent. *Journal of Materials Chemistry* **2011,** *21* (7), 2344-2350.

81.   Weber, C., Kreuter, J., Langer, K., Desolvation process and surface characteristics of HSA nanoparticles. *International Journal of pharmaceuticals* **2000,** *196*, 197-200.

82.   Marty, J. J., Oppenheim, R.C., Speiser, P., Nanoparticles-a new colloidal drug delivery system. *Pharmaceutica acta Helvetiae* **1978,** *53* (1), 17-23.

83.   Mehravar, R., Jahanshah, M., Sagatoleslami, N., Fabrication and evaluation of human serum albumin (HSA) nanoparticles for drug dlivery application. *International Journal of Nanoscience* **2009,** *8* (3), 319-322.

84.   Corporation, W. T., Wyatt Technology Corporation Handbook. (2011). 2011.

85.   Wacker, M.; Zensi, A.; Kufleitner, J.; Ruff, A.; Schutz, J.; Stockburger, T.; Marstaller, T.; Vogel, V., A toolbox for the upscaling of ethanolic human serum albumin (HSA) desolvation. *Int J Pharm* **2011,** *414* (1-2), 225-32.

86.   Alkilany, A. M., Thompson, Lucas B., Boulos, Stefano P., Sisco, Patrick N., Murphy, Catherine J., Gold nanorods: Their potential for photothermal therapeutics and drug delivery, tempered by the complexity of their biological interactions. *Advanced drug delivery reviews* **2012,** *64* (2), 190-199.

87.   Peralta;, D. V.; He;, J.; Wheeler;, D. A.; Zhang;, J. Z.; Tarr, M. A., Encapsulating Gold Nanomaterials into Size-Controlled Human Serum Albumin Nanoparticles for Cancer Therapy Platforms. *Journal of microencapsulation* **2014**.

88.   Kim, T. H.; Jiang, H. H.; Youn, Y. S.; Park, C. W.; Tak, K. K.; Lee, S.; Kim, H.; Jon, S.; Chen, X.; Lee, K. C., Preparation and characterization of water-soluble albumin-bound curcumin nanoparticles with improved antitumor activity. *Int J Pharm* **2011,** *403* (1-2), 285-91.

89.   Portal, A.; Pernot, S.; Siauve, N.; Landi, B.; Lepere, C.; Colussi, O.; Rougier, P.; Zaanan, A.; Verriere, B.; Taieb, J., Sustained response with gemcitabine plus Nab-paclitaxel after folfirinox failure in metastatic pancreatic cancer: report of an effective new strategy. *Clinics and research in hepatology and gastroenterology* **2014,** *38* (2), e23-6.

90.   Von Hoff, D. D.; Ramanathan, R. K.; Borad, M. J.; Laheru, D. A.; Smith, L. S.; Wood, T. E.; Korn, R. L.; Desai, N.; Trieu, V.; Iglesias, J. L.; Zhang, H.; Soon-Shiong, P.; Shi, T.; Rajeshkumar, N. V.; Maitra, A.; Hidalgo, M., Gemcitabine plus nab-paclitaxel is an active regimen in patients with advanced pancreatic cancer: a phase I/II trial. *Journal of clinical oncology : official journal of the American Society of Clinical Oncology* **2011,** *29* (34), 4548-54.

91.   Von Hoff, D. D.; Ervin, T.; Arena, F. P.; Chiorean, E. G.; Infante, J.; Moore, M.; Seay, T.; Tjulandin, S. A.; Ma, W. W.; Saleh, M. N.; Harris, M.; Reni, M.; Dowden, S.; Laheru, D.; Bahary, N.; Ramanathan, R. K.; Tabernero, J.; Hidalgo, M.; Goldstein, D.; Van Cutsem, E.; Wei, X.; Iglesias, J.; Renschler, M. F., Increased survival in pancreatic cancer with nab-paclitaxel plus gemcitabine. *The New England journal of medicine* **2013,** *369* (18), 1691-703.

92.   Kroeze, S. G. C.; van Melick, H. H. E.; Nijkamp, M. W.; Kruse, F. K.; Kruijssen, L. W. J.; van Diest, P. J.; Bosch, J. L. H. R.; Jans, J. J. M., Incomplete thermal ablation stimulates

proliferation of residual renal carcinoma cells in a translational murine model. *BJU International* **2012,** *110* (6b), E281-E286.

93.	Tang, H.; Kobayashi, H.; Niidome, Y.; Mori, T.; Katayama, Y.; Niidome, T., CW/pulsed NIR irradiation of gold nanorods: Effect on transdermal protein delivery mediated by photothermal ablation. *Journal of Controlled Release* **2013,** *171* (2), 178-183.

94.	Paal, K.; Muller, J.; Hegedus, L., High affinity binding of paclitaxel to human serum albumin. *European journal of biochemistry / FEBS* **2001,** *268* (7), 2187-91.

95.	Wang, L.; Li, J.; Pan, J.; Jiang, X.; Ji, Y.; Li, Y.; Qu, Y.; Zhao, Y.; Wu, X.; Chen, C., Revealing the Binding Structure of the Protein Corona on Gold Nanorods Using Synchrotron Radiation-Based Techniques: Understanding the Reduced Damage in Cell Membranes. *Journal of the American Chemical Society* **2013,** *135* (46), 17359-17368.

96.	Yoshimura, K.; Uemura, H., Role of vaccine therapy for renal cell carcinoma in the era of targeted therapy. *International Journal of Urology* **2013,** *20* (8), 744-755.

97.	Lundberg, B. B.; Risovic, V.; Ramaswamy, M.; Wasan, K. M., A lipophilic paclitaxel derivative incorporated in a lipid emulsion for parenteral administration. *Journal of controlled release : official journal of the Controlled Release Society* **2003,** *86* (1), 93-100.

98.	Sebaugh, J. L., Guidelines for accurate EC50/IC50 estimation. *Pharmaceutical statistics* **2011,** *10* (2), 128-34.

99.	Modabber, M.; Martin, J.; Athreya, S., Thermal Versus Impedance-Based Ablation of Renal Cell Carcinoma: A Meta-analysis. *Cardiovasc Intervent Radiol* **2014,** *37* (1), 176-185.

100.	Kim, S. C.; Yu, J.; Lee, J. W.; Park, E. S.; Chi, S. C., Sensitive HPLC method for quantitation of paclitaxel (Genexol in biological samples with application to preclinical pharmacokinetics and biodistribution. *Journal of pharmaceutical and biomedical analysis* **2005,** *39* (1-2), 170-6.

101.	Heuer, R.; Gill, I. S.; Guazzoni, G.; Kirkali, Z.; Marberger, M.; Richie, J. P.; de la Rosette, J. J., A critical analysis of the actual role of minimally invasive surgery and active surveillance for kidney cancer. *European urology* **2010,** *57* (2), 223-32.

102.	Fleury, F.; Kudelina, I.; Nabiev, I., Interactions of lactone, carboxylate and self-aggregated forms of camptothecin with human and bovine serum albumins. *FEBS Letters* **1997,** *406* (1–2), 151-156.

103.	Hsiang, Y.-H.; Liu, L. F.; Wall, M. E.; Wani, M. C.; Nicholas, A. W.; Manikumar, G.; Kirschenbaum, S.; Silber, R.; Potmesil, M., DNA Topoisomerase I-mediated DNA Cleavage and Cytotoxicity of Camptothecin Analogues. *Cancer Research* **1989,** *49* (16), 4385-4389.

104.	de la Loza, M. C.; Wellinger, R. E., A novel approach for organelle-specific DNA damage targeting reveals different susceptibility of mitochondrial DNA to the anticancer drugs camptothecin and topotecan. *Nucleic acids research* **2009,** *37* (4), e26.

105.	Chen, J.; Hu, R.-R.; Yang, X.-X.; Gu, W.; Tian, R.; Gong, F.; Luo, L.; Fang, F.; Chen, Z.-P.; Cai, B.-C., Antitumor efficacy, toxicity and pharmacokinetics of 9-nitrocamptothecin: role of lactone ratio. *Cancer Chemother Pharmacol* **2013,** *72* (4), 925-929.

106.	Gerweck, L. E.; Seetharaman, K., Cellular pH gradient in tumor versus normal tissue: potential exploitation for the treatment of cancer. *Cancer Res* **1996,** *56* (6), 1194-8.

107.	Kruszewski, S. K., D.M. , Affinity of new anticancer agent, 7-trimethylsilyl-ethyl-10-amino-camptothecin, to membranes and HSA determined by fluorescence spectroscopy methods. *Optica Applicata* **2008,** *38* (4), 625-633.

108. GIOVANELLA, B. C. H., N. ; MENDOZA, J. ; CAO, Z. ; LIEHR, J. ;; STEHLIN, J. S., Dependence of Anticancer Activity of Camptothecins on Maintaining Their Lactone Function. In *ANNALS NEW YORK ACADEMY OF SCIENCES*.

109. Ziomkowski, B. K., S.; Siuda, R.; Cyrankiewicz, M. , Deactivation rate of camptothecin determined by factor analysis of steady state fluorescence and absorption spectra. *optica applicata* **2006,** *36* (1), 10.

110. Aldrich, S. Camptothecin Data Sheet. www.SigmaAldrich.com.

Vita

The author was born in New Orleans, La. She obtained her B.S. in Chemistry from the Department of Chemistry at Loyola University, New Orleans in May 2002. She received her M.B.A. in Business Administration from University of Phoenix in 2008 and then continued her graduate education with the Department of Chemistry at the University of New Orleans in August 2010. During her time in the chemistry doctorate program at UNO, she was a member of Professor Matthew Tarr's research group.